

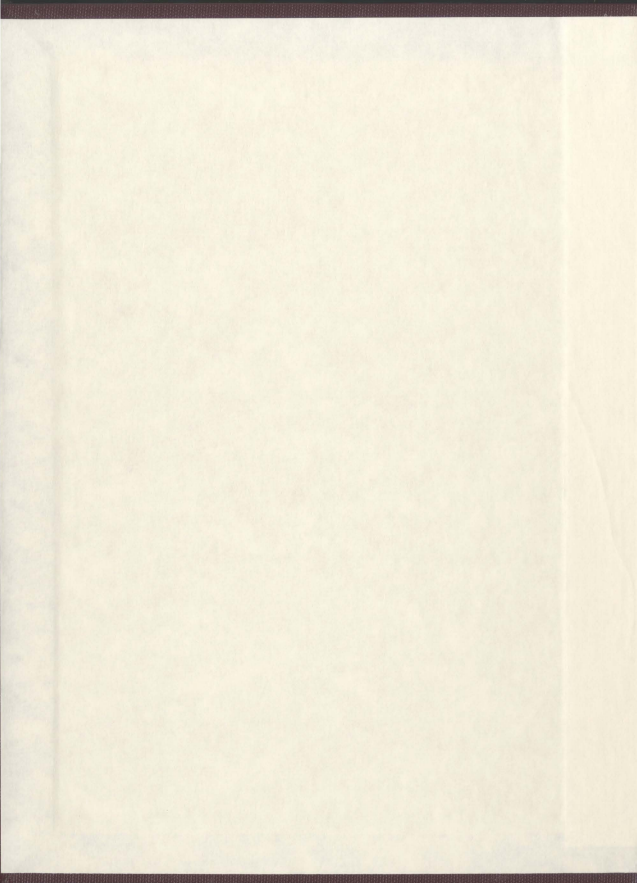
ACOUSTIC IMAGING OF DIEL VERTICAL
MIGRATION OF ZOOPLANKTON ON THE
NEWFOUNDLAND SHELF

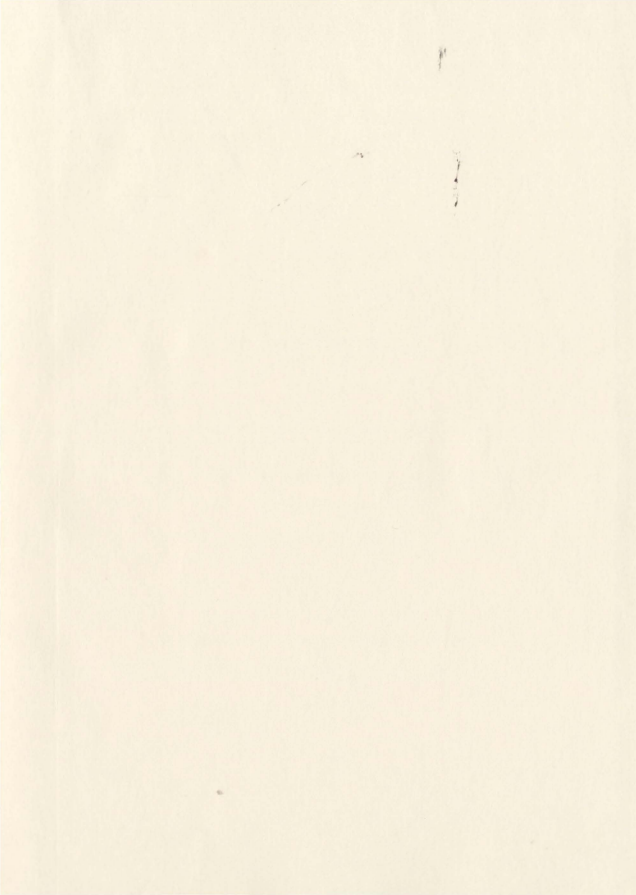
CENTRE FOR NEWFOUNDLAND STUDIES

**TOTAL OF 10 PAGES ONLY
MAY BE XEROXED**

(Without Author's Permission)

NICHOLAS RECORD





ACOUSTIC IMAGING OF
DIEL VERTICAL MIGRATION OF ZOOPLANKTON
ON THE NEWFOUNDLAND SHELF

by

© Nicholas Record

A thesis submitted to the
School of Graduate Studies
in partial fulfilment of the
requirements for the degree of
Master of Science

Department of Physics and Physical Oceanography

Memorial University of Newfoundland

August 2005

St. John's



Newfoundland

ABSTRACT

Diel vertical migration (DVM) of zooplankton is common to marine ecosystems around the world. Here, we examine the response of zooplankton vertical migration to changing physical conditions using acoustic Doppler current profilers (ADCPs) on the Newfoundland Shelf. Techniques for quantifying patterns of DVM in bioacoustic scattering layers are presented and evaluated, including both new methods and some taken from the literature. With these techniques, correlations of DVM patterns are examined in the horizontal, at scales of 10s of metres and 10s of kilometres, and an increase in correlation with proximity is found. Migrators are observed with high statistical significance ($p < 0.05$) to spend 10s of minutes more time at the surface in the morning and evening on overcast days than on clear days. Migration paths are coherent with isotherm depths at time scales longer than 20 days. Backscatter coefficient is modelled based on an empirical response to temperature and light.

ACKNOWLEDGEMENTS

There are many people to whom I would like to express my gratitude. Foremost, I thank my parents and my sisters immeasurably. My friends have also been an emboldening influence.

My supervisor, Brad de Young, has provided many opportunities to participate in field work and to work with scientists in many disciplines, creating the well-rounded educational experience that I was seeking. All the people on the Funk project gave me exposure to interesting ideas, and working with them was a pleasure. Thanks to Bill Montevecchi and Chantelle Burke for the work with the birds.

Many people helped in collecting the data discussed here, including Jack Foley, Chris Lang, Denise Davis, Gérard Morin, and numerous others. Thanks to Yakov Afanasyev and John Anderson for reviewing this thesis. The department staff have been exceptionally helpful. Daniel Bourgault provided valuable advice and also let me stay at his house when the cops came to mine.

Thanks to the Mertz family for their generous contribution to my education. The Department and University have been generous as well. Partial funding was also provided by the Natural Sciences and Engineering Research Council of Canada.

Finally, thanks to Edgar P., for his words on science, and to my brothers, for breakfast.

TABLE OF CONTENTS

ABSTRACT	ii
ACKNOWLEDGEMENTS	iii
TABLE OF CONTENTS	iv
LIST OF TABLES	vi
LIST OF FIGURES	viii
1 INTRODUCTION	1
1.1 Background	2
Hypotheses on adaptive value of migration	4
Environmental cues influencing migration	7
Context within larger trophic scheme	9
Bioacoustics	12
1.2 Goals of the study	13
2 ENERGETIC CONSIDERATIONS	16
2.1 Swimming expenditure	17
Continuous swimming	17
Hop-and-sink swimming	24
Drag coefficient and Reynolds number	25
2.2 Metabolic costs	27
2.3 Summary	29
3 DATA	31
3.1 Mooring information	31
3.2 Atmospheric data	36
3.3 Temperature data	47
3.4 ADCP data	55
3.5 Tow data	62
4 QUANTIFYING DIEL PATTERS IN BACKSCATTER DATA.....	65
4.1 Single statistics	68
Timing	68
Velocity	69
4.2 Time series	75
Choosing threshold values	75
Biomass median depth	81

Lagrangian particle path	88
4.3 Full data set	91
Simulating migration of scattering layers	91
Velocimetry from backscatter flux	94
4.4 Comparison of methods	99
5 ANALYSIS	112
5.1 Temporal and spacial persistence	113
Day-normalization	113
Daily averages	117
Horizontal homogeneity	124
5.2 Response to environmental cues	130
Light intensity	130
Temperature	138
5.3 Anomalies	149
Reverse migration	149
Midnight sinking	150
6 EMPIRICAL MODEL AND CONCLUSIONS	153
6.1 Model	153
Temperature-depth signature	154
Construction of backscatter array	157
6.2 Conclusions	167
REFERENCES	174
APPENDIX A	184
A.1 Energetic requirement for hovering at constant depth	184
A.2 Time and distance required to coast to a stop	187
A.3 Work requirement for hop-and-sink swimming at a nonzero mean velocity	188

LIST OF TABLES

Table 3.1.1 Mooring information for the four data sets.....	33
Table 3.3.1 Thermistor information for all moorings, including thermistor depths, water depth, ensemble time, deployment day, and recovery day.....	49
Table 3.4.1 Details of moored ADCPs, including deployment depth, water depth, signal frequency (Hz), vertical bin size (m), ensemble time (s), pings per ensemble, deployment day, and recovery day.....	57
Table 3.5.1 Dry weight data from bongo net tows, <i>Wilfred Templeman</i> trip # 553, broken into three size classes.....	63
Table 4.1.1 Mean and peak ascent and descent migration velocities averaged over the entire deployment duration, shown for all moorings.....	74
Table 4.4.1 Means and standard deviations of the three single-value time series described in § 4.2, for all moorings. Values are given in metres.....	108
Table 4.4.2 Summary of techniques for quantifying DVM patterns.....	111
Table 5.1.1 Mean correlation coefficient at each mooring between individual days and average day, using three different methods of quantification. Correlation coefficients are given for both with and without day-normalization.....	116
Table 5.1.2 Correlation coefficients r (upper right half) and associated p -values (lower left half) comparing daily averaged, day-normalized biomass median depth paths of individual beams at mooring A, Trinity Bay 2001, and beam averages at moorings A and B, Trinity Bay 2001.....	126
Table 5.1.3 Correlation coefficients r (upper right half) and associated p -values (lower left half) comparing daily-averaged, day-normalized biomass median depth paths of beam averages at the 12 moorings. Shaded regions indicate moorings were in the same deployment.....	128
Table 5.2.1 Difference of migration timing on overcast days from that on clear days, and associated p -values. Timings are obtained using an edge-detection algorithm on the bottom 20 m of backscatter data, then averaging times, eliminating the two outliers. The sample size varied from 70 to 80, with the exception of mooring B in Trinity Bay 2002, where the sample size was 38. Grey boxes are those with p -value of 0.05 or less.....	137
Table 6.1.1 Trinity Bay 2002, all moorings. Comparisons between the biomass median	

depth of measured backscatter data and that of simulated backscatter data. The difference used for the mean and standard deviation is *simulated - observed*. The day series and night series are constructed as in § 5.2.....160

LIST OF FIGURES

- Figure 1.1.1** Schematic of normal nocturnal diel vertical migration. Migrators move upwards around dusk and then return to deep waters around dawn..... 6
- Figure 1.1.2** Survey route and mooring location for the capelin ecosystem study, *Wilfred Templeman* trip # 553, August 2004..... 11
- Figure 3.1.1** Deployment areas for the Placentia Bay 1999, Trinity Bay 2001 and 2002, and Funk Island Bank 2004 data sets. Fig 3.1.2 shows zoom..... 34
- Figure 3.1.2** Mooring locations for the Placentia Bay 1999, Trinity Bay 2001 and 2002, and Funk Island Bank 2004 data sets. Triangles indicate ADCP and thermistor moorings. Cross indicates Bonavista weather station (AWOS)..... 35
- Figure 3.2.1** Cloud opacity obtained from ceilometer measurements at the Bonavista weather station for the time period spanning the Placentia Bay 1999 deployment. There is a two-month gap in the data..... 39
- Figure 3.2.2** Cloud opacity obtained from ceilometer measurements at the Bonavista weather station for the time period spanning the Trinity Bay 2001 deployment..... 40
- Figure 3.2.3** Cloud opacity obtained from ceilometer measurements at the Bonavista weather station for the time period spanning the Trinity Bay 2002 deployment..... 41
- Figure 3.2.4** Cloud opacity obtained from ceilometer measurements at the Bonavista weather station for the time period spanning the Funk Island Bank 2004 deployment..... 42
- Figure 3.2.5** Wind stress (Pa) calculated according to Large & Pond (1981) from wind velocity measurements obtained at the Bonavista weather station for the time period spanning the Placentia Bay 1999 deployment..... 43
- Figure 3.2.6** Wind stress (Pa) calculated according to Large & Pond (1981) from wind velocity measurements obtained at the Bonavista weather station for the time period spanning the Trinity Bay 2001 deployment..... 44
- Figure 3.2.7** Wind stress (Pa) calculated according to Large & Pond (1981) from wind velocity measurements obtained at the Bonavista weather station for the time period spanning the Trinity Bay 2002 deployment..... 45
- Figure 3.2.8** Wind stress (Pa) calculated according to Large & Pond (1981) from wind velocity measurements obtained at the Bonavista weather station for the time period spanning the Funk Island Bank 2004 deployment..... 46

Figure 3.3.1 An example temperature profile, linearly interpolated, taken at the Funk Island Bank mooring, August 2004, showing the presence of the CIL. Crosses mark thermistor depths.....	48
Figure 3.3.2 Isotherms at Trinity Bay 2001 mooring A. Profiles are linearly interpolated into 1 m bins. A moving average of ± 12 hours is taken here for visualization purposes.....	50
Figure 3.3.3 Isotherms at Trinity Bay 2001 mooring B. Profiles are linearly interpolated into 1 m bins. A moving average of ± 12 hours is taken here for visualization purposes.....	50
Figure 3.3.4 Isotherms at Trinity Bay 2001 mooring C. Profiles are linearly interpolated into 1 m bins. A moving average of ± 12 hours is taken here for visualization purposes.....	51
Figure 3.3.5 Isotherms at Trinity Bay 2002 mooring A. Profiles are linearly interpolated into 1 m bins. A moving average of ± 12 hours is taken here for visualization purposes.....	51
Figure 3.3.6 Isotherms at Trinity Bay 2002 mooring B. Profiles are linearly interpolated into 1 m bins. A moving average of ± 12 hours is taken here for visualization purposes.....	52
Figure 3.3.7 Isotherms at Trinity Bay 2002 mooring C. Profiles are linearly interpolated into 1 m bins. A moving average of ± 12 hours is taken here for visualization purposes.....	52
Figure 3.3.8 Isotherms at Trinity Bay 2002 mooring D. Profiles are linearly interpolated into 1 m bins. A moving average of ± 12 hours is taken here for visualization purposes.....	53
Figure 3.3.9 Isotherms at Trinity Bay 2002 mooring E. Profiles are linearly interpolated into 1 m bins. A moving average of ± 12 hours is taken here for visualization purposes.....	53
Figure 3.3.10 Isotherms at Trinity Bay 2002 mooring F. Profiles are linearly interpolated into 1 m bins. A moving average of ± 12 hours is taken here for visualization purposes.....	54
Figure 3.3.11 Isotherms at Funk Island Bank 2004 mooring. Profiles are linearly interpolated into 1 m bins. A moving average of ± 12 hours is taken for visualization purposes.....	54

Figure 3.4.1 Backscatter intensity (dB re $(4\pi\text{m})^{-1}$) and vertical velocity (mm/s) data from 8 days at Placentia Bay 1999 mooring A.....	58
Figure 3.4.2 Backscatter intensity (dB re $(4\pi\text{m})^{-1}$) and vertical velocity (mm/s) data from 8 days at Trinity Bay 2001 mooring A.....	59
Figure 3.4.3 Backscatter intensity (dB re $(4\pi\text{m})^{-1}$) and vertical velocity (mm/s) data from 8 days at Trinity Bay 2002 mooring A.....	60
Figure 3.4.4 Backscatter intensity (dB re $(4\pi\text{m})^{-1}$) and vertical velocity (mm/s) data from the Funk Island Bank 2004 mooring.....	61
Figure 4.0.1 Backscatter intensity (top) and vertical velocity (bottom) from the Funk Island Bank mooring, showing the presence of deep migrators and intermediate migrators.....	67
Figure 4.1.1 Cross sections of vertical velocity and backscatter at Trinity Bay 2001 mooring A, bin #3. Backscatter intensity (a), dashed line shows depth of bin #3. Vertical velocity (b), dashed line shows depth of bin #3. Vertical velocity at bin #3 (c). Backscatter intensity at bin #3 (d). Time gradient of backscatter intensity at bin #3 (e). In (c) – (e), solid vertical lines indicate sunrise and sunset times; dotted lines indicate nautical twilight times.....	71
Figure 4.1.2 Migration timing for Trinity Bay 2001 mooring A, 80 – 100 m. Ascent time based on evening peak upward w (a). Descent time based on morning peak downward w (b). Ascent time based on evening maximum dS_v/dt (c). Descent time based on morning minimum dS_v/dt (d).....	72
Figure 4.1.3 Migration velocities for Trinity Bay 2001 mooring A, averaged over the depth range 80 – 100 m, excluding two outliers.....	73
Figure 4.1.4 Trinity Bay 2001, mooring A. Distribution of upward and downward migration velocities averaged over the depth range 30 – 100 m, excluding two outliers, grouped by 5 mm s ⁻¹ bins.....	74
Figure 4.2.1 The number of occurrences of each dB value (± 0.5 dB) of the backscatter intensity data for the duration of the deployments of Placentia Bay 1999 mooring A (a) and mooring B (b).....	78
Figure 4.2.2 Trinity Bay 2001 mooring A: identifying migrating scatterers by associating high velocities with S_v values. Vertical velocity data (a). Regions of the vertical velocity data that lie outside of 2 standard deviations (b). Backscatter coefficient (c). Regions of	

the backscatter intensity data that are within 1 standard deviation of the set of S_v values associated with high velocities (d). Resulting backscatter range identified is from -86.5 to -80.8 dB..... 79

Figure 4.2.3 Trinity Bay 2001 mooring A: tracking maximum backscatter intensity. Volume backscatter intensity (a); depth of maximum S_v value at each measurement time (b); maximum S_v value at each measurement time (c)..... 80

Figure 4.2.4 Day-averaged (year days 220 - 233) backscatter coefficient (top) and standard deviation (bottom) for the Funk Island Bank mooring..... 85

Figure 4.2.5 Averaged backscatter and tow data for the Funk Island Bank mooring. Backscatter coefficient daily- and depth-averaged (a); bongo net tow data daily averaged and depth integrated, linearly interpolated to fill in gaps, and averaged over ± 30 minutes (b); log-linear regression between backscatter and dry weight averages shown, $r^2 = 0.77$ (c).....86

Figure 4.2.6 Trinity Bay 2001 mooring A: tracking biomass median depth. Backscatter coefficient (a); biomass median depth at each measurement time determined using a conversion formula from backscatter to biomass (b); S_v value at biomass median depth at each measurement time (c)..... 87

Figure 4.2.7 The numerical scheme used to track a Lagrangian particle through the measured vertical velocity with a temporal resolution higher than that of the ADCP..... 89

Figure 4.2.8 Trinity Bay 2001 mooring A: the path of a Lagrangian particle (dashed line) derived by integrating the vertical velocity field. Path is overlaid upon vertical velocity from which it is derived (a), and associated backscatter coefficient (b)..... 90

Figure 4.3.1 Tracking a profile of scatterers using the velocity field at Trinity Bay 2001 mooring A, according to Heywood (1996). Measured backscatter intensity data (a) (the first column is used to initialize the model); measured vertical velocity data (b); simulation of the scatterer profile using Heywood's model (c); Heywood simulation modified by empirical scatterer-biomass conversion formula (4.10) (d)..... 93

Figure 4.3.2 The method used to obtain vertical velocity from flux of scatterers. The difference between the two profiles in the segment above z_1 gives the flux of scatterers through z_1 over the time Δt between steps n and $n+1$96

Figure 4.3.3 Using a flux-velocimetry model to generate a velocity field from backscatter intensity data at Trinity Bay 2001 mooring A. Measured backscatter coefficient (a); measured vertical velocity (b); vertical velocity simulated using the flux-velocimetry method (c); vertical velocity simulated using the flux-velocimetry method with bootstrap

correction (d)..... 97

Figure 4.3.4 Cross sections at bin #5 (depth 80 m) of velocities obtained using the flux-velocimetry method for Trinity Bay 2001 mooring A: measured velocity (a), velocity calculated using the flux-velocimetry method (b), and velocity calculated using the flux-velocimetry method with the bootstrap correction (c).....98

Figures 4.4.1 - 4.4.4 Six methods for quantifying migration of scattering layers. (a) Backscatter coefficient from ADCP measurement. (b) Vertical velocity data from ADCP measurement. (c) Region outlined by threshold values determined by identifying S_v values associated with high velocities. (d) Depth of maximum S_v value. (e) Biomass median depth. (f) Path of Lagrangian particle obtained from measured velocity. (g) Simulated backscatter intensity using modified Heywood algorithm. (h) Simulated vertical velocity using flux-velocimetry method with bootstrap-correction. The first four days of each deployment are shown, using Placentia Bay 1999 mooring A (Fig. 4.4.1), Trinity Bay 2001 mooring A (Fig. 4.4.2), Trinity Bay 2002 mooring A (Fig. 4.4.3), and the Funk Island Bank mooring (Fig 4.4.4)..... 99

Figure 4.4.1 Placentia Bay 1999 mooring A (see above caption)..... 100

Figure 4.4.2 Trinity Bay 2001 mooring A (see above caption).....101

Figure 4.4.3 Trinity Bay 2002 mooring A (see above caption).....102

Figure 4.4.4 Funk Island Bank (see above caption)..... 103

Figure 4.4.5 Trinity Bay 2001 mooring A, bin 5. Daily maximum upward velocities (a) from observed data (thick line) and from flux-velocimetry simulation with bootstrap correction (thin line). Timing of daily maximum upward velocities (b) from observed data (thick line) and from flux-velocimetry simulation with bootstrap correction (thin line)..... 106

Figure 4.4.6 Trinity Bay 2001, mooring A. Distribution of upward migration velocities for observed velocities and velocities simulated using flux-velocimetry with the bootstrap correction. Values represent averages of three maxima in the depth range 80 – 100 m..... 107

Figure 4.4.7 Trinity Bay 2001 mooring A: normalized root-mean-square difference between backscatter intensity measured and simulated using Heywood's (1996) algorithm. Means are taken each day, over all data points..... 107

Figure 4.4.8 Mean backscatter profiles, both measured and simulated using Heywood's method, over four days at Trinity Bay 2001, mooring A..... 108

Figure 5.1.1 Trinity Bay 2001 mooring A, migration timing identified by maximum and minimum S_v gradients, and averaged over bins 1-5. Histograms of migration timing using ordinary local time (top) and day-normalized time (bottom). Sunrise and sunset times vary by approximately 90 minutes over this time series..... 115

Figure 5.1.2 Trinity Bay 2001 mooring B. Daily averaged day-normalized series and corresponding standard deviations of ADCP data: backscatter intensity daily average (a) and corresponding standard deviation (b), vertical velocity daily average (c) and corresponding standard deviation (d). Averages cover year days 141-232..... 119

Figure 5.1.3 Trinity Bay 2001 mooring B. Daily averaged day-normalized series and corresponding standard deviations of quantifications of scattering layers: method of identifying S_v values associated with high velocities (a), biomass median depth with standard deviation (b), depth of maximum S_v value with standard deviation (c), and Lagrangian particle path with standard deviation (d). Averages cover year days 141-232..... 120

Figure 5.1.4 Trinity Bay 2001 mooring B. Daily averaged day-normalized series and corresponding standard deviations of simulated ADCP data: backscatter intensity daily average simulated using the adjusted Heywood method (a) and corresponding standard deviation (b), vertical velocity daily average simulated using the flux-velocimetry method with the bootstrap correction (c) and corresponding standard deviation (d). Averages cover year days 141-232..... 121

Figure 5.1.5 Seasonal trends for Placentia Bay 1999 (top) and Trinity Bay 2001 (bottom). Normalized differences are of biomass median depth, between daily averaged day-normalized series and individual day-normalized days. The graph shows an average of ± 5 days..... 122

Figure 5.1.6 Seasonal trends for Trinity Bay 2002. Normalized differences are of biomass median depth, between daily averaged day-normalized series and individual day-normalized days. The graph shows an average of ± 5 days..... 123

Figure 5.1.7 Daily averages of day-normalized biomass median depth for individual beams (solid lines) and average beam (dotted line) at Trinity Bay 2001 mooring A, compared with average beam (dashed line) at Trinity Bay 2001 mooring B..... 127

Figure 5.1.8 Correlation coefficient r plotted against distance separating moorings. Correlations are only included between moorings within the same deployment, spanning the same time period. Mooring A at Trinity Bay 2001 is shown for beam to beam correlation. Time series correlated are (a) daily averages of biomass median depth (Fig 5.1.7), and (b) seasonal comparisons to daily averages (Fig 5.1.6). (Note: In (b), Trinity Bay 2002 mooring D is excluded because r values were very low.)..... 129

Figure 5.2.1 Effect of cloud opacity (a) on sea surface light intensity (b) based on Budyko (1974) formulation. Cloud data are from the Bonavista AWOS, 2002. Light intensity is normalized to I_{max} : the maximum light intensity for a clear summer solstice at latitude 0 °N. A sample of solar radiation ($W m^{-2}$) measured on the roof of the Chemistry and Physics building in St. John's is given for comparison (c)..... 136

Figure 5.2.2 Trinity Bay 2001 mooring A. Results of edge-detection algorithm used to determine migration timing from backscatter data..... 137

Figure 5.2.3 Trinity Bay 2002 mooring C. Scattering layers (white) defined by identifying a range of backscatter intensity values with high vertical velocities (outside of 2 standard deviations; see § 4.2). Series is day-normalized, and separated into day and night portions. Line shows $-0.5\text{ }^{\circ}C$ isotherm..... 142

Figure 5.2.4 Data from a 10 day period at Trinity Bay 2002 mooring A. Top: biomass median depth with 6-hour intervals centred at noon and midnight highlighted. Bottom: day and night time series derived by averaging the biomass median depth over the 6-hour intervals shown above..... 143

Figure 5.2.5 Trinity Bay 2002 mooring A. Left column shows day time series, and right column shows night time series. Top: biomass median depth and isotherm depth ($0\text{ }^{\circ}C$ for day and $1\text{ }^{\circ}C$ for night). Middle: correlation between the two time series as a function of time scale q , the time scale at which the running average is taken. Bottom: coherence between the power spectra of biomass median depth and isotherm depth..... 144

Figure 5.2.6 Trinity Bay 2002 mooring C. Left column shows day time series, and right column shows night time series. Top: biomass median depth and isotherm depth ($0\text{ }^{\circ}C$ for day and $1\text{ }^{\circ}C$ for night). Middle: correlation between the two time series as a function of time scale q , the time scale at which the running average is taken. Bottom: coherence between the power spectra of biomass median depth and isotherm depth..... 145

Figure 5.2.7 Trinity Bay 2002 mooring D. Left column shows day time series, and right column shows night time series. Top: biomass median depth and isotherm depth ($0\text{ }^{\circ}C$ for day and $1\text{ }^{\circ}C$ for night). Middle: correlation between the two time series as a function of time scale q , the time scale at which the running average is taken. Bottom: coherence between the power spectra of biomass median depth and isotherm depth..... 146

Figure 5.2.8 Trinity Bay 2002 mooring E. Left column shows day time series, and right column shows night time series. Top: biomass median depth and isotherm depth ($0\text{ }^{\circ}C$ for day and $1\text{ }^{\circ}C$ for night). Middle: correlation between the two time series as a function of time scale q , the time scale at which the running average is taken. Bottom: coherence between the power spectra of biomass median depth and isotherm depth..... 147

Figure 5.2.9 Trinity Bay 2002 mooring F. Left column shows day time series, and right column shows night time series. Top: biomass median depth and isotherm depth (0 °C for day and 1 °C for night). Middle: correlation between the two time series as a function of time scale q , the time scale at which the running average is taken. Bottom: coherence between the power spectra of biomass median depth and isotherm depth..... 148

Figure 5.3.1 Data anomaly that appears to be reverse migration, Trinity Bay 2001 mooring A, year day 198-199. Backscatter coefficient (a) and vertical velocity data (b) from ADCP, showing downward migration immediately following upward migration at 20:00. Simulations of backscatter intensity using the adjusted Heywood method (c) and of vertical velocity using the flux-velocimetry method with the bootstrap correction (d)..... 151

Figure 5.3.2 Data anomaly that appears to be midnight sinking, Trinity Bay 2002 mooring D, year day 234-235. Backscatter coefficient (a) and vertical velocity data (b) from ADCP, showing moderate sinking of the strong scattering layer just after 20:00 NST. Calculation of the biomass median depth (c) shows a similar path..... 152

Figure 6.1.1 Trinity Bay 2002 mooring C. Temperature-depth signature of S_v values. Colour plot shows the average S_v value for each temperature-depth pair. Solid lines show the distribution of temperature values at each depth. Averages are taken over the entire deployment period. Top: day. Bottom: night..... 161

Figure 6.1.2 Trinity Bay 2002 mooring D. Temperature-depth signature of S_v values. Colour plot shows the average S_v value for each temperature-depth pair. Solid lines show the distribution of temperature values at each depth. Averages are taken over the entire deployment period. Top: day. Bottom: night..... 162

Figure 6.1.3 Trinity Bay 2002 mooring E. Temperature-depth signature of S_v values. Colour plot shows the average S_v value for each temperature-depth pair. Solid lines show the distribution of temperature values at each depth. Averages are taken over the entire deployment period. Top: day. Bottom: night..... 163

Figure 6.1.4 Trinity Bay 2002 mooring A. Top: measured backscatter. Bottom: simulated backscatter using empirical model..... 164

Figure 6.1.5 Trinity Bay 2002 mooring A. Measured (top) and modelled (bottom) backscatter at a depth of 55 m..... 165

Figure 6.1.6 Trinity Bay 2002 mooring A. Measured (top) and modelled (bottom) backscatter at a depth of 30 m..... 165

Figure 6.1.7 Trinity Bay 2002 mooring A. Daily average of measured backscatter (a),

modelled backscatter (b), and absolute value of difference (c)..... 166

Figure 6.1.8 Trinity Bay 2002 mooring A. Biomass median depth of measured backscatter (a) and simulated backscatter (b)..... 166

Figure A.1.1 Schematic of a copepod hovering by producing a continuous downward flow..... 186

CHAPTER 1: INTRODUCTION

Marine ecosystems are fundamental to the global environment upon which humans are so dependent. Recent dramatic shifts in the global climate (IPCC, 2001) may have large impacts on these ecosystems. Hence it is important to develop a better understanding of ecosystem responses to the changing physical environment.

Ecosystem changes can take place on a wide range of time scales and across many trophic levels. It is often difficult to determine whether observed variations are inherent stochastic fluctuations, or represent a more fundamental response by the ecosystem to external forcing. This problem can be addressed by identifying ecosystem processes that are highly persistent, and whose variability can be easily measured with respect to this persistence. Variability can then be analysed in the context of environmental forcing.

In this thesis, we will focus on the diel vertical migration (DVM) of zooplankton. DVM patterns are highly persistent throughout much of the year and can be measured with relative ease using bioacoustic methods. This persistence and ease of measurement facilitate in-depth analyses of relatively long time series and correlation with environmental factors that may influence DVM. Furthermore, examining the pattern of DVM may reveal behavioural responses to the environment that other indicators, such as biomass or abundance, do not.

Zooplankton play a key role in the marine environment, both as predators and as prey. For example, over a period of about three years, the introduction of the ctenophore *Mnemiopsis leidyi* to the Black Sea is estimated to have had a greater effect on biological

communities and fish stocks than all other anthropogenic influences (Lalli & Parsons, 1993). Zooplankton DVM also occurs on such a large scale as to make significant contributions to biogeochemical processes, such as transport of dissolved inorganic carbon and nitrogen to deep water (Madin *et al.*, 2001; Hays, 2003).

Examination of the DVM of zooplankton warrants an interdisciplinary approach. Though some oceanographic questions can be addressed using methods from just one branch of oceanography, interdisciplinary approaches have often proven to be valuable or necessary for many oceanic problems. For example, physical, chemical, and biological processes are all important in assessing the impact of pollutant dispersal. Determining the fate of CO₂ in the oceans represents another problem that requires an integrated interdisciplinary approach. Many other questions related to climate change and ecosystem function are best answered with interdisciplinary approaches. Herein, for zooplankton DVM, we explore the link between physical and biological processes.

1.1 Background

The term plankton, from the Greek 'planktos' for 'wandering', refers to oceanic life that is primarily passively advected by water currents in the horizontal. Zooplankton makes up the animal constituent of plankton, with representatives from a high number of taxa—*e.g.* crustaceans, fish larvae, jellyfish. Zooplankton sizes cover a wide range, with classification into size groups: nanoplankton (< 2 μm), ultra microplankton (2-20 μm), microplankton (20-200 μm), mesoplankton (200-2000 μm), and megaplankton (> 2000 μm), the largest of which are jellyfish and may be many metres in diameter. Copepods

are the most dominant constituent of zooplankton, making up at least 70% of zooplankton in nearly every sampled area of the ocean (Raymont, 1983), though it should be noted that sampling methods using nets favour crustaceans like copepods over other more fragile forms of zooplankton (Lalli & Parsons, 1993).

Not all zooplankton movement is passive. It is common in nearly all of the world's oceans and many lacustrine environments to observe zooplankton undergoing a diel vertical migration (Figs 1.1.1, 4.0.1). Migration is typically nocturnal; zooplankton are near the surface at night, and descend to deeper waters, where they spend the day. However, alternate migration behaviours have been observed. Some zooplankton exhibit 'reverse' migration, spending dark hours at depth and light hours near the surface, while others exhibit 'twilight' migration, which is similar to nocturnal migration but with midnight sinking (Lalli & Parsons, 1993). Rare cases of diel horizontal migration have also been observed in freshwater environments, though the perceived rarity may be related to sampling methods (Burks *et al.*, 2002). Zooplankton DVM has been evidenced for over one hundred years using net tows, and more recently using bioacoustic techniques.

Despite many decades of study, neither the evolutionary mechanisms behind DVM nor the environmental cues influencing it are well understood. There remains much debate regarding both topics (*cf.* Lampert, 1989). Two fundamental assumptions are (1) that there is some energetic cost to swimming hundreds of metres every day (see Chapter 2), and (2) that there is a cost associated with low food availability at depth. In addition, migration may also carry costs related to metabolism and reduced birth rate

caused by lower temperatures at depth (Lampert, 1989). There must then be a significant evolutionary advantage to adopting this behaviour.

Hypotheses on adaptive value of migration

Many evolutionary hypotheses have been developed to explain the mechanisms behind zooplankton vertical migration. Predator evasion is currently the most favoured hypothesis. That is, zooplankton can more easily avoid visually hunting predators in darker waters. They inhabit deeper waters during the day, but migrate to the surface at night to feed under the cloak of darkness. This hypothesis is the most straight forward of many, and there exists supporting experimental evidence in the field (Zaret & Suffern, 1976) and in the laboratory (Dodson, 1988; Neill, 1990). Gliwicz (1986) examined the copepod *Cyclops abyssorum* in lakes with and without predatory fish, and concluded that natural selection is directly involved in the development of migratory behaviour.

The appeal of the predator avoidance hypothesis lies not only in its simplicity. There are also a number of spin-off predictions, such as reverse migration among smaller species, stronger migration tendencies among more conspicuous zooplankton, and altered migration behaviour depending upon presence of planktivorous fish (*cf.* Hays, 2003). Robertis (2002) predicted a size dependence of timing based on predation risk. The predator avoidance hypothesis also feeds well into simple theoretical models of multiple trophic levels that can predict complex migration characteristics. Iwasa (1982) developed a two-layer two-species game theoretical model, deriving DVM as an equilibrium solution. Hugie & Dill (1994) constructed a more elaborate game theoretical model.

Gabriel and Thomas (1988) approached the problem as a game between competing zooplankton populations. Clark and Levy (1988) modelled the vertical migration of the planktivorous sockeye salmon, assessing a number of migration hypotheses.

It has also been suggested that vertical migration provides metabolic advantages. McLaren (1963, 1974) has historically been the strongest voice behind the metabolic theory, arguing that under certain conditions in near-equilibrium populations, cooler waters provide a demographic advantage to the copepod *Pseudocalanus minutus* during certain developmental stages. Enright (1977b) developed a more elaborate model in which metabolic advantages in cool waters were combined with a daily decrease in foraging ability due to depletion of phytoplankton. In the proposed model, herbivorous zooplankton deplete the supply of phytoplankton so much during night time feeding that the metabolic advantage in migrating to lower depths outweighs that of remaining in the surface to feed on a scarce food source. Phytoplankton is replenished during the day by photosynthesis. Enright and Honegger (1977) tested the issue of predation versus metabolic advantages by examining migration timing relative to sunrise and sunset.

There has been a shortage of evidence backing the hypotheses of metabolic advantage. Furthermore, models based on this hypothesis are often highly constrained by assumptions, such as: food density during the night double that of the day, food intake directly proportional to availability, and the ability of zooplankton to greatly reduce metabolic expenditures (Enright, 1977b). In fact, many studies show the opposite, that migrators are at a metabolic disadvantage (Stich & Lampert, 1981; Lampert *et al.*, 1988).

A few other hypotheses have been explored. Hairston (1976) proposed that high

radiation levels are detrimental to certain copepods, depending upon pigmentation. Vertical migration may be a means of redistributing populations via horizontal currents that are vertically stratified (*cf.* Hays, 2003). Bosch and Taylor (1973) found DVM patterns in *Podon polyphemoides* to align with horizontal currents in such a way as to prevent the migrators from being advected out of the bay. Descent of herbivorous zooplankton may also be a mechanism for sustaining an equilibrium of food supply production (Kerfoot, 1970; McAllister, 1969), or simply a consequence of having gained mass due to consumption (*cf.* Hutchison, 1967). The lack of consensus suggests that no single hypothesis on its own fully explains the adaptive significance of DVM.

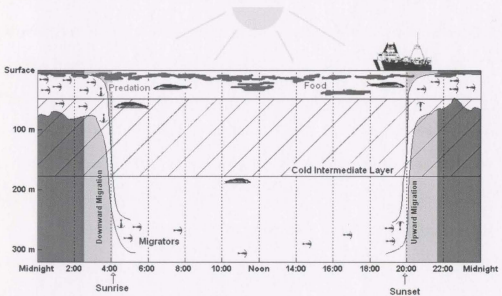


Figure 1.1.1 Schematic of normal nocturnal diel vertical migration. Migrators move upwards around dusk and then return to deep waters around dawn.

Environmental cues influencing migration

The extent to which zooplankton respond to different environmental cues is not well understood. In particular, it is not known how much of zooplankton behaviour is in response to the surrounding physical environment, and how much is in response to local concentrations of predators and prey. There may also be an endogenous rhythm cuing to the migration (Forward, 1988; Lorke *et al.*, 2004), and other internal factors, such as nutritional status or accumulated energy, may play a role (Sekino & Yamamura, 1999). Many different migration patterns are exhibited by different species of zooplankton, and even intra-species in different environmental settings. Most studies suggest that the migration behaviour is flexible and adaptable, depending upon the environmental characteristics (Ohman, 1990). The four primary cues considered to influence migrators in an immediate sense are: light level or changes in light level, food availability, temperature, and chemical cues from predators. Also under consideration are gravity (geotaxis) (Strickler, 1982), salinity (Lougee *et al.*, 2002), oxygen (LaRow, 1970), tides, hydrostatic pressure, and surface storms (*cf.* Hutchison, 1967; Mauchline, 1998). The relative importance of each cue is uncertain.

Light is believed to initiate and orient migration, although the manner by which light influences migration is unclear. The isolume hypothesis suggests that zooplankton migration is the result of an attempt to remain at a constant light level (Geller, 1986; Forward, 1988). This explains ordinary nocturnal migration, but not reverse or twilight migration. An alternate hypothesis is that changes in light intensity drive migration, in which case many migration patterns are possible. Clarke (1930, 1932) found in lab

experiments on *Daphnia* a strong phototropic response to changes in light intensity. He also found periodic changes in phototropic sign, suggesting an ability to adapt migration patterns despite consistent light cycles. Other studies have examined the effects of different wavelengths, polarization, extinction with depth, and other variables that zooplankton may detect (*cf.* Forward, 1988; Gal *et al.*, 1999).

Temperature is often regarded as playing a constraining role in migration. While light drives the daily repeating pattern, temperature stratification can determine the upper and lower bounds for migrators (Geller, 1986). Temperature may also be a seasonal cue that instigates migration for zooplankton that overwinter at depth (Mauchline, 1998).

Some zooplankton have been observed to respond to chemical stimuli emitted by predators. Dodson (1988) found a vertical response by *Daphnia* to three different predators in laboratory experiments, both by the introduction of predators, and by the introduction of water that had been exposed to predators, suggesting the ability to sense an emitted chemical cue. Tjossem (1990) observed greater migration intensity in *Chaoborus* larvae in water conditioned by planktivorous fish. Neill (1990) induced vertical migration in non-migrating *Diaptomus kenai* both with the introduction of predators, and with the introduction of water that had been exposed to predators.

Studies on the response to food availability are in conflict. Some specimens have been observed to increase migration amplitude with the increase of food availability (*cf.* Mauchline, 1998). Fiske and Giske (1995) demonstrated reduced migration behaviour in high food density. Sometimes no clear relationship is seen.

Recent models have been developed incorporating multiple cues. Han &

Straškraba (1988, 2001) combine the effects of light, temperature, predation, and food availability to derive a realized predation pressure to which zooplankton respond. Liu *et al.* (2003) model optimal food intake versus predation risk at different life stages. Fiske & Giske (1995) model individual maximization of reproductive value, combining physiological states with various environmental influences such as temperature, predation, and food.

Context within larger trophic scheme

The study area for observation of zooplankton DVM for this thesis lies around Newfoundland. The study was initiated as part of a Natural Sciences and Engineering Research Council of Canada strategic project: The importance of capelin (*Mallotus villosus*) biology in sustaining trophic interactions in the Northwest Atlantic. The primary goal of the strategic project is to assess predator-prey relationships in the marine environment on the Funk Island Bank, off the north-east coast of Newfoundland (Fig 1.1.2). The approach to this study involves a set of coordinated studies spanning various spatial and temporal scales and covering multiple trophic levels. Both the avian predators and zooplankton prey of capelin are of great interest. The vertical distribution and vertical movements of zooplankton and capelin are fundamental to this study.

The DVM of zooplankton may influence higher trophic levels in very direct ways. Carnivorous zooplankton that hunt based on tactile stimuli can forage in light or darkness, and can easily follow the migration pattern of zooplankton prey. Many fish hunt zooplankton visually, and their feeding patterns depend greatly upon the vertical

distribution of their prey (*cf.* Clark & Levy, 1988). Such fish can imitate the DVM pattern of their zooplankton prey both as a means of hunting and as a means of avoiding their predators that also hunt by sight, such as larger fish and sea birds. Nelson *et al.* (1997) observed dawn and dusk migrations by a megamouth shark (*Megachasma pelagios*) corresponding to a typical nocturnal diel pattern that suggests the relevance of migration of zooplankton upon which the megamouth preys. The vertical distribution of zooplankton predators in the water column also affects seabird diets, which are often used as an indicator of species abundance and distribution in marine ecosystems (Montevecchi & Myers, 1996).

In this study area, adult capelin were observed to undergo nocturnal DVM. This may be related to the DVM pattern of their copepod prey. Furthermore, gannets preying on capelin have been observed to have a distribution of feeding times with peaks during dawn and dusk twilight hours (Garthe *et al.*, 2003). This suggests the possibility that the capelin prey are below diving range of the gannets during the day, and that the gannets can best hunt during twilight migration times, when capelin inhabit shallower water and while there is still enough light to detect them. Changes in the character of zooplankton DVM may therefore have implications at higher trophic levels.

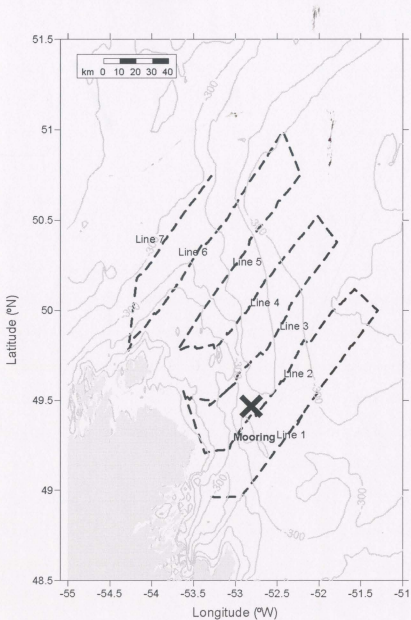


Figure 1.1.2 Survey route and mooring location for the capelin ecosystem study, *Wilfred Templeman* trip # 553, August 2004.

Bioacoustics

Towing nets remains a standard method to observe zooplankton *in situ*; however, such a time and labour intensive technique restricts the practical spatial and temporal resolutions of measurement. Nets also enter and influence zooplankton communities in the water column during sampling. Consequently, many studies involving cues for migration have been performed in the laboratory (Clarke, 1930, 1932; Dodson, 1988; Lougee *et al.*, 2002; Marcus, 1988; Neill, 1990). In recent decades acoustic techniques have become available with the advent of scientific acoustic echo sounders (*cf.* MacLennan & Holliday, 1996). Many acoustic systems, including scientific echo sounders (*e.g.* the BioSonics DTX, and simrad EK500) and other sensor systems such as the acoustic Doppler current profiler (ADCP), are now in common use in the ocean. The acoustic instrumentation offers much higher temporal resolution, as well as information on the entire water column, without disturbing zooplankton communities (Brierley *et al.*, 1998). ADCPs are primarily intended to measure water velocities, and can be moored and left for months at a time, recording data continuously.

Acoustic signals are scattered off objects in the water column, and the resulting backscatter is dictated by the physical properties of the scatterer, such as size, orientation, and morphology. Common scatterers include organisms, detritus, bubbles, turbulent features, and the sea floor and surface. Measured target strength, TS , in units of decibels (dB), is logarithmically related to the backscattering cross-section, σ_{bs} , by

$$TS = 10 \log \sigma_{bs} \quad (\text{Stanton } et al., 1996). \quad (1.1)$$

Other calibrations of the transducers are often necessary depending on the specifics of the

intended measurements (Flagg & Smith, 1989). DVM studies using bioacoustics have become quite common (Plueddemann & Pinkel, 1989; Flagg *et al.*, 1994; Heywood, 1996; Ashjian *et al.*, 1998; Rippeth & Simpson, 1998; Tarling *et al.*, 1998; Thomson & Allen, 2000; Lorke *et al.*, 2004; Sindlinger *et al.*, 2005).

1.2 Goals of the study

There are two main facets to the application of acoustic data to zooplankton studies. The first is an ongoing effort to correlate backscatter with the quantifications of zooplankton abundance, taxonomy, and size in a precise way. This can be approached as either the “forward problem” of mathematically modelling scattering based on assumptions about the properties of the animal (Stanton & Chu, 2000), or the “inverse problem” of determining the properties of the animal based on measured backscatter (Holliday & Pieper, 1995). These problems can be very difficult in complex multi-species zooplankton communities. They often require directed tow studies, high temporal resolution acoustic data, and sometimes multiple frequencies, as well as pre-calibration of the instrument (Brierley *et al.*, 1998). There are not enough tow data from the regions involved in this study to make a substantial contribution toward this goal, and no calibration was performed.

The second facet is the common use of backscatter to provide qualitative information on zooplankton behaviour—in particular diel migration and spatial distribution. Use of ADCPs for bioacoustic data in surveys and moorings has become quite common, and calibration data is often not available for conversion to zooplankton

abundance, taxonomy, and size. This need not limit assessments of these data to the qualitative type however. Because of the ease and regularity of collecting such data, it is valuable to develop quantitative techniques for their analysis.

Herein we provide a close examination of the migration characteristics of zooplankton on the Northeast Newfoundland Shelf. Using the data collected, we quantify the day to day variation and attempt to determine the influence of environmental factors on the observed DVM. The specific goals of this thesis are as follows:

1. Development, examination, and assessment of various methods for quantification of DVM of scattering layers in bioacoustic data;
2. Application of quantification techniques to determine the response of migrating layers to environmental cues in the data;
3. Development of an empirical model of this response that can model the variation in migration patterns caused by changes in the physical characteristics of the water column.

The outcome is that bioacoustic data can be used to address certain questions regarding DVM in a quantitative manner in the absence of calibration.

A brief discussion of the energetic costs of zooplankton migration is presented in Chapter 2, before examining the data. In addition to the capelin ecosystem project, past studies around Newfoundland provide a wealth of ADCP data that reveal DVM in the acoustic signals. There are also relevant temperature data from these studies, and climatological data from land-based weather stations that allow for examination of the influence of physical cues. Chapter 3 describes the collection and processing of data used

for this thesis.

Chapter 4 catalogues the methods found in the literature for quantifying acoustic backscatter data in a manner applicable to the DVM of zooplankton. Relevant new methods developed for this thesis are included, as well as inter-comparison of the methods.

Analyses of the data using these quantification methods are presented in Chapter 5. Primary questions of interest are those regarding migrator response to changes in light level, migrator response to changes in the vertical temperature profile, and horizontal homogeneity of zooplankton distribution. Anomalous behaviours are also identified.

Finally, the responses of migrators to environmental cues are modelled in an empirical manner for use in the ecosystem context of the capelin ecosystem study and other similar ecosystem-scale projects. This model is presented in the final chapter, followed by a brief summarizing discussion.

CHAPTER 2: ENERGETIC CONSIDERATIONS

A question at the core of the migration problem is that of energetic cost. In order to understand the evolutionary motives and physical cues driving migration, it is valuable to first understand how much energy is expended relative to basal metabolic expenditures. This is a very broad topic due to the large range in size, morphology, swimming behaviour, metabolism, forage and escape tactics, and many other characteristics of zooplankton biology.

The calculation of energy consumption of zooplankton can be estimated to first order as the sum two parts: swimming expenditure and metabolic expenditure. A discussion of zooplankton swimming requires many considerations, such as the mode of propulsion, Reynolds number in the generated flow, foraging and escape tactics, mechanical efficiency of the body, active versus passive descent, and bottom behaviour. There are also many parameters influencing the metabolic rate, such as temperature, depth, and increased respiration with swimming. Because of the complexity surrounding such a calculation, studies typically focus on one aspect of the problem for one type of organism. The discussion herein address the various approaches at an introductory level, and presents some initial estimates of the energetic cost of migration, illustrating how a range of differing estimates is possible.

For animals smaller than 10 mm, there is no reliable method for empirical estimates of energetic expenditure (Morris *et al.*, 1985), so estimates rely on theoretical hydrodynamic arguments and high speed video (Vlymen, 1970; Klyashtorin &

Yarzhombek, 1973; Enright, 1977a; Lehman, 1977; Strickler, 1977; Svetlichnyi *et al.*, 1977; Vlymen, 1977; Morris *et al.*, 1985). The consequence of the difficulty in measuring energetic expenditure is a wide range of estimates for migration costs. Vlymen (1970) calculated an energetic cost of migration to be 0.03% of the basal metabolic energy expenditure, while other studies have calculated swimming costs to be many times that of basal metabolism (Morris *et al.*, 1985). For measurements on larger animals, active metabolism is observed to be many times that of resting metabolism (Torres & Childress, 1983).

2.1 Swimming expenditure

Most theoretical studies focus on copepods, the most numerous zooplankton in the ocean. Within this subclass, there are many different propulsion techniques that lead to greatly differing estimates of energetic costs. Calanoid copepods propel themselves primarily via continuous movements of their mouthparts. Cycloid copepods swim in jerky movements, known as “hop and sink” swimming, which can range in frequency from 1 Hz on average to 120 Hz during escape (Strickler, 1975). Morris *et al.* (1985) note large differences in estimates of energetic costs between models that assume continuous swimming and models that assume hop and sink swimming. This discussion therefore considers both cases.

Continuous swimming

The simplest estimates of swimming energy assume a spherically shaped animal

with continuous propulsion. For an upward swimming zooplankter, the force required for steady ascent in simplified form is

$$F_{up} = F_D + F_g' , \quad (2.1)$$

where F_D is the drag force and F_g' is the buoyancy force on the organism relative to sea water. For a spherical shape, drag can be expressed as a function of velocity, w , using Stokes' law,

$$F_D = 6\pi\mu a w , \quad (2.2)$$

where μ is the dynamic viscosity of sea water ($1.4 \times 10^{-3} \text{ kg m}^{-1} \text{ s}^{-1}$ under typical conditions) and a is the radius. Stokes' law holds for a low Reynolds number; this is discussed later in greater detail. The buoyancy force is

$$F_g' = \Delta\rho \frac{4}{3}\pi a^3 g , \quad (2.3)$$

where $\Delta\rho$ is the density difference relative to sea water, and g is the gravitational constant (9.81 m s^{-2}), so that the net force required to swim upwards is

$$F_{up} = 6\pi\mu a w + \Delta\rho \frac{4}{3}\pi a^3 g , \quad (2.4)$$

and the total work in ascending a distance d is

$$W_{up} = F_{up} \cdot d . \quad (2.5)$$

For some example representative values ($a = 0.001 \text{ m}$, $w = 0.02 \text{ m s}^{-1}$, $\Delta\rho = 30 \text{ kg m}^{-3}$), $F \approx 1.8 \times 10^{-6} \text{ N}$. Over a distance of 100 m, the work done would be $1.8 \times 10^{-4} \text{ J}$.

An elaborated version of this approach is given by Jiang *et al.* (2002), where copepod propulsion is considered to be generated by moving a cephalic appendage. The associated force is expressed as a point force exerted outside the spherical body. Solving

the Stokes equation (Kundu & Cohen, 2002) for the flow generated gives a force approximately 2.3 times as large as the force determined here for an upward swimming copepod.

Downward migration may be accomplished through active swimming, passive sinking, or a combination of the two. A passively sinking zooplankter reaches terminal velocity, w_t , at $F_D = F_g'$, when the drag force balances the buoyancy force, so that

$$w_t = \frac{2}{9} \Delta \rho a^2 g \mu^{-1} . \quad (2.6)$$

For the example values suggested above, $w_t \approx 0.05 \text{ m s}^{-1}$, which corresponds to the highest downward velocities found in the data used in this project (see § 3.4). This implies that the swimming expenditure during descent is zero. However, for migrators descending at rates higher than w_t , the work required is

$$W_{down} = F_{down} \cdot d = (F_D - F_g') d . \quad (2.7)$$

Size may therefore play a large role in the energetic cost of descent. A zooplankter of length 10 times smaller ($a = 0.1 \text{ mm}$) would sink passively at a rate 100 times smaller ($w_t = 5 \times 10^{-4} \text{ m s}^{-1}$), and active swimming would be necessary for descent. Buskey *et al.* (1993) observed the copepod *Oithona plumifera* in its first naupliar stage to sink at speeds less than 0.1 mm s^{-1} .

A significant difference between measured ascent and descent velocities will be seen (§ 4.1). Descent velocities are consistently larger in magnitude, and this is likely related to the negative buoyancy of the zooplankton. Suppose, for example, that a zooplankter exerts the same force whether swimming up or down. That is

$$F_{down} = F_{up} \quad (2.8)$$

$$\Rightarrow F_{Dd} - F_g' = F_{Du} + F_g' \quad (2.9)$$

where F_{Dd} and F_{Du} are the magnitudes of the drag forces for downward and upward swimming, respectively. Using equations (2.2) and (2.3), the difference between the downward velocity magnitude, w_d , and the upward velocity magnitude, w_u , can be written

$$\Delta w = w_d - w_u = \frac{2F_g'}{6\pi\mu a} \quad (2.10)$$

Substituting the representative values chosen above gives $\Delta w = 0.1 \text{ m s}^{-1}$. This is a fairly large estimate due to the simplifying assumptions.

This type of argument can be valuable in interpreting measured migration velocities given detailed information on the size, morphology, and swimming behaviour of a particular specimen. Mauchline (1998) has catalogued this information for calanoid copepods, and these values are used here. Consider *Calanus finmarchicus*—one of the most abundant copepods in the Northwest Atlantic (Planque, 1996). A specimen with prosome length $PL = 0.001 \text{ m}$ has volume $V = 6.34 \times 10^{-11} \text{ m}^3$. The animal's density is approximately $1,045 \text{ kg m}^{-3}$, so take $\Delta\rho = 20 \text{ kg m}^{-3}$. Expressing (2.10) as

$$\Delta w = \frac{2\Delta\rho V g}{6\pi\mu(PL)} \quad (2.11)$$

gives $\Delta w \approx 0.001 \text{ m s}^{-1}$. This estimate is in accordance with measured values (see § 4.1).

Between migrations, zooplankton remain at a near constant depth, either near the surface or in deep water. They must continue swimming for the purposes of foraging, escaping predators, and to keep from sinking. The energetic cost of swimming behaviour at a constant depth can be expressed as a sum of energy spent in foraging and escaping, and energy spent against buoyancy:

$$W_c = W_f + W_b \quad (2.12)$$

The first term can be estimated from the mean foraging velocity, u_f , which has been measured for different types of zooplankton in laboratory studies (Bundy *et al.*, 1993). Foraging is not considered to take place at depth, so this term only considers time spent at the surface, t_f . The total distance covered while foraging is then $d_f = u_f \cdot t_f$, and the work spent foraging is

$$W_f = F_d \cdot d_f = 6 \pi \mu a u_f^2 t_f \quad (2.13)$$

This formula represents a broad generalization of foraging and escaping expenditure. For example, *Neocalanus cristatus* uses a stationary suspension-feeding tactic, generating a current to entrain food; *Euchaeta elongata* cruises for food; *Calanus pacificus* uses a hop-and-sink tactic (Greene, 1988). Escape tactics typically require very high accelerations over very short periods of time, and require very high energy expenditures (Morris *et al.*, 1985), so W_f may be underestimated in the above formula. Swimming patterns also influence detectability by predators (Buskey *et al.*, 1993).

The work expended against buoyancy is calculated assuming that a constant flow must be generated to keep from sinking:

$$W_b = \left[\frac{(2 F_g')^{3/2}}{(2 \rho \pi a^2)^{1/2}} \right] t_T \quad (2.14)$$

where t_T is the total time spent hovering, including both time at the surface and time at depth (see Appendix A.1 for derivation). This term is appropriate for stationary suspension feeders. For example, *Temora longicornis* produces a continuous feeding flow by moving the mouthparts, just balancing the downward buoyancy force (Tiselius &

Jonsson, 1990). The term is not appropriate for zooplankton that use the hop-and-sink tactic. The latter case is dealt with separately.

Daylight hours are spent resting in the deep, dark water, with no foraging or predator evasion. The total work for a day of swimming and migrating for a spherical copepod in this scenario is then the sum,

$$W_T = W_{up} + W_f + W_b + W_{down} \quad (2.15)$$

If sinking is passive, then $W_{down} = 0$.

For the values chosen above, migration takes approximately 80 minutes each way. Suppose the remainder of the day is divided evenly between time at the surface and time at depth—10 hours and 40 minutes each, so that $t_f = 10$ hr 40 min, and $t_r = 2t_f$ —and suppose a mean foraging velocity of $u_f = 0.01$ m s⁻¹ (Bundy *et al.* 1993). The total energetic swimming requirement for one day is then $W_T \approx 0.18 \times 10^{-3}$ J + 0.10×10^{-3} J + 3.75×10^{-3} J + 0 J = 4.03×10^{-3} J. Note that the work spent against buoyancy is an order of magnitude higher than the values for the other terms because this effort is ongoing throughout nearly the entirety of the day.

For a hypothetical zooplankton that does not adopt a migration strategy, remaining instead at the surface all day, the first and last terms are both zero, and t_r and t_f both become 24 h. The total work is $W_T \approx 0.23 \times 10^{-3}$ J + 4.22×10^{-3} J = 4.45×10^{-3} J. Under these assumptions, the energetic requirements of remaining at the surface all day are actually greater than those of adopting a migrating strategy, though the difference is an order of magnitude smaller than the total energetic requirements. The increase in energetic cost for a non-migrator is due to the additional amount of energy required for

foraging and escaping at the surface. These additional costs are not present during migration or during time spent at depth.

For these estimates, we assume 100 % mechanical efficiency in the mode of propulsion. In reality, there will be some inefficiency, and so the actual energetic requirement of the animal is higher, and can be expressed as

$$E_{swim} = \frac{1}{\eta} W_T, \quad (2.16)$$

where η is the mechanical efficiency as a fraction of 1. Klyashtorin & Yarzombek (1973) estimate η in active swimming to be about 0.05 for planktonic crustaceans. This is based on upper limits of efficiency in cellular synthesis of ATP, cell to muscle transmission, and paddle propulsion. The energetic burden on zooplankton is then larger by a factor of 20 than the estimates calculated above. The energetic difference between migration and non-migration strategies, however, remains an order of magnitude smaller than the total energetic cost.

Torres (1984) calculated efficiency in *Euphausia pacifica* as a ratio of theoretical drag to measured metabolic swimming requirements, and found a large dependence upon swimming speed. A better representation of the energetic requirement for migration must therefore include a velocity-dependent efficiency:

$$E_{swim} = \frac{1}{\eta(w)} W(w). \quad (2.17)$$

Since velocity varies significantly with time, particularly during surface foraging, the total energetic requirement becomes a complicated integral taken over time. One would also expect a dependence of efficiency upon propulsion technique.

Hop and sink swimming

The energetic expenditure for a zooplankter that swims by discontinuous jumps is different from one that swims by generating a continuous current. The simplest scenario is to assume that swimming is divided into two behaviours: jumping upward at a constant velocity w_j , and sinking downward at the terminal velocity w_t . Acceleration and deceleration times are considered small enough to neglect (see Appendix A.2).

For hovering, a zooplankter is considered to repeatedly hop and sink the same distance, so that the net displacement is zero. If each jump covers a distance z_j , then the time spent jumping is $t_j = z_j/w_j$, and the time spent sinking is $t_s = z_j/|w_t|$. The total number of jumps required to hover by hopping and sinking for an elapsed time of t_T is $N = t_T/(t_j+t_s)$. The total work required is

$$W_T = F_{up} \cdot N \cdot z_j = F_{up} \left[\frac{w_j |w_t|}{w_j + |w_t|} \right] t_T \quad (2.18)$$

This calculation assumes a mean velocity of $\bar{w}=0$. That is, over the course of a time period t_T , the total distance covered hopping is equal to the total distance covered sinking. If the mean velocity is not equal to zero, such as during migration, then

$$W_T = F_{up} \left[\frac{w_j (\bar{w} + |w_t|)}{w_j + |w_t|} \right] t_T \quad (\text{see Appendix A.3}). \quad (2.19)$$

However, under these assumptions, for both migrators and non-migrators, the net displacement over the course of one day is zero, implying a mean velocity of zero. The energetic cost is therefore equal in the two cases, with the implicit assumption that all downward movement is passive. Assuming a hopping velocity of $w_j = 0.03 \text{ m s}^{-1}$, and

other parameter values as before, $W_T = 1.8 \times 10^{-6} \text{ N} \cdot 1.62 \times 10^3 \text{ m} = 2.9 \times 10^{-3} \text{ J}$. At 100% efficiency, this value is of the same order of magnitude as the value calculated assuming continuous swimming, though the energetic cost of adopting a migrating strategy is zero.

In reality, the swimming path of a copepod may be a combination of large scale hops ($z > 10 \text{ mm}$) and fine scale movements ($z < 10 \text{ mm}$), and is a complicated 3-dimensional path (Bundy *et al.*, 1993). Furthermore, energetic costs increase with consideration of factors involved in the mode of propulsion, such as energy losses during recovery strokes (Morris *et al.*, 1985).

Drag coefficient and Reynolds number

Thus far, drag force, F_D , has been assumed to be linearly proportional to the velocity, w (2.2). Validity of this assumption depends upon the value of the Reynolds number, a dimensionless parameter defined by

$$\text{Re} = \frac{Ul}{\nu} \quad , \quad (2.20)$$

where U is a characteristic velocity, l is a characteristic length scale, and ν is the kinematic viscosity of the fluid. The Reynolds number expresses a ratio of inertial forces to viscous forces, and (2.2) only holds for $\text{Re} \ll 1$ (Kundu & Cohen, 2002). For a 1 mm zooplankter, this means that swimming velocity must be smaller than 1 mm s^{-1} .

Measured swimming velocities indicate that the Reynolds number may be larger, and for a typical swimming copepod, $\text{Re} \sim 1$ (Jiang *et al.*, 2002). For $\text{Re} \gg 1$, drag is due to turbulent wake, and is proportional to the square of the swimming velocity,

$$F_D \propto \rho w^2 A \quad , \quad (2.21)$$

where ρ is the fluid density, and A is the cross-sectional area (Kundu & Cohen, 2002).

The effect of drag in a more realistic scenario, where Reynolds number may vary and where the zooplankter is not assumed to be spherical, can be gauged by the dimensionless drag coefficient,

$$C_D \equiv \frac{F_D}{\rho U^2 A/2} \quad (\text{Kundu \& Cohen, 2002}). \quad (2.22)$$

The drag coefficient is a function of the Reynolds number, and for $Re \ll 1$ is proportional to $1/Re$. It is extremely difficult to determine the drag coefficient theoretically at $Re \gg 1$ for realistic object shapes. The value is typically determined empirically. However, on the millimetre scale, there is no effective experimental method to accomplish this (Vlymen, 1970).

Zooplankton swimming varies in many respects, between migration, foraging, and escaping. Even considering foraging alone, swimming behaviour depends upon the abundance of food (Bundy *et al.*, 1993). This variability makes the effects of drag, and consequently the energetic requirements, difficult to determine when simplifying assumptions are not made. Consequently, innovative laboratory experiments are devised to measure energetic requirements for swimming. For example, Alcaraz and Strickler (1988) attached a copepod to a spring and calculated work using the spring constant and elongation. Gill (1987) recorded frequency of appendage movements using an impedance pneumograph for different species of calanoid copepods.

2.2 Metabolic costs

Comparing energetic costs of swimming to basal metabolism disregards the general effects of swimming on metabolism, such as the increased respiratory rate. Furthermore, other environmental factors such as temperature and pressure can also influence metabolic rates, so that energetic costs and benefits of migrating are not simply a function of the work required to migrate.

For larger zooplankton, the relationship between swimming velocity and metabolic requirements can be measured using a respirometer and an oxy-calorific conversion (Torres & Childress, 1983). Torres (1984) calculated the total metabolic power required for euphausiids swimming at different speeds. Based on the assumption that total metabolic power is a function of swimming speed alone, a comparison can be made of the energetic cost between migrating and non-migrating strategies.

The following argument is based on the assumption that a normal migrator can forage at a rate such that the daily energy expenditure balances the daily energy consumed during foraging. Suppose the day is divided into three intervals for a migrator: time spent at the surface, time spent at depth, and time spent migrating, of respective lengths t_S , t_D , t_M (with $t_S + t_D + t_M = 1$ day). Each time interval is characterized by a different swimming velocity, so that the metabolic power requirements are P_S , P_D , P_M , respectively (downward migration is ignored for simplicity). The total energetic requirement for a single day is

$$E_T = P_S t_S + P_D t_D + P_M t_M \quad (2.23)$$

The migrator must be able to consume this amount of energy in the time spent at the surface. A foraging rate can then be expressed

$$\Phi = \frac{1}{t_S} [P_S t_S + P_D t_D + P_M t_M] , \quad (2.24)$$

where Φ is the effective amount of energy consumed per unit time. For this migrator, the amount of energy consumed equals the amount expended over one day.

Suppose a similar animal adopts the non-migrating strategy, remaining at the surface for the entire day. The energy required to remain at the surface all day is

$$E_S = P_S (t_S + t_D + t_M) , \quad (2.25)$$

and the energy consumed through an entire day of foraging is

$$E_\phi = \Phi \cdot (1 \text{ day}) = \left(\frac{t_S + t_D + t_M}{t_S} \right) [P_S t_S + P_D t_D + P_M t_M] . \quad (2.26)$$

The net energetic gain by the non-migrator, or equivalently the energetic cost E_C sustained by adopting a migrating strategy, is

$$E_C = E_F - E_S = \left(\frac{t_S + t_D + t_M}{t_S} \right) [P_D t_D + P_M t_M] , \quad (2.27)$$

or

$$E_C = \left(\frac{1}{1 - t_D - t_M} \right) [P_D t_D + P_M t_M] , \quad (2.28)$$

if time is expressed in days.

This cost can be evaluated using values from Torres (1984), who gives metabolic power requirements for swimming at speeds of 1 – 20 cm/s for *E. pacifica*. At depth, take the minimum value, $P_D = 1.681 \times 10^{-5} \text{ J s}^{-1}$ (at 8 °C). Suppose migrators travel at a velocity of 5 cm s⁻¹: $P_M = 8.404 \times 10^{-5} \text{ J s}^{-1}$. Suppose migration lasts 1 hr, and time spent at depth is 12 hr. The net cost of migrating is then $E_C \approx 2.24 \text{ J}$. In comparison, the energy

spent just for migration is 0.30 J. Swimming all day at 2 cm/s would require $3.362 \times 10^{-5} \text{ J s}^{-1} \times 86,400 \text{ s} = 2.90 \text{ J}$. For *E. pacifica*, the net daily energetic cost of adopting a migrating strategy is then of the same order of magnitude as the daily energetic expenditure, while the energy spent migrating is an order of magnitude smaller.

Respiration is also a function of temperature and body size (Small & Hebard, 1967). Hirche (1987) found respiration rates in various calanoid copepods to obey the Arrhenius equation,

$$V = V_0 e^{-\mu/RT}, \quad (2.29)$$

where V is the respiration rate, T is temperature ($^{\circ}\text{K}$), V_0 and μ are empirically determined coefficients, and R is the gas constant ($1.987 \text{ kcal mol}^{-1}$). Migration energetic calculations must therefore consider the temperature stratification of the water column. Temperature profiles through which zooplankton migrate have a great deal of seasonal and regional variation, so that quantifying the effect on the metabolism of migrators is complex. As a generalization, deep waters are cooler than surface waters, so that migrating to depth may have a metabolic benefit.

2.3 Summary

The simplest estimates of energetic expenditures for migration of a 1 mm zooplankter are on the order of 10^{-4} J , with daily swimming expenditures on the order of 10^{-3} J . If mechanical efficiency is taken into account, these values increase, but the expenditure for migration is still an order of magnitude smaller than that for daily swimming activity. This result is due to the fact that zooplankton are expending energy

between migration events in foraging activity, predator evasion, and countering the buoyancy force. For continuous swimmers, a migration strategy may actually save energy under the assumption that predator evasion and foraging do not take place at depth during the day. For a zooplankter that is larger by a factor of ten ($a \sim 0.01$ m), the energetic values increase by a factor of 1000, but the migration expenditure (0.1 J) is still an order of magnitude smaller than the daily expenditure (1 J).

When metabolic effects are taken into account using measurements on larger zooplankton ($a \sim 0.01$ m), the energetic cost of migration appears to be larger, on the order of 1 J—the same order of magnitude as daily expenditures. This is a consequence not only of swimming expenditures, but also of the assumption that zooplankton remaining at the surface can forage continuously—an assumption that is not necessarily valid (Marcus, 1988). However, the energy required for the act of migration itself in this scenario is still an order of magnitude smaller, on the order of 0.1 J.

These preliminary calculations neglect a number of other considerations that may influence migration energetics. Swimming, feeding tactics, and metabolism depend not only on the animal, but also on the developmental stage; it is possible that the energetic cost of migration varies substantially throughout the life of a migrator. Foraging tactics and velocities depend on the availability of food (Bundy *et al.*, 1993); energetic cost may therefore depend on the horizontal patchiness of the food source. The energetic cost of ingestion also depends upon the composition of the food source (Hein *et al.*, 1993).

CHAPTER 3: DATA

The focus in this thesis is on the physical cues that influence migration. This involves an examination of the physical properties of the water column—in particular, light, temperature, and the presence and velocity of detectable acoustic scatterers. Relevant data are discussed in the following sections, including methods of collection as well as the quirk of having data from a range of different sources, originally collected for different purposes. The primary data analysed here include cloud opacity and wind velocity and direction from a weather station in Bonavista; temperature data from moored thermistors and moored ADCPs; velocity and backscatter data from moored ADCPs; and dry sample weights from bongo net tows.

The data are initially unfiltered. To facilitate analysis, data are presented using the local time scale, Newfoundland Standard Time (NST), *with no daylight savings*. This is because DVM behaviour is coordinated with the solar cycle. Year days are measured beginning at 0 for January 1st.

3.1 Mooring information

Most of the data for this study were originally collected as part of four separate projects. They are divided here accordingly into four data sets corresponding to the four time periods over which they were collected (Table 3.1.1). These four data sets cover three regions in coastal Newfoundland (Figs 3.1.1, 3.1.2). The first data set runs from April-June 1999 in Placentia Bay, with two moored ADCPs. The second runs from May-

August 2001 in Trinity Bay, with three moored ADCPs. The third runs from May-August 2002 in Trinity Bay, with six moored ADCPs. The fourth data set covers two weeks in August 2004 on the Funk Island Bank, with one mooring containing two ADCPs (Fig 3.1.2). In all data sets but the first, moorings also included thermistors spaced at intervals. More details on thermistors and ADCPs are given in § 3.3 and 3.4 respectively.

The bottom depths were verified from the surface using echo-sounding and confirmed from the chart location (Table 3.1.1). Equipment remained below the surface during the deployment period and was recovered using an acoustic release system.

Each of these four deployments was designed with a different purpose in mind. The data from Placentia Bay were used to analyse the circulation around the bay (Schillinger *et al.*, 2000). The 2001 Trinity Bay deployment was intended to quantify local physical features of the bay (Tittensor *et al.*, 2002a). The 2002 Trinity Bay deployment collected data for analysing overall circulation and hydrography (Tittensor *et al.*, 2002b). The Funk Island Bank deployment was designed as part of the capelin ecosystem project, with one purpose being observation of the diel vertical migration of zooplankton in the water column.

The inconsistency between data sets in duration, sample interval, and ADCP depth is a consequence of these differing purposes. Only in retrospect were the first three data sets seen to contain valuable data regarding the vertical migration of zooplankton. They are interesting because the long time series allow for more rigorous statistical analyses, particularly of the seasonal phenomena. In contrast, the Funk Island Bank 2004 data set utilized a smaller ensemble time to better resolve the migration phenomena, but was

limited in duration to two weeks. The 2004 data set was also designed to cover more of the water column by using two ADCPs, but the downward-looking ADCP malfunctioned and did not collect any data.

Climate data such as wind velocity and cloud opacity were not measured at the mooring sites, but rather at weather stations on land. Details are presented in the next section.

<i>Data Set</i>	<i>Mooring</i>	<i>Latitude (°N)</i>	<i>Longitude (°W)</i>	<i>Water Depth (m)</i>	<i>Year Day Deployed</i>	<i>Year Day Recovered</i>
Placentia Bay 1999	A	47°24.63	54°24.17	428	107	180
	B	47°24.56	54°04.27	304	107	180
Trinity Bay 2001	A	48°04.83	53°24.53	240	140	234
	B	48°03.59	53°17.98	244	140	234
	C	47°54.68	53°31.74	301	140	234
Trinity Bay 2002	A	47°47.53	53°36.17	340	126	240
	B	47°56.72	53°23.47	400	126	240*
	C	47°52.16	53°34.69	350	126	240
	D	47°57.67	53°27.19	449	126	240
	E	48°04.57	53°23.31	239	126	240
	F	48°03.47	53°19.60	300	126	240
Funk Island Bank 2004		49°27.85	52°51.30	327	219	233

Table 3.1.1 Mooring information for the four data sets. * No data after year day 187.

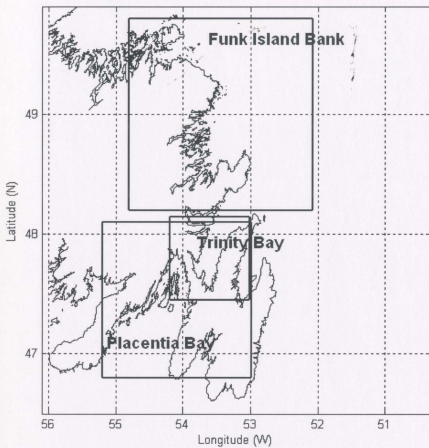


Figure 3.1.1 Deployment areas for the Placentia Bay 1999, Trinity Bay 2001 and 2002, and Funk Island Bank 2004 data sets. Fig 3.1.2 shows zoom.

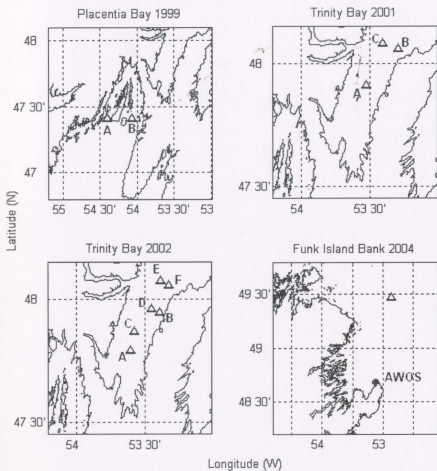


Figure 3.1.2 Mooring locations for the Placentia Bay 1999, Trinity Bay 2001 and 2002, and Funk Island Bank 2004 data sets. Triangles indicate ADCP and thermistor moorings. Cross indicates Bonavista weather station (AWOS).

3.2 Atmospheric data

Zooplankton behaviour is influenced not only by oceanographic phenomena, but also by conditions above the sea surface. In particular, since zooplankton have been observed to respond to sun-induced light intensity (see § 1.1), atmospheric data are relevant. No such data exist for the mooring sites, but nearby land-based weather stations provide good sources of representative data. The following discusses the usage of and problems associated with these data.

Atmospheric data are collected by Environment Canada using Automated Weather Observation Systems (AWOSs). The weather station used for this project is located on the Bonavista peninsula (48.68 N, 53.12 W at an elevation of 27 m). The available forms of data that are used in analysis are cloud opacity and wind velocity and direction. Cloud opacity is valuable because of its substantial influence on sea surface light levels. Wind stress plays a role in many oceanographic processes, such as density stratification and upwelling. Cloud data (Figs 3.2.1 – 3.2.4) and wind data (Figs 3.2.5 – 3.2.8) were obtained from Environment Canada for the years 1999-2004, spanning the deployment times of the four data sets.

Cloud opacity is the only available form of data regarding light intensity in the regions of interest. It is calculated from laser ceilometer measurements (resolution 50 feet, measures every 30 seconds) at the Bonavista AWOS. Hourly opacities represent the history of cloud coverage over the course of the hour, as opposed to instantaneous measurements. Coverage is based on the percentage of time for which layers of clouds are present over the station, with the viewing window scaled according to the height of

the cloud layer. Cloud opacity is registered only for clouds below a height of 3048 m (10,000 feet). Opacity is measured in tenths, with 0 indicating clear skies and 10 indicating overcast skies. Clouds located at heights greater than 3048 m are measured as 0 tenths (Environment Canada, 2004).

The presence of clouds has a substantial effect on the amount of solar irradiance that reaches the surface of the earth. In extreme cases, clouds can absorb and reflect up to 90% of the solar radiation (Kirk, 1994). Cloud opacity is only an approximate measure of this effect, as other variables, such as the characteristics of the albedo, also influence the amount of absorbed radiation at the surface. Furthermore, some discrepancy is to be expected because the measurements were taken over land, where it is generally less cloudy than over the ocean (Kirk, 1994). This effect should be minimized by the weather station's close proximity to the ocean, and location at the tip of a peninsula. Additional error will arise because clouds at heights greater than 3048 m are not recorded. For the four deployment periods, there are a few small gaps in the cloud data, as well as one large gap that spans most of the 1999 Placentia Bay deployment period (Fig 3.2.1). An AWOS located closer to Placentia Bay, at Argentia, also recorded no cloud opacity data for this deployment period.

Wind data collected at the Bonavista AWOS included velocity and direction. The directional data measured by the station are accurate up to $\pm 2^\circ$, but the data obtained from Environment Canada were provided in tens of degrees. Velocities are accurate up to $\pm 1 \text{ m s}^{-1}$ (2 knots) for speeds up to 10.3 m s^{-1} (20 knots), and $\pm 10\%$ for speeds greater than 10.3 m s^{-1} .

As with the cloud opacity data, some discrepancy is to be expected because the wind data were collected over land rather than at the mooring sites. Smith and MacPherson (1987) found a 20 – 40 % increase in wind velocity with distance from shore, as well as a clockwise rotation due to orographic effects. No compensation was made here because relative magnitudes sufficed for analysis.

Wind velocity is converted to wind stress according to the formulation of Large and Pond (1981):

$$\tilde{\tau} = \rho_{AIR} C_D |\tilde{U}| \tilde{U} \quad , \quad (3.1)$$

where $\tilde{\tau}$ is the surface wind stress, ρ_{AIR} is the density of air,

$$C_D = \begin{cases} .00114, & \text{if } |\tilde{U}| \leq 10 \text{ ms}^{-1} \\ .00049 + .000065|\tilde{U}|, & \text{if } 10 \text{ ms}^{-1} < |\tilde{U}| \end{cases} \quad (3.2)$$

is a dimensionless drag coefficient with bounds extended from Large and Pond (1981), and \tilde{U} is the wind velocity at 10 m above the water surface. There were no substantial gaps in the wind data for the four deployment periods (Figs 3.2.5 – 3.2.8).

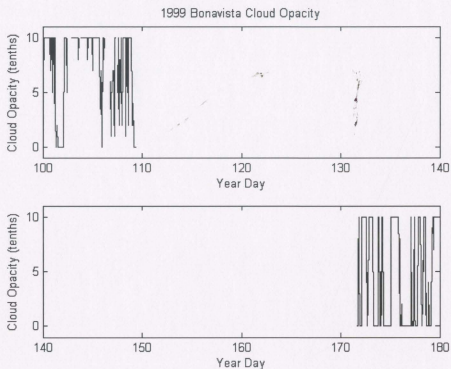


Figure 3.2.1 Cloud opacity obtained from ceilometer measurements at the Bonavista weather station for the time period spanning the Placentia Bay 1999 deployment. There is a two-month gap in the data.

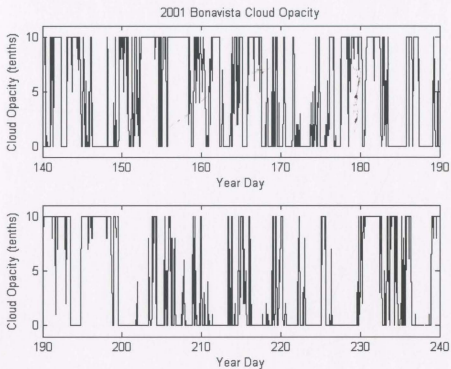


Figure 3.2.2 Cloud opacity obtained from ceilometer measurements at the Bonavista weather station for the time period spanning the Trinity Bay 2001 deployment.

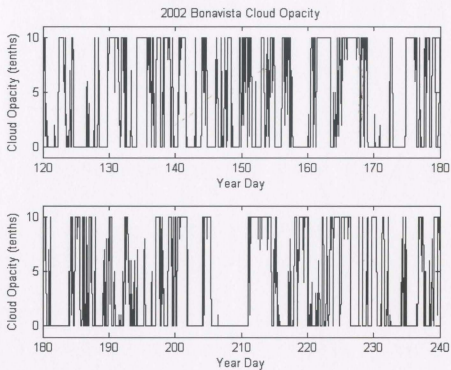


Figure 3.2.3 Cloud opacity obtained from ceilometer measurements at the Bonavista weather station for the time period spanning the Trinity Bay 2002 deployment.

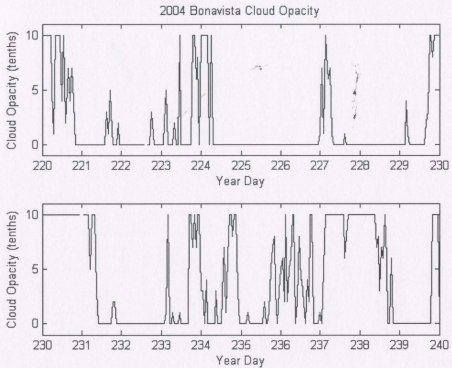


Figure 3.2.4 Cloud opacity obtained from ceilometer measurements at the Bonavista weather station for the time period spanning the Funk Island Bank 2004 deployment.

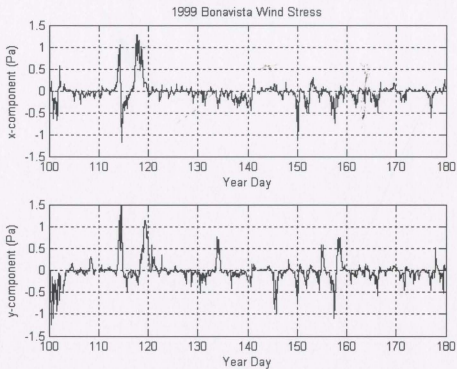


Figure 3.2.5 Wind stress (Pa) calculated according to Large & Pond (1981) from wind velocity measurements obtained at the Bonavista weather station for the time period spanning the Placentia Bay 1999 deployment.

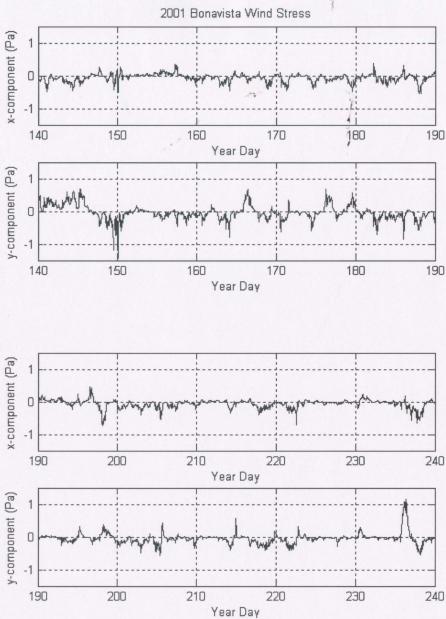


Figure 3.2.6 Wind stress (Pa) calculated according to Large & Pond (1981) from wind velocity measurements obtained at the Bonavista weather station for the time period spanning the Trinity Bay 2001 deployment.

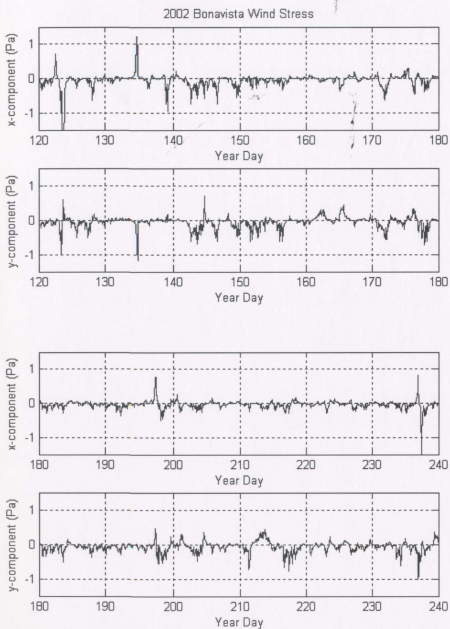


Figure 3.2.7 Wind stress (Pa) calculated according to Large & Pond (1981) from wind velocity measurements obtained at the Bonavista weather station for the time period spanning the Trinity Bay 2002 deployment.

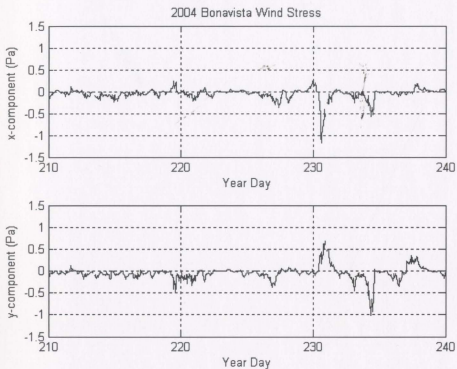


Figure 3.2.8 Wind stress (Pa) calculated according to Large & Pond (1981) from wind velocity measurements obtained at the Bonavista weather station for the time period spanning the Funk Island Bank 2004 deployment.

3.3 Temperature data

Ocean temperatures are more strongly stratified in the vertical than the horizontal. A typical ocean profile decreases in temperature as depth increases, with a well mixed upper layer, a relatively steep temperature gradient known as the thermocline, and a colder lower layer (Pickard & Emery, 1990). Profiles in the Northwest Atlantic surrounding Newfoundland deviate from this norm, exhibiting a seasonal Cold Intermediate Layer (CIL) extending from depths of around 50 m to depths of 150 m or more, containing water colder than that at greater depths. The CIL is typically defined as the region of water with temperature less than or equal to 0 °C. Over the Northeast Newfoundland Shelf, the CIL is most apparent during the summer period, when surface water is warmest, for example at the Funk Island Bank mooring in August 2004 (Fig 3.3.1).

Cold water has an effect on the metabolism of zooplankton as well as egg developmental time of zooplankton and fish (McLaren, 1974; Gabriel & Thomas, 1988; Nielsen *et al.* 2002). Zooplankton predators such as capelin are also affected by low sea temperatures (Carscadden *et al.*, 1997, 2001). Therefore, temperature profiles at the mooring sites are of interest.

All moorings, excepting those from Placentia Bay in 1999, included thermistors spaced at intervals (Table 3.3.1). In addition, the ADCPs record temperature. Thermistors are generally spaced to give higher resolution within 100 m of the surface because that is the region of highest temperature variability. Profiles were linearly interpolated into 1 m bins, with a moving average of ± 12 hours taken over the time series

for visualization purposes here (Figs 3.3.2 – 3.3.11). A CIL is present at each mooring, through its deployment duration. The data from Trinity Bay 2001 mooring C appeared faulty in that a warmer layer occurred within the CIL. This is most likely due to the unnoticed accidental swapping of two thermistors at some point during data collection. The data used here have been accordingly corrected (Fig 3.3.4).

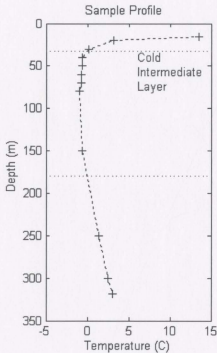


Figure 3.3.1 An example temperature profile, linearly interpolated, taken at the Funk Island Bank mooring, August 2004, showing the presence of the CIL. Crosses mark thermistor depths.

<i>Data Set</i>	<i>Moorings</i>	<i>Thermistor Depths (m)</i>	<i>Water Depth (m)</i>	<i>Ensemble Time (s)</i>	<i>Year Day Dep.</i>	<i>Year Day Rec.</i>
Placentia Bay 1999	A	NONE	428	N/A	N/A	N/A
	B	NONE	304	N/A	N/A	N/A
Trinity Bay 2001	A	55, 105 (ADCP), 155, 200, 233	240	1200	140	234
	B	51, 101 (ADCP), 151, 201, 238	244	1200	140	234
	C	50, 100 (ADCP), 150, 200, 294	301	1200	140	234
Trinity Bay 2002	A	20, 30, 40, 50, 75 (ADCP), 100, 200	340	1200	126	240
	B	20, 30, 40, 50, 75 (ADCP), 100, 200, 383	400	1200	126	240*
	C	20, 30, 40, 50, 75 (ADCP), 100, 200, 338	350	1200	126	240
	D	20, 30, 40, 50, 75 (ADCP), 200, 432	449	1200	126	240
	E	20, 30, 40, 50, 74 (ADCP), 100, 200	239	1200	126	240
	F	20, 30, 40, 50, 75 (ADCP), 100, 200	300	1200	126	240
Funk Island Bank 2004		15, 20, 30, 40, 50, 60, 70, 80, 110 (ADCP), 150, 250, 300	327	600	219	233

Table 3.3.1 Thermistor information for all moorings, including thermistor depths, water depth, ensemble time, deployment day, and recovery day. * No data after year day 187.

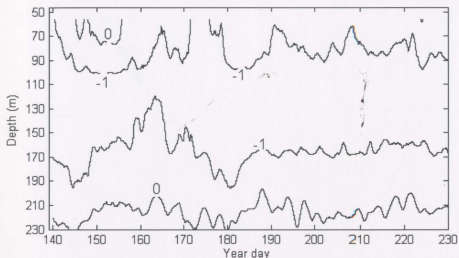


Figure 3.3.2 Isotherms at Trinity Bay 2001 mooring A. Profiles are linearly interpolated into 1 m bins. A moving average of ± 12 hours is taken here for visualization purposes.

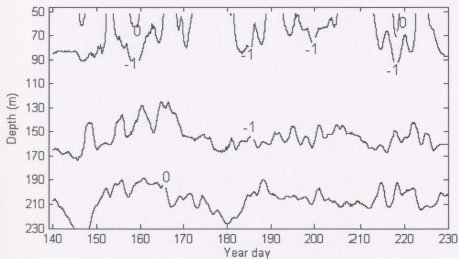


Figure 3.3.3 Isotherms at Trinity Bay 2001 mooring B. Profiles are linearly interpolated into 1 m bins. A moving average of ± 12 hours is taken here for visualization purposes.

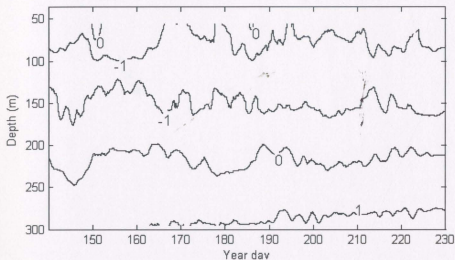


Figure 3.3.4 Isotherms at Trinity Bay 2001 mooring C. Profiles are linearly interpolated into 1 m bins. A moving average of ± 12 hours is taken here for visualization purposes.

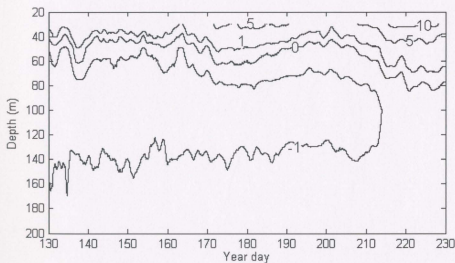


Figure 3.3.5 Isotherms at Trinity Bay 2002 mooring A. Profiles are linearly interpolated into 1 m bins. A moving average of ± 12 hours is taken here for visualization purposes.

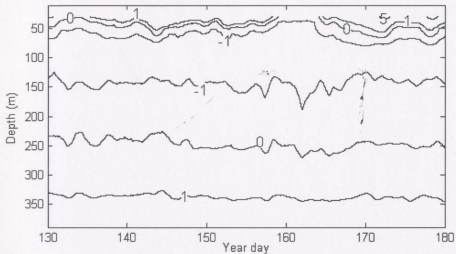


Figure 3.3.6 Isotherms at Trinity Bay 2002 mooring B. Profiles are linearly interpolated into 1 m bins. A moving average of ± 12 hours is taken here for visualization purposes.

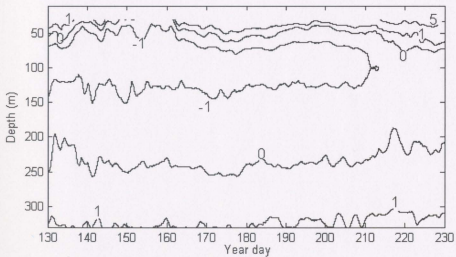


Figure 3.3.7 Isotherms at Trinity Bay 2002 mooring C. Profiles are linearly interpolated into 1 m bins. A moving average of ± 12 hours is taken here for visualization purposes.

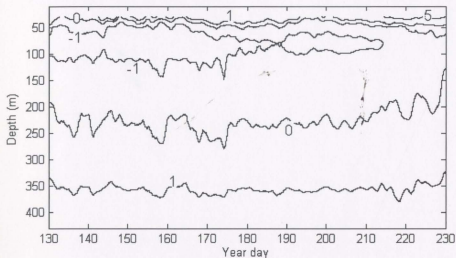


Figure 3.3.8 Isotherms at Trinity Bay 2002 mooring D. Profiles are linearly interpolated into 1 m bins. A moving average of ± 12 hours is taken here for visualization purposes.

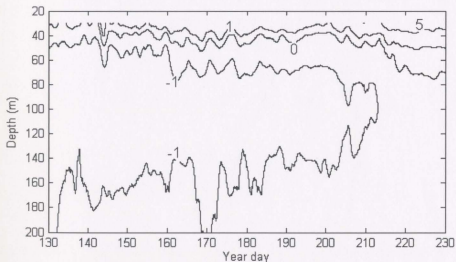


Figure 3.3.9 Isotherms at Trinity Bay 2002 mooring E. Profiles are linearly interpolated into 1 m bins. A moving average of ± 12 hours is taken here for visualization purposes.

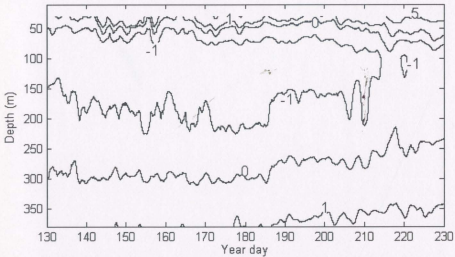


Figure 3.3.10 Isotherms at Trinity Bay 2002 mooring F. Profiles are linearly interpolated into 1 m bins. A moving average of ± 12 hours is taken here for visualization purposes.

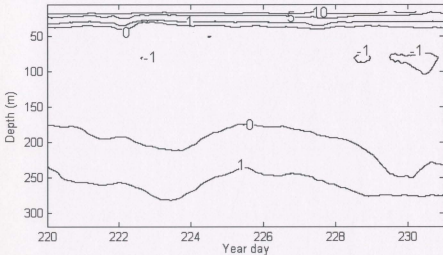


Figure 3.3.11 Isotherms at Funk Island Bank 2004 mooring. Profiles are linearly interpolated into 1 m bins. A moving average of ± 12 hours is taken for visualization purposes.

3.4 ADCP data

Velocities of currents in the ocean are measured by ADCPs using Doppler shifts from emitted acoustic signals hitting scatterers. A single beam yields a one-dimensional velocity vector. Composition of at least three beams oriented at different angles gives the complete velocity vector. Each beam also records the intensity of the backscattered signal, giving a profile of information on the scatterers in the water column.

The ADCP data of particular interest for this thesis are the backscatter intensity data, as given by the calculated backscatter coefficient S_n , and the vertical velocity data. Backscatter data are important because they show the presence of any signal scatterers in the water column. With the acoustic frequency on the scale of hundreds of kHz, detected scatterers will be on the millimetre scale, and will thus be primarily composed of hard body zooplankton of that size (Renard, 2003). The vertical velocity data is particularly interesting because although the ADCP is intended to measure the velocity of water currents, it instead measures the velocity of migrating zooplankton during twilight hours. This effect is due to the high concentration of migrating zooplankton during twilight, and it is quite clearly seen in the data and is consistent daily throughout all four data sets (Figs 3.4.1 – 3.4.4).

All ADCPs (Table 3.4.1) used an upward-facing 4-beam Janus configuration with a beam angle of 21°. Data from ADCPs in all four data sets were recorded in 4 m bins. The top few bins, near or above the surface, were removed and disregarded because the signal was distorted by side-lobe interference. Profiles were recorded as 10 minute ensembles at 6 seconds per ping for the Funk Island Bank data set, and 20 minute

ensembles for all other data sets, at 17 - 24 seconds per ping. All ADCPs had a frequency of 302.7 kHz. Artefacts in the vertical velocity data were recognized by extremely large values, were identified by a threshold value of $\pm 100 \text{ mm s}^{-1}$, and were replaced by NaN ("Not a Number").

Backscatter intensity was corrected following standard techniques (Deines, 1999), using a working version of the sonar equation solved for the backscatter coefficient:

$$S_v = C + 10 \log_{10}((T_x + 273.16) R^2) - L_{DBM} - P_{DBW} + 2\alpha R + K_C(E - E_r) \quad (3.3)$$

where: S_v gives the backscattering strength in dB referenced to $(4\pi\text{m})^{-1}$; $L_{DBM} = 10 \log_{10}$ (transmit pulse length (m)); $P_{DBW} = 10 \log_{10}$ (transmit power (W)); T_x is the transducer temperature ($^{\circ}\text{C}$); R is the along-beam slant range to the scatterers (m); α is the absorption coefficient of water (dB m^{-1}); and

$$C = 10 \log_{10} \left[\frac{8 k F B_N \cos(\theta)}{\pi E_x d^2} \right] \quad (3.4)$$

where: k is Boltzmann's constant ($1.38 \times 10^{-23} \text{ J } ^{\circ}\text{K}^{-1}$); F is the Receiver Noise Factor; B_N is the Noise bandwidth (Hz); θ is the beam angle from the system vertical; E_x is the transducer efficiency; and d is the transducer diameter (m). The slant range to each depth cell is given by,

$$R = \left[\frac{B + (L + D)/2 + ((N - 1) \times D) + (D/4)}{\cos(\theta)} \right] \times \frac{c'}{c_1} \quad (3.5)$$

where B , L , and D are the ADCP parameters: respectively, blank after transmit (m), transmit pulse length (m), and depth cell length (m); N is the number of the depth cell in question; c' is the average sound speed from the transducer to the range cell; and c_1 is the speed of sound used by the instrument. For further detail, see Deines (1999). The

resulting volume backscatter coefficient has units $\text{dB re } (4\pi\text{m})^{-1}$. Henceforth, all backscatter data will be expressed with these dB units.

The quantity of ADCP data used in this study is too great to display all of it here without condensing it to the point where daily phenomena are indiscernible. Instead, only samples of the first three data sets are included, followed by the entire data set from the Funk Island Bank mooring, as it is a small data set (Figs 3.4.1 – 3.4.4). In all data sets, both backscatter data and vertical velocity data show corresponding daily events that are easily recognizable as DVM of zooplankton.

<i>Data Set</i>	<i>Mooring</i>	<i>ADCP Depth (m)</i>	<i>Water Depth (m)</i>	<i>Freq. (kHz)</i>	<i>Bin Size (m)</i>	<i>Ens. Time (s)</i>	<i>Pings per Ens.</i>	<i>Year Day Deployed</i>	<i>Year Day Recovered</i>
Placentia	A	110	428	307.2	4	1200	70	107	180
Bay 1999	B	110	304	307.2	4	1200	70	107	180
Trinity	A	105	240	307.2	4	1200	50	140	234
Bay 2001	B	101	244	307.2	4	1200	50	140	234
	C	100	301	307.2	4	1200	50	140	234
Trinity Bay 2002	A	76	340	307.2	4	1200	50	126	240
	B	75	400	307.2	4	1200	50	126	240*
	C	75	350	307.2	4	1200	50	126	240
	D	75	449	307.2	4	1200	50	126	240
	E	74	239	307.2	4	1200	50	126	240
	F	75	300	307.2	4	1200	50	126	240
Funk Island Bank 2004		110	327	307.2	4	600	100	219	233

Table 3.4.1 Details of moored ADCPs, including deployment depth, water depth, signal frequency (Hz), vertical bin size (m), ensemble time (s), pings per ensemble, deployment day, and recovery day. * No data after year day 187.

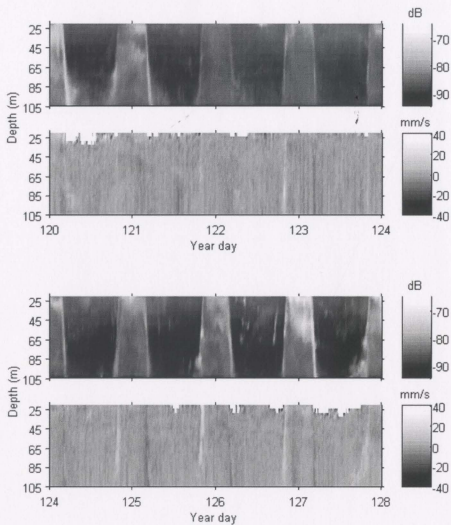


Figure 3.4.1 Backscatter intensity ($\text{dB re } (4\pi\text{m})^{-1}$) and vertical velocity (mm/s) data from 8 days at Placentia Bay 1999 mooring A.

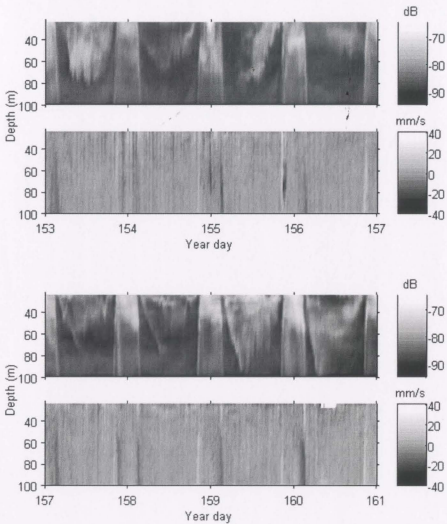


Figure 3.4.2 Backscatter intensity ($\text{dB re } (4\pi\text{m})^{-1}$) and vertical velocity (mm/s) data from 8 days at Trinity Bay 2001 mooring A.

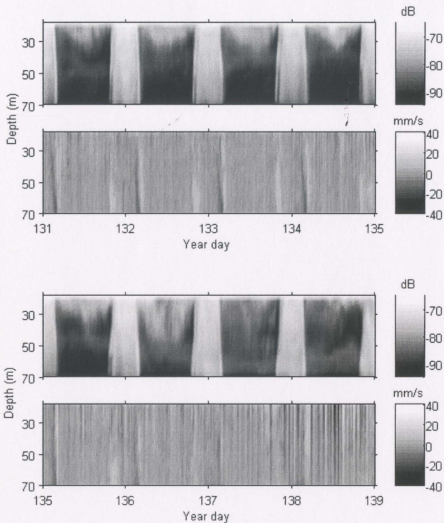


Figure 3.4.3 Backscatter intensity ($\text{dB re } (4\pi\text{m})^{-1}$) and vertical velocity (mm/s) data from 8 days at Trinity Bay 2002 mooring A.

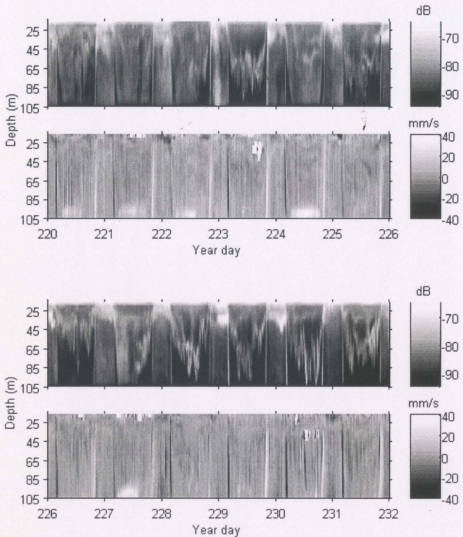


Figure 3.4.4 Backscatter intensity ($\text{dB re } (4\pi\text{m})^{-1}$) and vertical velocity (mm/s) data from the Funk Island Bank 2004 mooring.

3.5 Tow data

Tows were performed from the *Wilfred Templeman*, trip # 553, as part of the capelin ecosystem project. The survey covered a large region off the northeast coast of Newfoundland (Fig 1.1.2), spanning two weeks in August 2004. Bongo nets were lowered to depths of around 100 m during the survey, and to varying depths during a one day directed study (Table 3.5.1).

Bongo nets are primarily designed to sample copepods, so the large majority of sampled organisms are copepods, although the nets will also catch amphipods and euphausiids. Samples were performed using oblique tows, where nets are gradually lowered to depth, then raised to the surface, sampling the entire water column as the ship moves.

Data were processed by the Department of Fisheries and Oceans, Newfoundland, and were obtained from the capelin ecosystem project database. Samples are divided into 3 size classes: 0.232 mm, 1 mm, and 2 mm. The samples comprised mostly of copepods, and this study will examine the scattering layer as a whole, so no further distinction is provided here. The 2005 field season for the strategic project will address the taxonomy issue in greater detail. The 2 mm size class did include a small number of other organisms, such as euphausiids, decapods, and gastropods.

There are no available tow data from Trinity Bay or Placentia Bay that correspond to the deployment periods.

Stn	Dry Wt (g)			Time	Duration (min)	Tow Depth (m)
	2 mm	1 mm	0.232 mm			
1	2.580	0.340	2.380	10:15	17	100
2	1.610	3.520	4.980	19:35	24	100
3	3.130	3.570	2.700	00:46	19	101
4	2.090	8.500	2.350	06:33	17	101
5	1.450	1.910	2.950	11:12	21	100
7	15.460	1.890	2.030	21:08	20	101
8	4.080	10.390	4.930	01:56	19	100
9	1.520	0.780	1.660	06:37	20	101
10	1.750	3.380	2.060	13:54	21	101
11	1.180	2.130	3.600	18:50	18	101
12	3.760	9.270	5.950	23:11	23	100
13	0.480	2.000	4.300	04:50	30	100
14	0.260	5.850	5.970	09:23	20	86
15	0.160	2.760	2.760	13:52	8	38
16	0.750	7.870	4.880	00:32	13	53
17	0.910	3.450	4.090	04:08	15	100
18	3.410	2.740	4.350	08:14	21	101
19	0.540	1.880	2.170	12:00	17	101
20	0.820	2.460	0.690	16:05	15	101
21	2.640	3.120	4.540	19:44	20	101
22	4.800	6.780	1.870	00:03	20	101
23	2.840	4.750	1.360	04:30	18	100
24	0.940	0.990	2.040	08:16	20	100
25	2.230	2.960	1.450	12:08	24	100
26	1.660	2.880	1.530	16:14	19	101

Table 3.5.1 Dry weight data from bongo net tows, *Wilfred Templeman* trip # 553, broken into three size classes. Times are local, 24-hour, with no daylight savings.

Stn	Dry Wt (g)			Time	Duration (min)	Tow Depth (m)
	2 mm	1 mm	0.232 mm			
27	5.790	5.510	5.710	20:48	24	100
28	3.340	6.320	3.640	00:08	26	100
29	0.470	11.490	3.210	04:30	18	96
30	4.450	9.560	4.740	08:16	23	101
31	1.390	4.290	2.150	12:10	19	100
32	1.530	3.750	2.020	15:55	21	101
33	1.650	6.410	2.740	20:09	22	100
34	5.270	6.130	1.480	23:41	20	101
35	2.750	2.610	0.570	03:41	15	101
36	1.550	4.980	2.650	07:47	21	100
37	3.110	2.750	2.010	11:56	18	101
38	0.540	1.400	1.860	15:20	16	101
39	2.620	2.390	3.220	19:19	20	100
40	3.720	9.640	4.700	23:23	21	100
41	0.540	9.380	3.710	03:46	17	101
42	1.030	8.090	6.280	22:16	21	101
43	5.910	5.160	1.770	02:09	19	100
44	1.870	4.770	3.220	06:23	19	100
45	2.060	2.030	2.220	09:54	18	100
47	8.150	53.150	11.420	17:27	62	333
47	1.080	2.690	4.150	18:15	15	60
48	13.720	19.380	5.770	01:19	54	328
48	10.150	7.750	6.290	02:30	14	60
49	5.410	12.720	4.300	09:30	64	301
49	1.560	4.970	5.210	10:23	15	61
50	2.190	10.610	6.270	16:09	60	335
50	0.180	2.880	3.970	16:52	11	61

Table 3.5.1 (continued)

CHAPTER 4: QUANTIFYING DIEL PATTERNS IN BACKSCATTER DATA

The backscatter intensity data and the vertical velocity data clearly show the DVM of scattering layers. Both the persistence and the day to day variability of this pattern are of interest. The long time series (about 100 days at each mooring, except for the Funk Island Bank mooring, which is 13 days) provide adequate data for an in-depth analysis of the features and character of this migration phenomenon. The daily pattern is easily identifiable. The goal here is to develop quantitative, objective techniques to identify the prominent features of the DVM as observed on the Northeast Newfoundland Shelf.

To begin, there are often two distinct groups of migrators (Fig 4.0.1). Both occupy the surface waters at night. In the morning, a group of “deep migrators” travels abruptly to depths below the ADCPs, re-emerging as abruptly in the evening. This migration is marked by very large vertical velocities. A group of “intermediate migrators” descends for the daytime but remains at depths within ADCP range most of the time (50 – 100 m). This group is not always detectable in the vertical velocity data; that is, the migration velocities are often indistinguishable from the background velocities.

Historical data offer a speculative interpretation of these two groups. Copepods are the most numerous zooplankton in this part of the ocean, and in terms of biomass, *Calanus finmarchicus* is dominant (Dalley *et al.*, 2001). *C. finmarchicus* is known to be a shallow migrator relative to other zooplankton (Cushing, 1951), suggesting that they are likely to contribute significantly to the intermediate migrators seen in the ADCP signal.

The deep migrators may be composed of other vertical migrators known to be abundant in this region, including amphipods and euphausiids (Dalley *et al.*, 2001). A directed tow study is necessary to make conclusive identifications.

Beyond distinguishing between these two groups, many characteristics of the scattering layers must be quantified, such as velocity, thickness, and migration timing, intensity and duration, as well as the identification of anomalies. Quantification is difficult given the complexity of the geometry and variation in these characteristics. In addition, oceanographic features other than the DVM of zooplankton, and the presence of zooplankton, are responsible for features observed with the ADCPs.

There are many different techniques found in the literature for quantifying aspects of migration for analysis (Heywood, 1996; Rippeth & Simpson, 1998; Ashjian *et al.*, 2002; Lorke *et al.* 2004). A discussion and comparison of these techniques is required. Existing and new approaches to the analysis of these data are presented, and then applied to the available ADCP data. The different techniques are evaluated for usefulness, and for determining which aspects of migration each best elucidates. Strengths and weaknesses of the various techniques are determined through application to the available ADCP data for the Newfoundland Shelf.

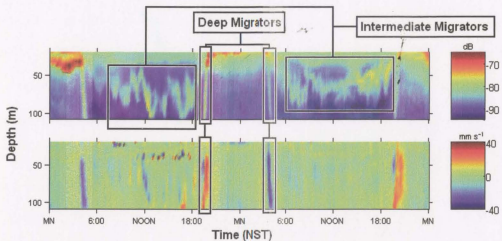


Figure 4.0.1 Backscatter intensity (top) and vertical velocity (bottom) from the Funk Island Bank mooring, showing the presence of deep migrators and intermediate migrators.

4.1 Single statistics

We begin with the simplest quantifications of the observed migration patterns, providing general information on the day to day changes in migration, without intensive calculation. The three primary migration statistics of interest are (1) timing, (2) velocity (or intensity), and (3) duration. Simple methods for quantifying timing and velocity are introduced here. Duration is not addressed because of the absence of data below the ADCPs. Other methods, based on more elaborate quantifying techniques, are described in § 4.2 and § 4.3.

Timing

Zooplankton have been observed to respond to seasonally changing twilight times by adjusting their migration timing accordingly. Ashjian *et al.* (1998) observed in the Mid-Atlantic Bight that copepods synchronized migration timing to threshold light levels. Luo *et al.* (2000) found copepod migration in the Arabian sea to have a consistent relationship to sunrise and sunset times, despite variation in duration and intensity. Ashjian *et al.* (2002) found migration to occur consistently preceding local sunrise and sunset times in the Arabian Sea, with some regional variation. Vertical velocity and backscatter intensity data taken at a given depth or depth range can be used to identify the timing of migration at dusk and dawn of each day.

The following analysis was performed for each bin. An ascent time for each day was found by locating the time of peak upward velocity w between the hours of 18:00 and 0:00 NST. Searching within a consistent time range rather than within twilight hours

prevents any statistical bias to the seasonally changing twilight times. In most cases, the peak upward vertical velocity value in this time interval is also the maximum for the entire day. Evening nautical twilight hours always fell within the range 19:00 – 22:00 NST. A descent time was found similarly by locating the time of peak downward velocity between the hours of 0:00 and 6:00 NST. Morning nautical twilight hours always fell within the range 2:00 – 5:00 NST. The same process was performed for the temporal derivative of backscatter intensity (cf. Lorke *et al.*, 2004), dS_v/dt , yielding another set of migration times (Fig 4.1.1).

An overall relationship between migration timing and sunrise and sunset times is apparent (Fig 4.1.2), as well as significant variability, the causes of which are examined in detail in the next chapter. Some bins are more appropriate for this analysis than others. For example, in the bins nearer the surface, the velocity of migrators is more difficult to discern. There is also a marked difference in the values and long-term trends obtained between the two methods. To account for the discrepancy, an edge detection algorithm is applied, identifying the maximum temporal derivative of S_v across a range of depths. The average time, excluding the maximum and minimum outliers, is taken to be the time of migration.

Twilight, sunrise, and sunset times have been rounded to correspond to the temporal resolution of the ADCP measurements—in this case, 20 minutes.

Velocity

The literature indicates that zooplankton can alter their vertical velocity in

response to their surroundings. Neill (1990) found increased migration rates in copepods after the introduction of a predator. Ashjian *et al.* (2002) found a significant seasonal variation in migration velocity.

A by-product of the migration timing calculation is a migration speed for each day at each bin. That is, the vertical velocity associated with time of migration is the peak (upward or downward) velocity. This value is taken to represent the intensity of migration.

One drawback to this method is that a peak velocity may be an anomaly and therefore may not be a good representative of migration velocity. This can be addressed by averaging velocities over a range of depths, though there is some subjectivity in choosing the depth range. To account for extreme unrepresentative values, the two outliers are omitted from the average (Fig 4.1.3).

An immediate result of this method is a distribution that shows descent velocities consistently higher than ascent velocities (Fig 4.1.4). This pattern holds for nearly all of the moorings, both for velocities averaged over a depth range, and for absolute maxima (Table 4.1.1). The largest difference is seen in Trinity Bay. The difference is on the order of 1 mm s^{-1} , which is in agreement with the estimate calculated in § 2.1 for *Calanus finmarchicus*.

There is still some question as to whether ADCP velocities can be considered to be a direct measurement of migration velocities (Luo *et al.* 2000; Ott, 2005). Alternative means of determining migration velocities come out of the more elaborate quantification methods described in the next sections.

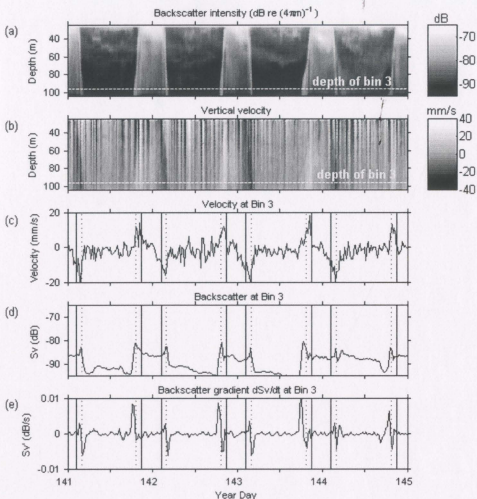


Figure 4.1.1 Cross sections of vertical velocity and backscatter at Trinity Bay 2001 mooring A, bin #3. Backscatter intensity (a), dashed line shows depth of bin #3. Vertical velocity (b), dashed line shows depth of bin #3. Vertical velocity at bin #3 (c). Backscatter intensity at bin #3 (d). Time gradient of backscatter intensity at bin #3 (e). In (c) – (e), solid vertical lines indicate sunrise and sunset times; dotted lines indicate nautical twilight times.

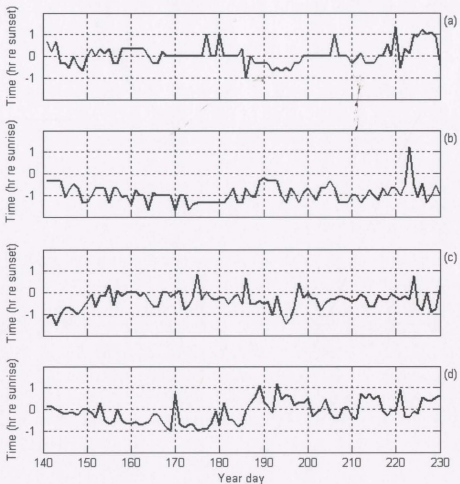


Figure 4.1.2 Migration timing relative to sunset and sunrise for Trinity Bay 2001

mooring A, 80 – 100 m. Ascent time based on evening peak upward w (a). Descent time based on morning peak downward w (b). Ascent time based on evening maximum dS/dt (c). Descent time based on morning minimum dS/dt (d).

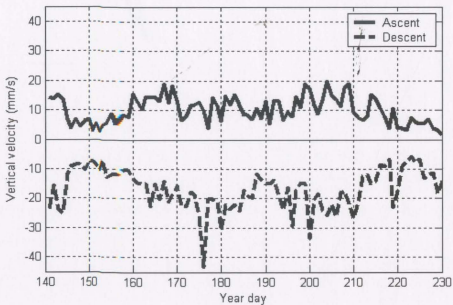


Figure 4.1.3 Migration velocities for Trinity Bay 2001 mooring A, averaged over the depth range 80 – 100 m, excluding two outliers.

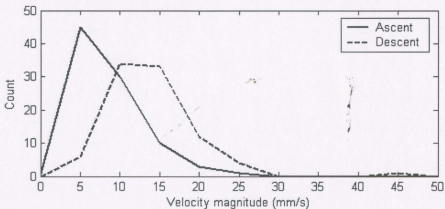


Figure 4.1.4 Trinity Bay 2001, mooring A. Distribution of upward and downward migration velocities averaged over the depth range 30 – 100 m, excluding two outliers, grouped by 5 mm s⁻¹ bins.

Mooring		Ascent velocity (mm/s)		Descent velocity (mm/s)	
		mean	max	mean	max
Placencia Bay 1999	A	10.1	18.6	-10.8	-19.4
	B	9.4	21.0	-10.0	-19.7
Trinity Bay 2001	A	8.4	14.9	-14.1	-22.2
	B	12.7	21.1	-15.5	-26.4
	C	10.4	18.8	-13.8	-22.6
Trinity Bay 2002	A	6.7	15.0	-10.2	-19.5
	B	5.9	11.1	-10.0	-18.6
	C	7.0	14.2	-10.3	-17.5
	D	8.9	16.1	-10.7	-18.6
	E	9.3	15.3	-8.7	-14.6
	F	12.1	22.1	-8.9	-17.0
Funk Island Bank 2004		25.2	37.7	-22.5	-31.2

Table 4.1.1 Mean and peak ascent and descent migration velocities averaged over the entire deployment duration, shown for all moorings.

4.2 Time series

A time series of scattering layer depth as a function of time provides information on the response of zooplankton to environmental conditions that single statistics do not reflect. Time series can also be used to extract the statistics discussed in the previous section by locating the daily maximum and minimum temporal gradients. Different methods for creating time series from the ADCP backscatter data are found in the literature. Ashjian *et al.* (1998) converted backscatter intensity to a biomass median depth. Rippeth & Simpson (1998) generated a particle path from the vertical velocity data. The following describes various methods for generating such time series from analysis of ADCP data.

Choosing threshold values

One method for reducing complicated backscatter patterns to a single layer is to choose a range of S_v values considered to represent the layer. This isolates the diel pattern from the background data. Choosing the range of values sometimes follows some subjective assessment of the data and is likely particular to a specific region. The distribution at Placentia Bay mooring B (Fig 4.2.1 b) suggests the possibility of two distinct scattering layers identified by the two dominating maxima, while the distribution at Placentia Bay mooring A (Fig 4.2.1 a) is more difficult to interpret. It should also be pointed out that a high count of a particular range of S_v values does not necessarily represent a migrating backscattering layer, but may instead simply indicate some common background scatterers.

The method proposed here is to identify the S_v values that represent migrating scatterers by examining the vertical velocity data. During the twilight hours, migrating scatterers should be associated with abnormally high vertical velocity values—values that are very unlikely to be water velocities. These values are identified in the vertical velocity data by using Chauvernet's criterion. That is, measurement of migrating velocity is treated as a measurement error, and is identified as any values that are >2 standard deviations from the mean (Taylor, 1982). This identifies regions where scatterers are known to be migrating (Fig 4.2.2 a,b). The S_v values that fall within these regions make up a new data set of known migrators. A migrating scattering layer is then defined by all S_v values in the backscatter intensity data that fall within one standard deviation of the mean of the new data set (Fig 4.2.2 c,d).

This method is useful for outlining the complex-shaped scattering layers. It has the potential to catch both the deep migrators and the intermediate migrators, as well as some variability that takes place during the night. It does, however, omit the surface concentration that appears at night because the surface has a much higher concentration of strong scatterers than migrating groups. Unfortunately, because the result retains much of the complexity of the original scattering layers, it remains difficult to work with statistically. It can be a tool for visualization of trends and for identifying important isolines of S_v , as well as providing an index of layer thickness.

The path of a scattering layer can be reduced so that at each time, the scattering layer depth is a single value. This is more convenient to work with than a time series with breadth in the vertical dimension. Some essential characteristics are lost, such as

variation in layer breadth or the presence of multiple layers. In cases where there is a single layer with fairly consistent breadth, such methods can greatly facilitate analysis.

One method for reducing a path to a single line is to follow an iso-line in the backscatter intensity, such as one of the threshold values obtained from the method just described. The maximum S_v path can also be tracked (Luo *et al.*, 2000). This is found by determining at each time step the depth at which the maximum S_v value occurs (Fig 4.2.3). The typical effect is that during the day, the path follows a signal near the surface of around -85 dB, and at night the path follows a signal near the surface of around -75 dB, indicating perhaps that two distinct groups of migrators are being tracked. The abrupt deep migration at twilight is seen as downward spikes dividing night from day. Results of this method are somewhat difficult to interpret because the series produced does not vary much from the uppermost bin.

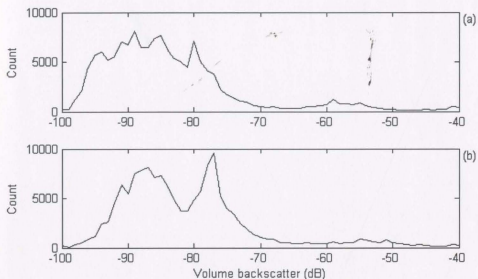


Figure 4.2.1 The number of occurrences of each dB value (± 0.5 dB) of the backscatter intensity data for the duration of the deployments of Placentia Bay 1999 mooring A (a) and mooring B (b).

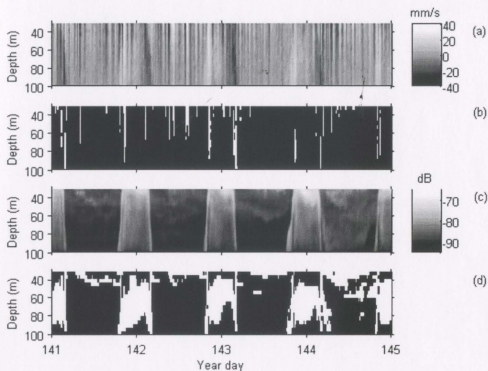


Figure 4.2.2 Trinity Bay 2001 mooring A: identifying migrating scatterers by associating high velocities with S_v values. Vertical velocity data (a). Regions of the vertical velocity data that lie outside of 2 standard deviations (white regions) (b). Backscatter coefficient (c). Regions of the backscatter intensity data that are within 1 standard deviation of the set of S_v values associated with high velocities (white regions) (d). Resulting backscatter range identified is from -86.5 to -80.8 dB.

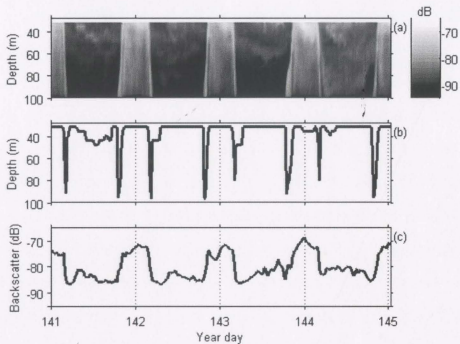


Figure 4.2.3 Trinity Bay 2001 mooring A: tracking maximum backscatter intensity. Volume backscatter intensity (a); depth of maximum S_v value at each measurement time (b); maximum S_v value at each measurement time (c).

Biomass median depth

Independent biological measurements are necessary for quantification and better understanding of scattering layers observed acoustically. Relating backscatter intensity to a biological measurement such as dry weight is a tricky process with many parameters to take into account (Heywood *et al.*, 1991, Ashjian *et al.*, 1994; Stanton *et al.*, 1994; Martin *et al.* 1996; Wiebe *et al.*, 1996; Fielding *et al.* 2004). To formulate a reliable conversion, pre-calibration of the ADCP is optimal (Flagg & Smith, 1989), and tow data should be directed to this purpose for taxonomic differentiation. The deployments in Placentia Bay and Trinity Bay were designed to collect data primarily regarding physical processes in the bays, and no biological data were collected. The biological data collected during the Funk Island Bank deployment covered a region approximately 100 km across (Fig 1.2.2). Estimating biomass based on backscatter intensity at the location of the mooring is therefore very difficult.

Even without absolute calibration, biomass and abundance estimates can still be useful in a relative sense. One method for reducing a scattering layer path to a single-value time series is to track scattering layers based on the median depth of relative biomass estimates (Ashjian *et al.*, 1998; Ashjian *et al.*, 2002). Based upon the consistency of the daily migratory cycle, backscatter intensity data can be converted to biomass by correlating S_v values to dry weights from tow samples. A scattering layer is then converted into a single time series by choosing at each time step the biomass median depth. That is, the depth that divides the water column with the same biomass above and below. Because the desired result is a median depth, it is not necessary that the biomass

estimates are accurate in an absolute sense. It is sufficient that the converting formula yield a biomass estimate that is accurate in a relative sense.

We present a method for determining a relative index of biomass, resulting in a conversion formula from backscatter intensity to relative biomass. The nature of the available data introduces a high degree of uncertainty to the conversion formula, which is why the resulting formula is only considered useful in a relative sense. Sources of uncertainty will be noted as they are introduced into the calculation.

Tow data from the *Templeman* cruise (§ 3.5) were used in comparison with backscatter data from the Funk Island Bank mooring. The mooring site is near the centre of the survey region (Fig 1.1.2). It is treated as representative of the diel backscatter cycle for the entire region. This is based on the assumption of horizontal homogeneity of scattering layers and introduces a degree of uncertainty. The issue of horizontal homogeneity is discussed in § 5.1. The analogous assumption is made for the tow data. That is, variation with regard to location within the survey region is considered to be small as compared to variation based on the diel cycle.

Backscatter intensity data from this mooring is averaged in a daily sense to give a representative daily backscatter cycle. That is, if $S_v(t,z)$ gives the backscatter intensity at any time t and depth z then the daily-average is given by

$$S_{v\text{daily}}(z,t) = \frac{1}{N} \sum_{i=D_1}^{D_N} S_v(z, i+t) \quad , \quad (4.1)$$

where t and i are given in days, t ranging from 0 to 1, and (D_1, \dots, D_N) give the year days included in the study. An associated standard deviation is also calculated (Fig 4.2.4). No adjustments were made for the changing twilight times because the deployment spanned

only two weeks, during which twilight times only changed by about 20 minutes, or 2 ensemble intervals. Use of this mean to represent the daily cycle in backscatter is based on the assumption that the day to day variation is small relative to the consistency of the repeating pattern, a small source of uncertainty as indicated in the standard deviation plot (Fig. 4.2.4). Both the mean backscatter intensity and the standard deviation were highest at night near the surface.

Most of the tows (85%) integrated over the entire ADCP depth range, so no variation in the vertical is reflected. Backscatter intensity was therefore depth-averaged by

$$\overline{S}_v \equiv S_{v, \text{depth, day}}(t) = \frac{1}{n} \sum_{z=B_1}^{B_n} S_{v, \text{day}}(t, z) \quad , \quad (4.2)$$

where B_1, \dots, B_n denote the n bins of backscatter data (Fig 4.2.5 a).

Tow data were also represented as a daily average of sampled weight \overline{DW} , calculated as

$$\overline{DW}(t) = \frac{1}{n} \sum_{i=1}^n \frac{DW_i}{T_i} \quad , \quad (4.3)$$

where n is the number of samples that occurred at time of day t , DW is the sample dry weight, and T is the tow duration. The calculated sample weights were averaged into 10 minute bins to correspond to the backscatter data. To account for gaps where no samples were taken, the resulting time series was linearly interpolated and averaged over ± 30 minutes (Fig. 4.2.5 b).

A best fit was found using linear regression, relating \overline{S}_v to $\log(\overline{DW})$ since the backscatter coefficient is logarithmically related to volume (*cf.* Ashjian *et al.*, 2002) (Fig.

4.2.5), with an r -squared value of 0.77. Without linear interpolation of tow data, the r -squared value is slightly lower, at 0.75. The resulting conversion formula is

$$\log(\overline{DW}) = 0.07\overline{S}_v + 5.01 \quad , \quad (4.4)$$

and is essentially a linear fit of two groups of data points—day and night. The formula is then applied directly, without averages, to the backscatter intensity data, to obtain a biomass index at any point that is considered to be accurate in a relative sense, with arbitrary units. The same biomass index is used at all moorings.

Copepods composed the majority of tow data, so this index is more accurately a copepod biomass index. The fairly high correlation with backscatter suggests that copepods compose a substantial portion of the detected scatterers. However, high correlation to backscatter does not necessarily indicate high numerical abundance relative to other taxa (Wiebe *et al.*, 1996). Copepod migration may also be aligned with migration of some other zooplankton that dominates the backscatter. On one occasion, Dr. P. Pepin (DFO, personal communication) found a similar night-time acoustic signal in Trinity Bay to correspond to a high concentration of jellyfish.

Biomass median depth at each time is calculated as the depth below which is 50% of the biomass (Fig. 4.2.6). This method tracks the deep migrators at night and the intermediate migrators during the day. This method is optimally used when just one dominating scattering layer is present (Ashjian *et al.*, 2002), and its entire migration cycle is within range of observation. This latter is not the case for the data available here, but biomass median depth is still a valuable quantification technique if day and night are considered separately.

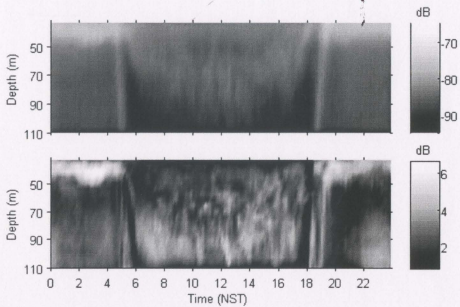


Figure 4.2.4 Day-averaged (year days 220 - 233) backscatter coefficient (top) and standard deviation (bottom) for the Funk Island Bank mooring.

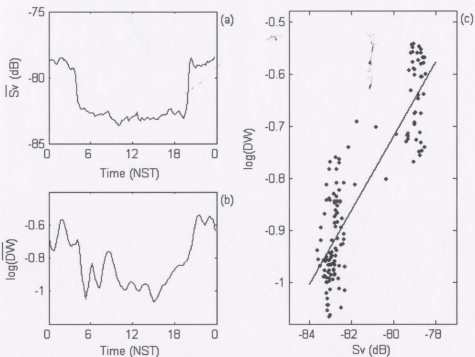


Figure 4.2.5 Averaged backscatter and tow data for the Funk Island Bank mooring.

Backscatter coefficient daily- and depth-averaged (a); bongo net tow data daily averaged and depth integrated, linearly interpolated to fill in gaps, and averaged over ± 30 minutes (b); log-linear regression between backscatter and dry weight averages shown, $r^2 = 0.77$ (c).

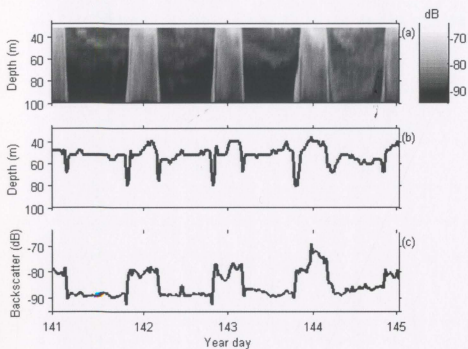


Figure 4.2.6 Trinity Bay 2001 mooring A: tracking biomass median depth. Backscatter coefficient (a); biomass median depth at each measurement time determined using a conversion formula from backscatter to biomass (b); S_v value at biomass median depth at each measurement time (c).

Lagrangian particle path

The vertical velocity data make up a velocity array that should be integrable to give the path in the z -direction of the dominating scatterers. The method used here is to track a single Lagrangian particle through the vertical velocity field. The resulting path can then be compared to backscatter data to test how well it represents the movement of the migrating layer (Rippeth & Simpson, 1998).

The grid is determined by the ensemble time intervals and bin size (4 m) of the measured data. The particle originates at the bottom of the lowest bin, and its position z is updated according to

$$dz = w \cdot dt \quad (4.5)$$

where w indicates the vertical velocity value at the current location of the particle. Time steps are typically 1,200 s, except for the Funk Island Bank mooring, where $\Delta t = 600$ s. This is enough time in many cases for the particle to cross many bins. To account for this, a smaller Δt is used to recalculate position by iterating many times within a time step, adjusting w appropriately as the particle passes through different bins. The final position after all iterations gives z_{n+1} (Fig 4.2.7). Calculation is not intensive, so a very small Δt can be used. A forward-in-time numerical scheme is satisfactory. A more advanced scheme, such as Runge-Kutta, makes negligible difference because of the high number of iterations within each time step.

The particle is clearly restricted from travelling below the ADCP, the bottom of the lowest bin (Fig 4.2.8), but the water column extends about 200 m below. Based on the backscatter data, the most intensely migrating scatterers appear to migrate to below

the ADCP. The particle path follows the migrators down to the lowest bin during morning twilight, and remains thereabouts throughout daylight hours, disallowed from going any deeper. In the evening, as these scatterers re-enter ADCP range and migrate quickly toward the surface, the particle path tracks back up toward the higher bins. The resulting effect is that the particle path tracks the group of deep migrators, while ignoring, for the most part, the intermediate migrators. In addition, the path is essentially reset to bin #1 every day, eliminating residual effects from day to day. This facilitates normalization of the path and unbiased day-to-day comparisons.

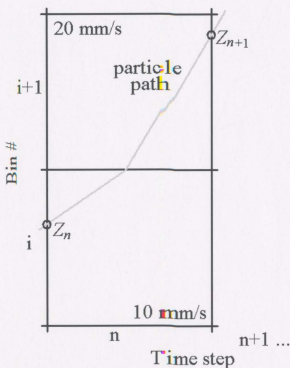


Figure 4.2.7 The numerical scheme used to track a Lagrangian particle through the measured vertical velocity with a temporal resolution higher than that of the ADCP.

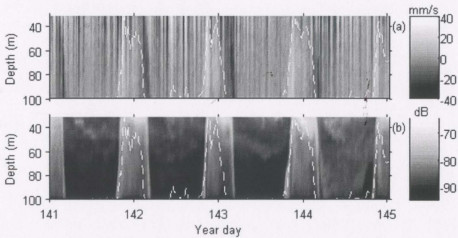


Figure 4.2.8 Trinity Bay 2001 mooring A: the path of a Lagrangian particle (dashed line) derived by integrating the vertical velocity field. Path is overlaid upon vertical velocity from which it is derived (a), and associated backscatter coefficient (b).

4.3 Full data set

This section describes two methods of simulating two-dimensional time-depth arrays of ADCP data. The first is taken from Heywood (1996) and models the backscatter array based on the measured velocity. The second performs the converse, modelling the vertical velocity array based on velocimetry of measured backscatter data.

Simulating migration of scattering layers

An elaboration of the particle tracking method is to track the entire collection of scatterers. That is, initialize the water column using a profile from the backscatter intensity data. For each time step, redistribute the scatterers based on the velocity field:

$$\frac{\partial S}{\partial t} = \frac{\partial(wS)}{\partial z}, \quad (4.6)$$

where S is the concentration of scatterers. The numerical scheme shown here is taken from Heywood (1996). As in the previous section, vertical velocity data are assumed to primarily represent the vertical velocity of migrating scatterers. At each time step n , the concentration of scatterers S in the i th bin is adjusted according to

$$S_{n+1}^i = S_n^i - \frac{\Delta t}{\Delta z} |w_n^i| S_n^i + S_n^{*i-1} + S_n^{*i+1} \quad (4.7)$$

where

$$S_n^{*i-1} = \begin{cases} \frac{\Delta t}{\Delta z} |w_n^{i-1}| S_n^{i-1} & \text{if } w_n^{i-1} < 0 \\ 0 & \text{otherwise} \end{cases} \quad (4.8)$$

and S_n^{*i+1} is defined similarly; $\Delta t = 1200$ s (or 600 s for the Funk Island Bank mooring), $\Delta z = 4$ m, and w is the vertical velocity at the appropriate time and bin. The quantity of

scatterers S is obtained from the backscatter coefficient using a simple antilog, since S_v is logarithmic, and converted back to backscatter by taking a logarithm, according to Heywood (1996).

As noted in the previous section, velocities are high enough for scatterers to move many bins over a single time step. This model only allows for motion to the neighbouring bin and in fact is unstable for $w > \Delta z / \Delta t$. As before, this is remedied by reducing Δt and iterating many times between time steps. Because this algorithm requires a great deal more calculation than the algorithm generating a Lagrangian particle path, a Δt as large as possible is preferable. If a maximum migrating velocity, w_{max} , is assumed, then the time interval must meet the following criterion for stability:

$$\Delta t < \frac{\Delta z}{w_{max}} \quad (4.9)$$

For $w_{max} = 80 \text{ mm s}^{-1}$ (a very high estimate), $\Delta t < 50 \text{ s}$. This method captures more of the intermediate migration than does the particle tracking technique and exaggerates certain features (Fig 4.3.1 c). Heywood (1996) reinitializes the model just before sunrise and sunset every day to eliminate residual effects. However, as with the particle tracking technique, this model reinitializes itself in effect every day when the scatterers migrate out of range below the ADCP.

An improvement upon Heywood's log-antilog conversion is to use the empirical conversion formula (4.4). S and S_v are related by

$$\log(S) = 5.01 + 0.07 S_v \quad (4.10)$$

A relative estimate of scatterer abundance is acceptable here because all values are converted back to dB. The result is that the scattering layer is more focused within the

appropriate dB range (Fig. 4.3.1 d). The model was constrained so that the minimum S_v value corresponded to the minimum value measured by the ADCP in the absence of migrating scatterers.

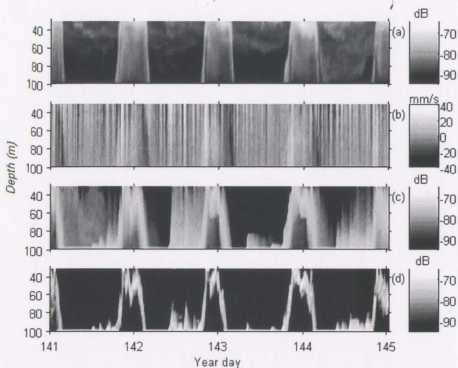


Figure 4.3.1 Tracking a profile of scatterers using the velocity field at Trinity Bay 2001 mooring A, according to Heywood (1996). Measured backscatter intensity data (a) (the first column is used to initialize the model); measured vertical velocity data (b); simulation of the scatterer profile using Heywood's model (c); Heywood simulation modified by empirical scatterer-biomass conversion formula (4.10) (d).

Velocimetry from backscatter flux

The converse of the previous method can be performed. That is, rather than using the velocity data to simulate the backscatter data, a velocity array can be derived by tracking the movement of scatterers in the backscatter data. The standard method typically performed on fluids is particle image velocimetry (PIV). PIV calculates velocity based on the movement of tracer particles between subsequent time steps.

PIV generally requires a set of distinct particles to track (Westerweel, 1997). In the backscatter data, the scatterers move as a collection rather than as distinguishable particles or identifiable objects. Thus a more appropriate method of velocimetry is desired.

The method used here to track scatterers is simpler than PIV and relies on the fact that the data are one-dimensional. This assumption follows from the horizontal homogeneity of backscattering layers (see § 5.1). The surface can be taken as a closed boundary. The 1-D flux of scatterers at a depth z_1 can be obtained from the change in the number of scatterers between z_1 and the closed surface boundary (Fig. 4.3.2). That is,

$$F_S(z_1) = \frac{1}{\Delta t} \sum_{z=z_1}^{\text{surface}} [S(z)_{n+1} - S(z)_n] . \quad (4.11)$$

The backscatter measurement at depth z_1 gives a 1-D scatterer density at that depth:

$$D_S(z_1) = \frac{S(z_1)}{\Delta z} . \quad (4.12)$$

This value is appropriate because it gives the ensemble averaged density over the period of time through which the flux takes place. Thus the velocity at depth z_1 is obtained by

$$w(z_1) = \frac{F_S(z_1)}{D_S(z_1)} = \left(\frac{\Delta z}{\Delta t} \right) \frac{\sum_{z=z_1}^{\text{surface}} [S(z)_{n+1} - S(z)_n]}{S(z_1)} \quad (4.13)$$

In order for this method to work, S must represent the relative concentration of scatterers. Since S_v is logarithmically related to measures of scatterer abundance, a conversion is performed. If S_v is used directly, the method may capture the dominant features, but the velocity values are unrealistic. Thus, S is obtained from S_v using the empirical formula (4.10). The resulting simulation is very close to the measured velocity (Fig. 4.3.3 c).

The top few bins of the ADCP contain bad data, so the practical upper boundary is actually below the surface. Some scatterers might then pass through this boundary, affecting the calculated velocity at lower depths. A bootstrap technique is added to correct for this. For each time step, at each bin, velocity is first calculated using the above technique. The resulting velocity is then used to determine a maximum range of vertical movement at that time step. Velocity is then recalculated using a closed upper boundary prescribed by this range, rather than the surface boundary. This technique removes noise from the simulated velocity, better emphasising the dominant features (Fig. 4.3.3 d).

This quantification technique is designed to filter out velocities that are not related to movement of migrators. When the bootstrap correction is used, the high frequency variation occurring between migration events is filtered out, leaving peaks that correspond to migration events. These peaks are very well defined and have higher values than those in the measured velocity data (Fig 4.3.4).

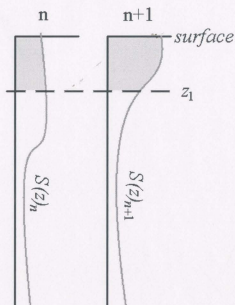


Figure 4.3.2 The method used to obtain vertical velocity from flux of scatterers. The difference between the two profiles in the segment above z_1 gives the flux of scatterers through z_1 over the time Δt between steps n and $n+1$.

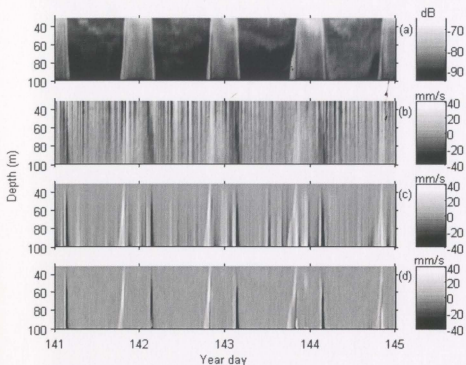


Figure 4.3.3 Using a flux-velocimetry model to generate a velocity field from backscatter intensity data at Trinity Bay 2001 mooring A. Measured backscatter coefficient (a); measured vertical velocity (b); vertical velocity simulated using the flux-velocimetry method (c); vertical velocity simulated using the flux-velocimetry method with bootstrap correction (d).

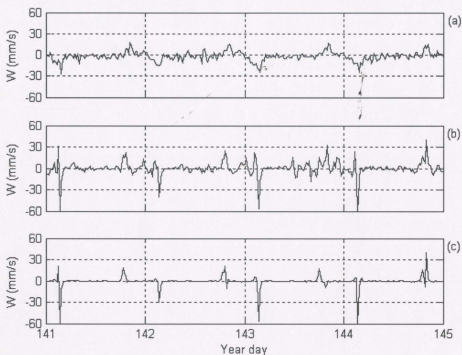


Figure 4.3.4 Cross sections at bin #5 (depth 80 m) of velocities obtained using the flux-velocimetry method for Trinity Bay 2001 mooring A: measured velocity (a), velocity calculated using the flux-velocimetry method (b), and velocity calculated using the flux-velocimetry method with the bootstrap correction (c).

4. 4 Comparison of Methods

The different methods for quantification of backscattering layers should be assessed to judge the relative usefulness and best applications of each. Much of this assessment will result implicitly from their application in the next chapter when they are correlated with physical properties of the environment. This section presents a preliminary assessment, with some quantitative comparison between methods.

Samples of all quantification methods are shown (Figs 4.4.1 - 4.4.4) of the first four days at one mooring of each deployment. Differences in the effectiveness of each method between deployments are apparent. There also exists some seasonal variation in the effectiveness of each method that cannot be seen in four-day samples.

Figures 4.4.1 - 4.4.4 Six methods for quantifying migration of scattering layers. (a) Backscatter coefficient from ADCP measurement. (b) Vertical velocity data from ADCP measurement. (c) Region outlined by threshold values determined by identifying S_v values associated with high velocities. (d) Depth of maximum S_v value. (e) Biomass median depth. (f) Path of Lagrangian particle obtained from measured velocity. (g) Simulated backscatter intensity using modified Heywood algorithm. (h) Simulated vertical velocity using flux-velocimetry method with bootstrap-correction. The first four days of each deployment are shown, using Placentia Bay 1999 mooring A (Fig. 4.4.1), Trinity Bay 2001 mooring A (Fig. 4.4.2), Trinity Bay 2002 mooring A (Fig. 4.4.3), and the Funk Island Bank mooring (Fig 4.4.4).

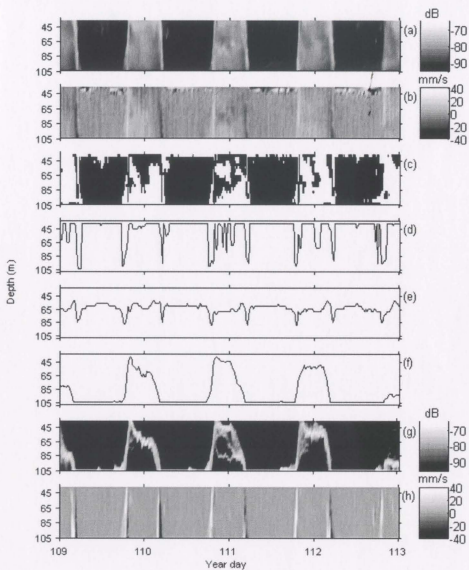


Figure 4.4.1 Placentia Bay 1999 mooring A (see above caption).

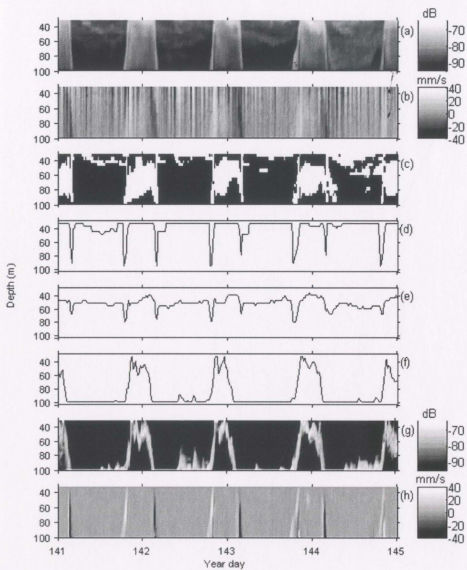


Figure 4.4.2 Trinity Bay 2001 mooring A (see above caption).

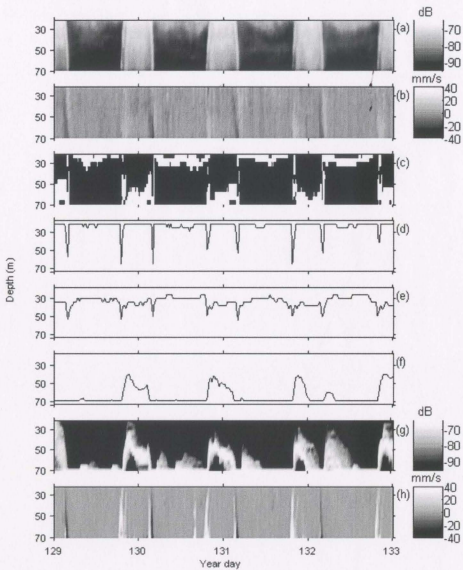


Figure 4.4.3 Trinity Bay 2002 mooring A (see above caption).

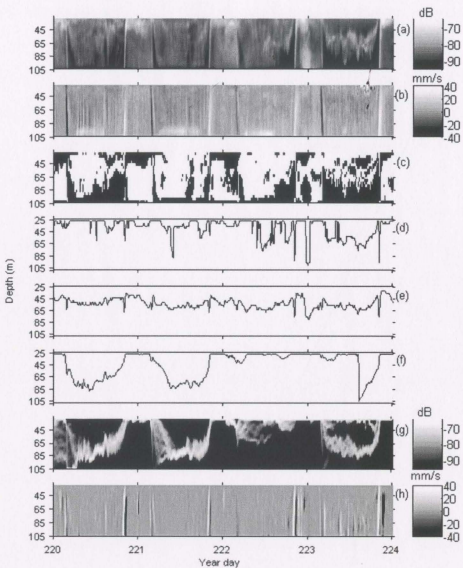


Figure 4.4.4 Funk Island Bank (see above caption).

The three methods that yield a single depth per sample time are the maximum S_v depth, the biomass median depth, and the Lagrangian particle path. At every mooring, the Lagrangian particle path is consistently the deepest, and the maximum S_v depth is consistently the shallowest (Table 4.4.1). A further analysis of the persistence and variability of each series is presented in Chapter 5.

Velocities obtained using the flux-velocimetry method were compared to measured velocities with respect to the timing and magnitude of the peak values that are associated with migration events. Most other velocities are successfully filtered out by the flux-velocimetry method. Time series of migration timing and velocity were constructed from both measured and simulated velocity using the methods described in § 4.1. Results show that the flux-velocimetry method with the bootstrap correction generates migrating velocities greater than measured velocities by an average factor of about 4. Migration timing is also highly affected, though the average remains the same (Fig 4.4.5, 4.4.6).

The flux-velocimetry method is successful in filtering out velocities that are not associated with migration. Simulated velocities in between migration events are very close to zero. The high simulated values associated with migration events may be largely due to the fact that the surface is not a true closed boundary. Violation of this assumption also leads to occasional spikes in simulated velocity values. The velocimetry method is expected to be more consistent for data collected by a downward-looking ADCP, where the sea floor can be used as a closed boundary. Horizontal patchiness may also cause some error in the simulated values. However, it is also possible that measured velocities

underestimate migration velocities—a possibility also suggested by the low values generated by the Lagrangian particle path. Velocimetry may be used to elucidate to what extent measured velocities correspond to scatterer migration. Measured vertical velocities are sometimes taken to represent migration velocities, though Ott (2005) showed a small influence by migration on measured vertical velocities, and Luo *et al.* (2000) found measured velocities to be smaller than the velocity of the migrating layer obtained by tracking the depth of maximum S_v .

To evaluate simulated backscatter, Heywood (1996) compares the simulated backscatter array to the measured backscatter array using a normalized root-mean-square (rms), taking into account the logarithmic nature of S_v , defined by

$$Q = \log \frac{\sqrt{\sum_1^k \left(\frac{\exp(S_v(\text{simulated})) - \exp(S_v(\text{observed}))}{\exp(S_v(\text{observed}))} \right)^2}}{k}, \quad (4.14)$$

where k is the number of valid data points. This calculation is awkward, however. A perfect simulation gives a non-real Q value of $\log(0)$.

Since Heywood's algorithm already takes into account the logarithmic relationship between S_v and the volume of scatterers in the simulation of dB values, as does the modified algorithm designed in § 4.3, it is better to calculate a normalized rms directly from the observed and simulated dB values. This is given by

$$Q = \sqrt{\frac{1}{k} \sum_1^k \left[\frac{S_v(\text{simulated}) - S_v(\text{observed})}{S_v(\text{observed})} \right]^2}, \quad (4.15)$$

where lower values indicate good simulations. For Trinity Bay 2001 mooring A, the unmodified algorithm had a lower rms (Fig. 4.4.7), but when all 12 moorings are

considered, neither algorithm has a consistently lower rms. Both algorithms show a tendency of scatterers toward the lower bins (Fig 4.4.8). The modified algorithm is preferred because of its calibration with tow data and because it better emphasizes the scattering layer.

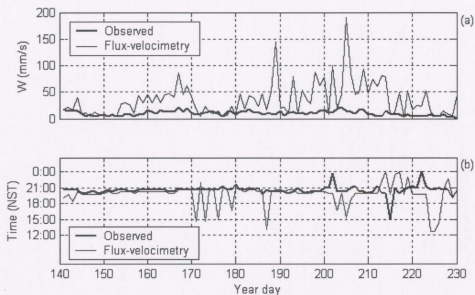


Figure 4.4.5 Trinity Bay 2001 mooring A, bin 5. Daily maximum upward velocities (a) from observed data (thick line) and from flux-velocimetry simulation with bootstrap correction (thin line). Timing of daily maximum upward velocities (b) from observed data (thick line) and from flux-velocimetry simulation with bootstrap correction (thin line).

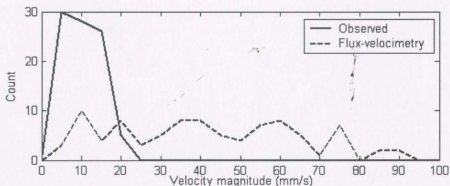


Figure 4.4.6 Trinity Bay 2001, mooring A. Distribution of upward migration velocities for observed velocities and velocities simulated using flux-velocimetry with the bootstrap correction. Values represent averages of three maxima in the depth range 80 – 100 m.

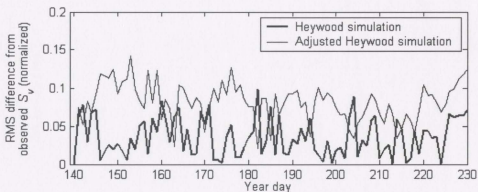


Figure 4.4.7 Trinity Bay 2001 mooring A: normalized root-mean-square difference between backscatter intensity measured and simulated using Heywood's (1996) algorithm. Means are taken each day, over all data points.

Mooring		Maximum Sv depth		Biomass median depth		Lagrangian particle path	
		mean	st. dev.	mean	st. dev.	mean	st. dev.
Placentia Bay 1999	A	44	20	58	9	97	12
	B	42	17	58	7	95	13
Trinity Bay 2001	A	41	19	49	9	90	13
	B	38	21	47	10	80	19
	C	37	19	45	9	83	16
Trinity Bay 2002	A	14	3	20	8	61	9
	B	28	16	35	8	62	8
	C	28	14	34	8	59	12
	D	30	15	35	8	55	15
	E	28	15	34	9	44	19
	F	31	17	36	9	49	17
Funk Island Bank		43	15	56	8	63	24

Table 4.4.1 Means and standard deviations of the three single-value time series described in § 4.2, for all moorings. Values are given in metres.

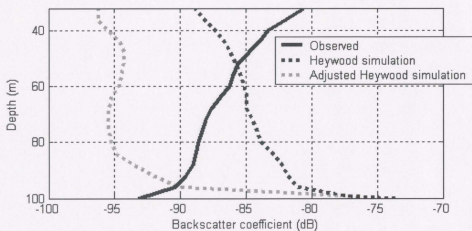


Figure 4.4.8 Mean backscatter profiles, both measured and simulated using Heywood's method, over four days at Trinity Bay 2001, mooring A.

The techniques described in this chapter provide a toolbox for quantification and subsequent analysis of DVM patterns in the ADCP data. Each technique has strengths and weaknesses, and each is best suited for emphasizing some particular aspect of the DVM pattern (Table 4.4.2).

The simple edge-detection techniques described in § 4.1 provide time series of velocity and timing of migration. These time series are small data sets, and analysis is not intensive. Edge-detection is applied over a depth range rather than across a single bin so that the values obtained are not biased by unrepresentative extreme values. There is some degree of subjectivity involved in choosing the depth range.

Of the methods described in § 4.2 that reduce the scattering layer to a single time series, the preferred quantification technique is the biomass median depth. It is the most representative of the depth of the scattering layer, and captures characteristics of both the deep migrators and the intermediate migrators. The method of tracking the depth of maximum backscatter generates a series that tends toward the uppermost bin, except during migration events. The method of tracking a Lagrangian particle generates a series that tends toward the lowermost bin, particularly during the day. The biomass median depth is therefore preferred for the analysis presented in Chapter 5. The major disadvantage to using the biomass median depth is that its formulation relies on biological samples. However, only a relative index of biomass is required, so limited biological data will suffice.

The two methods described in § 4.3 for simulating backscatter and vertical velocity both rely on the assumption that the DVM pattern is essentially one-dimensional.

This can lead to poor simulations in the presence of large horizontal currents and patchy distribution of zooplankton. Both methods are useful in examining to what extent measured vertical velocities and scatterer movement are related. They do not produce series that are convenient for correlation with environmental forcing.

<i>Technique</i>	<i>Application</i>	<i>Strengths</i>	<i>Weaknesses</i>
<i>Edge-detection</i>	Identify migration timing and velocity	<ul style="list-style-type: none"> • Small data sets • Simple analysis 	<ul style="list-style-type: none"> • Maxima and minima not always representative of migrator behaviour • Subjectivity in choosing depth range
<i>Range of backscatter associated with high velocities</i>	Isolate scattering layers from background	<ul style="list-style-type: none"> • Retains complex characteristics of migration such as multiple layers and layer thickness 	<ul style="list-style-type: none"> • Complex geometry difficult to analyse
<i>Depth of maximum backscatter</i>	Reduce backscatter to a single layer	<ul style="list-style-type: none"> • Calculation not intensive 	<ul style="list-style-type: none"> • Tends to be shallower than apparent layer depth • Influenced by limited ADCP range
<i>Biomass median depth</i>	Reduce DVM pattern to a single layer based on measured backscatter	<ul style="list-style-type: none"> • Good representation of apparent layer depth • Calculation not intensive 	<ul style="list-style-type: none"> • Requires tow data for relative biomass index • Influenced by limited ADCP range
<i>Lagrangian particle path</i>	Reduce DVM pattern to a single layer based on measured velocity	<ul style="list-style-type: none"> • Calculation not intensive • Path represents measured velocities 	<ul style="list-style-type: none"> • Tends to be deeper than apparent layer depth • Influenced by limited ADCP range
<i>Simulation of scattering layers</i>	Reconstruct backscatter array based on measured velocity	<ul style="list-style-type: none"> • Able to simulate multiple layers 	<ul style="list-style-type: none"> • Calculation intensive • Underestimates backscatter near surface • 1-D assumption
<i>Velocimetry from backscatter flux</i>	Reconstruct velocity array based on observed scatterer movement	<ul style="list-style-type: none"> • Filters velocities caused by currents 	<ul style="list-style-type: none"> • Simulated velocities may be overestimated • 1-D and closed-boundary assumptions • Calculation intensive

Table 4.4.2 Summary of techniques for quantifying DVM patterns.

CHAPTER 5: ANALYSIS

The persistent diel pattern is first established, both spatially and temporally, using the quantification techniques described in Chapter 4. Seasonal trends, horizontal correlation, and responses to physical cues are then analysed in the context of variability in this diel pattern. The final section (§ 5.3) makes note of interesting anomalies in the data.

Some features of these data make them difficult to analyse. Foremost is the fact that the ADCPs only view the upper portion of the water column. This means that we only see the migrators for a fraction of the day, thus restricting analysis of their behaviour and affecting the continuity of the data. The general solution will be to separate data into day and night portions. Our analysis would be more effective if the data included the entire water column; however, no such data were collected in the study area, so the methods of quantification and analysis must be robust enough to accommodate the available data.

The temporal resolution of 20 minutes (except for the Funk Island Bank mooring) limits analyses on migration timing somewhat. Temperature data is also missing from some of the deployments. For the Trinity Bay 2001 deployment, the shallowest thermistors are at depths of around 50 m, so that for the upper half of the ADCP range, temperatures are unknown. The Placentia Bay 1999 deployment did not include thermistors. Despite these limitations, valuable quantitative results are obtained.

5.1 Temporal and spacial persistence

Variability in migration is analysed with respect to the repeating diel pattern; therefore the pattern must first be established. This is accomplished through the processes of “day-normalization,” defined below, and daily averaging. Horizontal homogeneity is then examined with respect to separation distances between moorings and between individual beams of a single ADCP.

Day-normalization

The daily average synthesizes the repeating pattern well for short deployments (*cf.* Fig 4.2.4). However, most deployments span approximately 3 months, during which twilight times vary by as much as 90 minutes. If migration events correspond to twilight times, then taking a daily mean will obscure their characteristics, blurring them over this temporal range. The solution follows Ashjian *et al.* (2002), time-standardizing each day so that sunrise occurs at 6:00 and sunset occurs at 18:00.

This “day-normalization” is based on the assumption that migration events consistently align with the solar cycle, changing with the changing twilight times. This is often taken as a given, and migration timing is measured relative to sunrise or sunset timing. To be thorough, it is important to confirm this. It is not obvious from the distribution that migration timing varies according to seasonally changing twilight times (Fig. 5.1.1), and it may be that migrators follow endogenous rhythms rather than light cues (Forward, 1988; Lorke *et al.* 2004). Furthermore, because of higher frequency variation, polynomial fits of migration timing (*cf.* Fig 4.1.2) using the least-squares

method, both with and without day-normalization, show comparable coefficients of order 1 and 2 for migration timing. If migration timing corresponds with twilight times, coefficients of order 1 and 2 should diminish noticeably with day-normalization.

The procedure used to test the validity of day-normalization is as follows. For any given method of quantifying diel vertical migration, the average day is taken, analogous to equation (4.1). Each day of the deployment is correlated with this average day by determining the correlation coefficient,

$$r = \frac{\sum_i (x_i - \bar{x})(y_i - \bar{y})}{\sqrt{\sum_i (x_i - \bar{x})^2 \sum_i (y_i - \bar{y})^2}}, \quad (5.1)$$

where x and y are the series being correlated, and over-bars indicate means. The mean correlation coefficient over all days is taken. The resulting value gives an indication of how closely the time series correlates with the average day. The procedure is carried out both with and without performing day-normalization. Results show that migration paths consistently correlate more highly with day-normalized average days than with average days that are not day-normalized (Table 5.1.1), implying that migration timing is correlated with sunrise and sunset, and thereby justifying day-normalization. The exception is the particle-path method, which shows no consistent preference. This method may not be a good indicator of migration timing because of its tendency to produce a path that descends at variable times during the night.

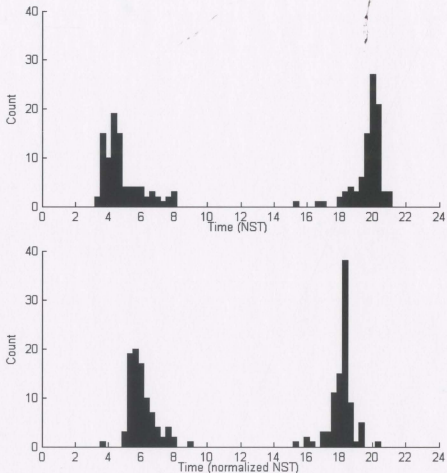


Figure 5.1.1 Trinity Bay 2001 mooring A, migration timing identified by maximum and minimum S_v gradients, and averaged over bins 1-5. Histograms of migration timing using ordinary local time (top) and day-normalized time (bottom). Sunrise and sunset times vary by approximately 90 minutes over this time series.

Mooring		Correlation coefficient (<i>r</i>)					
		With day-normalization			Without day-normalization		
		Median depth	Max Sv depth	Particle path	Median depth	Max Sv depth	Particle path
Placentia	A	0.43	0.39	0.68	0.37	0.28	0.65
Bay 1999	B	0.48	0.50	0.74	0.42	0.44	0.73
Trinity	A	0.66	0.44	0.63	0.62	0.37	0.64
Bay 2001	B	0.64	0.39	0.74	0.61	0.34	0.74
	C	0.56	0.37	0.74	0.54	0.32	0.75
Trinity	A	0.46	0.39	0.66	0.38	0.33	0.65
Bay 2002	B	0.50	0.41	0.75	0.49	0.38	0.77
	C	0.51	0.45	0.58	0.45	0.40	0.58
	D	0.66	0.48	0.75	0.60	0.40	0.75
	E	0.64	0.45	0.61	0.59	0.39	0.59
	F	0.54	0.36	0.68	0.48	0.30	0.67
Funk Island Bank		0.49	0.54	0.80	0.47	0.50	0.80

Table 5.1.1 Mean correlation coefficient at each mooring between individual days and average day, using three different methods of quantification. Correlation coefficients are given for both with and without day-normalization.

Daily averages

Daily averaged day-normalized series and their associated standard deviations then provide a good synthesis of the persistence of the daily cycle. This calculation can be performed for any of the quantification methods described in Chapter 4, as well as for the backscatter coefficient and vertical velocity data. In all cases, the diel pattern is extremely clear (Figs 5.1.2 – 5.1.4), with the exception of the method of identifying threshold S_v values associated with abnormally high velocities (Fig 5.1.3, a).

Daily averages of backscatter and vertical velocity measured by the ADCP show that migration in the top 100 m of the water column occurs just before sunrise (6:00) and just after sunset (18:00), during nautical twilight hours (Fig 5.1.2). Large standard deviations are associated with these times, however, indicating that there is some variation in migration timing. For backscatter intensity data, both measured by the ADCP and simulated using the adjusted Heywood method, highest standard deviations follow the path of the migrating layer. In the vertical velocity data, both measured by the ADCP and simulated by the flux-velocimetry method, the highest standard deviations are during migration times (Fig 5.1.2, 5.1.4). The daily average of the flux-velocimetry data shows an area of downward velocity following the upward migration in the evening, also associated with a high standard deviation. This will be discussed further in § 5.3.

The daily average produced by the method of identifying S_v associated with high velocities is meaningless (Fig 5.1.3 a). This is because the method does not work well over long time scales. The biomass median depth and the maximum backscatter depth both show clear, symmetrical diel patterns (Fig 5.1.3 b, c). The Lagrangian particle path

method also yields a clear diel pattern but with a noticeable asymmetry, in that downward migration appears much more gradual than upward migration (Fig 5.1.3 d). Standard deviations for the biomass median depth are fairly consistent, whereas those for the maximum S_v depth and the particle path differ greatly between day and night. The particle path is also consistently 40 - 60 m deeper than the other two paths, and tends to sink gradually throughout the night in a manner unrepresentative of the actual scatterers.

Time series from an entire deployment can then be related to the day-normalized daily average to observe long term trends and deviations from the generally persistent pattern. A normalized difference is calculated between individual days and the daily average using the biomass median depth paths. All days are day-normalized. A positive value indicates that the biomass median depth is shallower than the average, and a negative value indicates a deeper than average path.

Results show seasonal trends that are consistent between moorings within the same deployment. The Placentia Bay 1999 and Trinity Bay 2001 deployments show shallower than average paths near the summer solstice, year day 171 (Fig 5.1.5), while the Trinity Bay 2002 deployment shows deeper than average paths at this time (Fig 5.1.6). The consistency between moorings within the same deployment is analysed in the following subsection in the context of horizontal homogeneity. The dips in biomass median depth around year day 170 in the Trinity Bay 2002 deployment are discussed in § 5.2 in the context of a response to changes in temperature stratification.

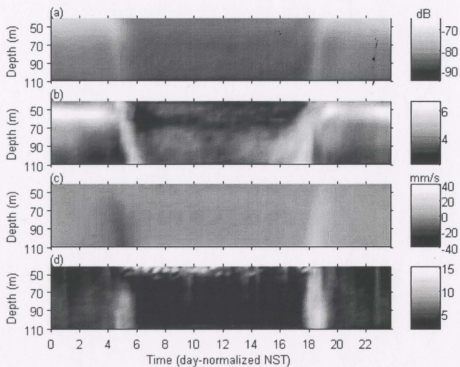


Figure 5.1.2 Trinity Bay 2001 mooring B. Daily averaged day-normalized series and corresponding standard deviations of ADCP data: backscatter intensity daily average (a) and corresponding standard deviation (b), vertical velocity daily average (c) and corresponding standard deviation (d). Averages cover year days 141-232.

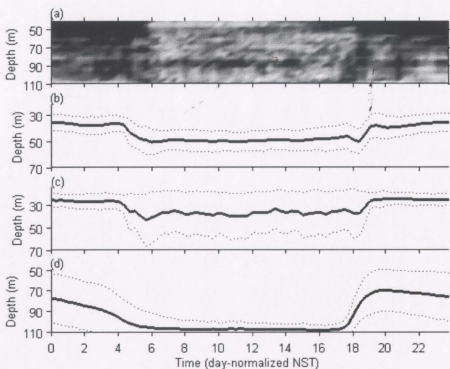


Figure 5.1.3 Trinity Bay 2001 mooring B. Daily averaged day-normalized series and corresponding standard deviations of quantifications of scattering layers: method of identifying S_v values associated with high velocities (a), biomass median depth with standard deviation (b), depth of maximum S_v value with standard deviation (c), and Lagrangian particle path with standard deviation (d). Averages cover year days 141-232.

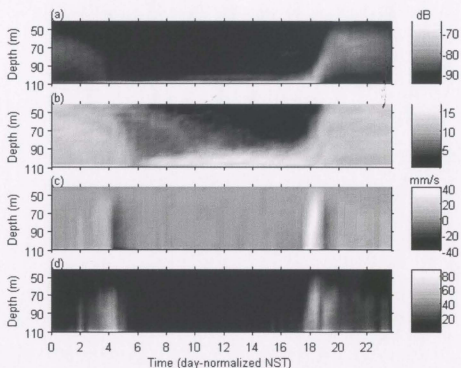


Figure 5.1.4 Trinity Bay 2001 mooring B. Daily averaged day-normalized series and corresponding standard deviations of simulated ADCP data: backscatter intensity daily average simulated using the adjusted Heywood method (a) and corresponding standard deviation (b), vertical velocity daily average simulated using the flux-velocimetry method with the bootstrap correction (c) and corresponding standard deviation (d). Averages cover year days 141-232.

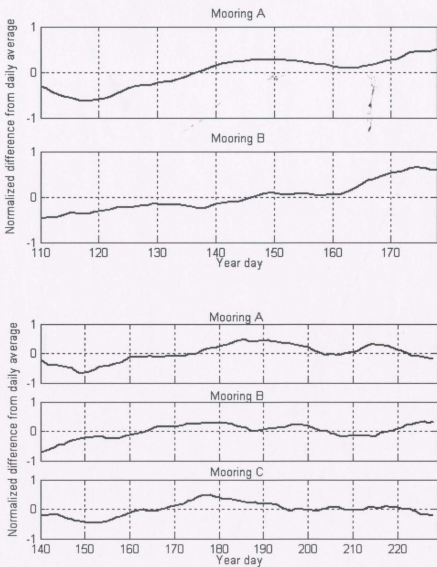


Figure 5.1.5 Seasonal trends for Placentia Bay 1999 (top) and Trinity Bay 2001 (bottom). Normalized differences are of biomass median depth, between daily averaged day-normalized series and individual day-normalized days. The graph shows an average of ± 5 days.

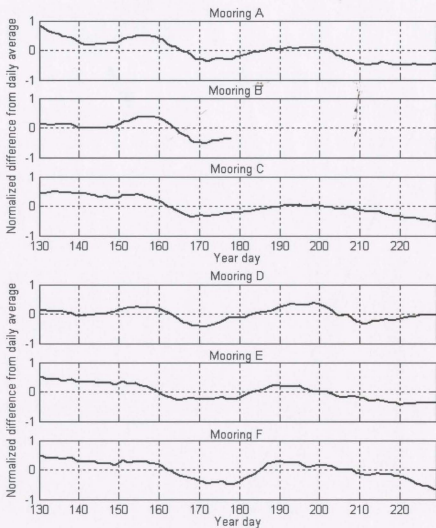


Figure 5.1.6 Seasonal trends for Trinity Bay 2002. Normalized differences are of biomass median depth, between daily averaged day-normalized series and individual day-normalized days. The graph shows an average of ± 5 days.

Horizontal homogeneity

A common difficulty in collecting oceanographic data is the practical limitation for sampling given the ocean's extremely large horizontal scale. Data from a single mooring are often used to represent the characteristics of a large region. In the case of the Funk Island Bank mooring, the survey region extended over 100 km across, with only one moored ADCP to measure the vertical characteristics (Fig 1.1.2). Some assumption of horizontal homogeneity is clearly made, though zooplankton distributions likely have some degree of patchiness in the horizontal (Marcus, 1988).

For the 2001 and 2002 Trinity Bay deployments, there are multiple moorings within the bay, spaced on the order of 10 km apart. These are good data sets for gauging variability in the horizontal. Furthermore, each ADCP collects 4 beams of backscatter data, each beam oriented at 21° from the vertical. Near the ADCP, the beams are close together, but near the surface, they are separated by distances of 10s of metres. Degrees of horizontal homogeneity can thus be determined with respect to different horizontal scales.

Biomass median depths were calculated, day-normalized, and averaged daily. Correlation coefficients were found between resulting paths. At first, this was done for individual beams within the same ADCP, which were correlated to each other, to the average beam path, and to the path of another mooring from the same deployment (Fig 5.1.7). Because the beams coincide at the ADCP, the calculation only included bins 8-18, with beam separation ranging from about 20 m to about 50 m. There is some variation between beams, but there is consistently a higher correlation when compared to each

other or to the average beam ($r = 0.99$) than when compared to another mooring in the vicinity ($r = 0.95$). These values are representative of the variation between distances of 10s of metres as compared to 10s of kilometres (Table 5.1.2).

Beam averages were then used in the same manner to find correlations between moorings in all deployments. Correlation coefficients were found between daily averages of all 12 moorings (Table 5.1.3), showing high correlations between moorings within the same region during the same time period ($r \approx 0.90$), and even within Trinity Bay between years 2001 and 2002 ($r \approx 0.85$). Correlations dropped off somewhat with the Funk Island Bank mooring ($r \approx 0.60$), and quite a bit with the Placentia Bay moorings ($r \approx 0$).

It should be noted that the higher temporal resolution at the Funk Island Bank mooring has some effect on the algorithms' outputs. Also, this mooring was deployed for only 2 weeks in August, whereas the other moorings collected data for about 100 days each, during approximately the same seasons. In addition, correlations are expected to drop off for inter-year comparisons since they do not compare the same time period.

The two moorings separated by the greatest horizontal distance in the Trinity Bay 2002 deployment were moorings A and E. These moorings still had a high correlation coefficient ($r = 0.89$), suggesting that a single mooring gives a fairly good representation of the diel pattern of zooplankton vertical distribution over 10s of kilometres in the horizontal. There is a trend, however, of decreasing correlation with increasing distance between moorings (Fig 5.1.8 a).

The same analysis can be performed for season-scale time series (Fig 5.1.6). The correlation coefficient r is determined as a function of separation distance (Fig 5.1.8 b).

Time series derived from moorings within the same deployment, with separation distance of 10s of km, are correlated fairly highly (average $r = 0.77$, excluding mooring D, Trinity Bay 2002, which was consistently uncorrelated with the other moorings). The relationship between mooring separation distance and r is less clear here than in the previous analysis (Fig 5.1.8), and r values are not high enough to suggest that seasonal variation on scales of 10s of km can be represented by a single mooring. Time series derived from different beams within the same mooring, on the scale of 10s of m, correlate very highly ($r > 0.95$), so some relationship to separation distance is clear. The consistently low correlation between mooring D and any other mooring, regardless of separation distance, suggests that local phenomena may also influence migration patterns.

Mooring	A					B	
	1	2	3	4	AVE	AVE	
A	1	-	0.995	0.993	0.998	0.998	0.933
	2	0.000	-	0.997	0.995	0.998	0.921
	3	0.000	0.000	-	0.992	0.997	0.914
	4	0.000	0.000	0.000	-	0.998	0.952
	AVE	0.000	0.000	0.000	0.000	-	0.952
B	AVE	0.000	0.000	0.000	0.000	0.000	-

Table 5.1.2 Correlation coefficients r (upper right half) and associated p -values (lower left half) comparing daily averaged, day-normalized biomass median depth paths of individual beams at mooring A, Trinity Bay 2001, and beam averages at moorings A and B, Trinity Bay 2001.

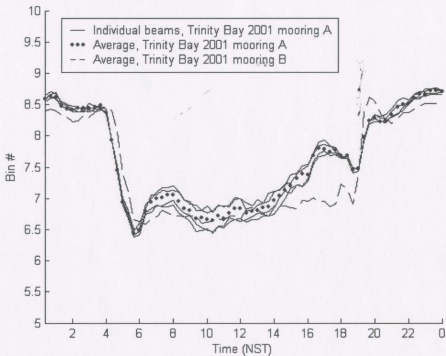
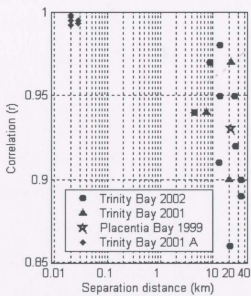


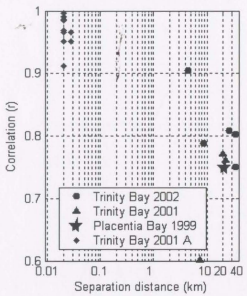
Figure 5.1.7 Daily averages of day-normalized biomass median depth for individual beams (solid lines) and average beam (dotted line) at Trinity Bay 2001 mooring A, compared with average beam (dashed line) at Trinity Bay 2001 mooring B.

Mooring	Trinity Bay 2001			Trinity Bay 2002						Funk I. Bank	Placentia Bay 1999		
	A	B	C	A	B	C	D	E	F	A	B		
Trinity Bay 2001	A	-	0.94	0.90	0.83	0.59	0.92	0.89	0.97	0.86	0.64	-0.05	-0.15
	B	0.00	-	0.87	0.73	0.63	0.84	0.89	0.94	0.85	0.65	-0.12	-0.26
	C	0.00	0.00	-	0.87	0.70	0.94	0.92	0.91	0.90	0.51	0.10	0.05
Trinity Bay 2002	A	0.00	0.00	0.00	-	0.58	0.97	0.86	0.89	0.90	0.56	0.13	0.10
	B	0.00	0.00	0.00	0.00	-	0.63	0.81	0.68	0.82	0.09	0.48	0.41
	C	0.00	0.00	0.00	0.00	0.00	-	0.91	0.95	0.92	0.61	0.05	0.02
	D	0.00	0.00	0.00	0.00	0.00	0.00	-	0.95	0.98	0.42	0.20	0.08
	E	0.00	0.00	0.00	0.00	0.00	0.00	0.00	-	0.94	0.61	0.03	-0.08
	F	0.00	0.00	0.00	0.00	0.00	0.00	0.00	0.00	-	0.46	0.26	0.15
Funk I. Bank	0.00	0.00	0.00	0.00	0.44	0.00	0.00	0.00	0.00	0.00	-	-0.45	-0.48
Placentia Bay 1999	A	0.68	0.31	0.39	0.28	0.00	0.68	0.09	0.80	0.03	0.00	-	0.93
	B	0.22	0.03	0.70	0.40	0.00	0.90	0.53	0.50	0.20	0.00	0.00	-

Table 5.1.3 Correlation coefficients r (upper right half) and associated p -values (lower left half) comparing daily-averaged, day-normalized biomass median depth paths of beam averages at the 12 moorings. Shaded regions indicate moorings were in the same deployment.



(a)



(b)

Figure 5.1.8 Correlation coefficient r plotted against distance separating moorings.

Correlations are only included between moorings within the same deployment, spanning the same time period. Mooring A at Trinity Bay 2001 is shown for beam to beam correlation. Time series correlated are (a) daily averages of biomass median depth (Fig 5.1.7), and (b) seasonal comparisons to daily averages (Fig 5.1.6). (Note: In (b), Trinity Bay 2002 mooring D is excluded because r values were very low.)

5.2 Response to environmental cues

Variability from the diel pattern is now correlated with environmental data. Not all cues believed to influence migration are represented in the data. There are no data regarding cues emitted by predators or food availability, for example. Therefore there will be some unexplained variability in migration behaviour. The two cues of interest here are light intensity and temperature stratification. Light intensity is derived from cloud cover (§ 3.2), and temperature is obtained from moored thermistors (§ 3.3). Wind data were also analysed, but no relationship with migration was found.

Light intensity

Zooplankton have been observed for many decades in the laboratory to respond to changes in light intensity (Clarke, 1930). *In situ*, the coordination of migrating times to changing twilight times is further evidence of this connection (Ashjian *et al.*, 2002), though Lorke *et al.* (2004) found migration timing in *Chaoborus flavicans* larvae to be unaffected by changes in cloud cover. The data from the two Trinity Bay deployments revealed a response by migrators to changing light conditions.

The only light data available for the deployments in this study are cloud opacity data from weather stations on land (see § 3.2). Cloud opacity is not a perfect measure of light intensity, as other atmospheric factors and the surface albedo have an effect, as well as attenuation through the water column. Furthermore, there is some question as to the spectral sensitivities of different species of zooplankton (Forward, 1988; Gal *et al.*, 1999). Another source of uncertainty comes from the fact that cloud data are taken from

a single land-based location, and applied to multiple mooring locations at sea. While cloud cover differs from land to ocean (Kirk, 1994), the fact that the weather station was on the tip of a peninsula near the mooring locations reduces this effect. In short, the cloud data available were an adequate enough source of light intensity data to find a statistically significant response by migrators, but a better gauge of sea surface light intensity and of light attenuation should be sought for future studies of this kind.

A commonly used relationship between cloud cover and light intensity is based on Budyko (1974):

$$Q = Q_0[1 - an - bn^2] \quad , \quad (5.2)$$

where Q_0 is the incoming irradiance unaffected by cloud, and Q is the resulting irradiance reaching the surface. The coefficient a depends upon latitude, and for the study region $a = 0.40$ (at 50 °N), and $b = 0.38$ at any latitude (Budyko, 1974). Cloud cover n is given as a number from 0 to 1, with 0 indicating clear skies and 1 indicating overcast skies. Thus on a clear day, $Q = Q_0$, and on an overcast day, $Q = 0.22 Q_0$. Consider the daily light cycle to be sinusoidal from sunrise to sunset, giving surface light intensity as

$$I = \left\{ \begin{array}{ll} I_0 & \text{if } t < R \text{ or } t > S \\ I_0 + Q \sin\left(\pi \frac{t-R}{S-R}\right) & \text{if } R \leq t \leq S \end{array} \right\} \quad , \quad (5.3)$$

where R and S are respectively the times of sunrise and sunset, and I_0 is a minimum night-time intensity, taken to be zero. This model for light suggests that cloud cover can play a large role in determining the light that reaches the surface (Fig 5.2.1).

Light then decays exponentially with depth, depending upon its wavelength and the properties of the water column. The question of which wavelengths are perceived by

the migrating zooplankton requires species differentiation within the migrating layer as well as more thorough light data, so this question is not addressed in the current study. Rather the response of the layer as a whole is examined.

The uncertainties in the cloud data discussed earlier suggest that a functional relationship between light intensity and some characteristic of migration will be difficult to perceive. Therefore a simpler relationship is sought. Days are divided into two groups: overcast and clear. Overcast days are those with cloud opacity 10 tenths during time of migration. Clear days are those with cloud opacity 0 tenths during time of migration. These two cases make up the majority of days, and intermediate cases are ignored for this analysis. The goal is to find a significant difference between overcast days and clear days in migration behaviour.

The deployments in Trinity Bay provide the best data for this analysis. Cloud data from the 1999 deployment in Placentia Bay contain a large gap that spans most of the deployment period. The Funk Island Bank mooring was too brief to obtain any statistically significant results. The Trinity Bay deployments provide more complete data sets, each spanning approximately 3 months, and the cloud data for this period contain only a few brief gaps.

The quantification methods described in § 4.1 and § 4.2 can each be used to determine timing of upward and downward migration. In § 4.1, a method is described for obtaining migration timing by locating times of peak upward or downward velocity w , or peak upward or downward backscatter gradient dS/dt . These times can be found for individual bins or averaged over many bins. The methods in § 4.2 for reducing ADCP

data to a single time series can also be used to quantify migration timing by locating the time of maximum or minimum gradient. The result is a statistically significant difference in migration timing between clear and overcast days.

If the cue for upward migration is a decrease in light beyond a certain threshold, then the hypothesis is that upward migration will occur earlier on overcast evenings than on clear evenings. Similarly, darkness is slower to recede on overcast mornings, so migration should occur later on overcast mornings than on clear mornings. The response to light by zooplankton is likely more complex than this, and variant between different species, but this relationship is apparent and statistically significant based on the data used in this study.

The highest statistical significance was found using the methods described in § 4.1—in particular, using an edge-detection algorithm based on the maximum and minimum temporal derivatives of S_v (Fig 5.2.2). In 2001 the significance was higher for morning migration, and in 2002 the significance was higher for evening migration. In most cases, evening migration was approximately 20 minutes earlier on overcast days than on clear days, and morning migration was approximately 20 minutes later on overcast days than on clear days. Results showed a high statistical significance ($p < 0.05$) in almost half of the tests, and a fairly high significance ($p < 0.2$) in two thirds of the tests (Table 5.2.1). If the edge-detection algorithm is applied to the entire depth range of the ADCP data, $p < 0.05$ for nearly all Trinity Bay 2002 moorings, but statistical significance decreases for Trinity Bay 2001. When an entire deployment is taken as a single data set, rather than individual moorings, t-tests always show high statistical significance.

Various other t-tests were performed to test for numerical quirks. The ADCP data have a temporal resolution of 20 minutes while sunrise and sunset times are known to much higher resolution. Sunrise and sunset times were rounded to the nearest 20 minute time for these analyses. Using a higher resolution did not decrease the statistical significance. Further tests were performed using cloud data from time periods that did not correspond to those of the ADCP data—essentially random cloud data. This was to check for systematic numerical phenomena that may appear statistically significant. The results showed no statistical significance.

A response to cloud opacity was only seen when comparing completely overcast days to completely clear days. Still, these results are promising, particularly given the limitations of the available data in representing light intensity and in proximity to the moorings. Migrators are ascending earlier and descending later on cloudy days than on clear days. As suggested in § 1.2, such changes in migration timing by zooplankton may have implications throughout higher trophic levels, particularly regarding diel patterns in foraging.

There exists debate as to whether migration is cued by light crossing a certain threshold or by changes in light intensity (Geller, 1986; Forward, 1988). In the model presented here, the maximum change in light intensity occurs at sunrise and at sunset both on days that are completely clear and on days that are completely overcast. The time at which light levels reach any given threshold changes, however. The implication is that under this model, *in situ* migration timing is cued by light crossing a certain threshold level. This is consistent with the predation avoidance hypothesis in that a threshold light

level would render zooplankton at risk of predation.

Determining a more precise functional response of migrators to light intensity will require better data on light intensity and more information on the species composition of the migrating layers. Light intensity should be measured at the sea surface near the mooring location, and taxonomy should be determined from net tows. These objectives have been included in the plan for the 2005 field season for the capelin ecosystem strategic project.

The same analysis was performed using the velocity data. Migration velocities were found using a variety of methods analogous to the methods used to find migration timing, as described in § 4.1 and § 4.2. Velocities on clear days were compared to velocities on overcast days. No statistically significant difference was found, nor was any consistent pattern revealed.

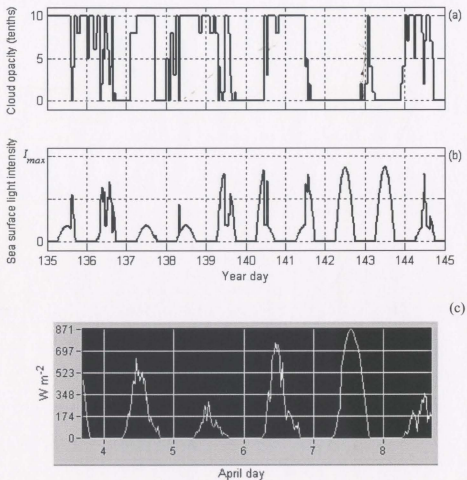


Figure 5.2.1 Effect of cloud opacity (a) on sea surface light intensity (b) based on Budyko (1974) formulation. Cloud data are from the Bonavista AWOS, 2002. Light intensity is normalized to I_{max} : the maximum light intensity for a clear summer solstice at latitude 0 °N. A sample of solar radiation ($W m^{-2}$) measured on the roof of the Chemistry and Physics building in St. John's is given for comparison (c).

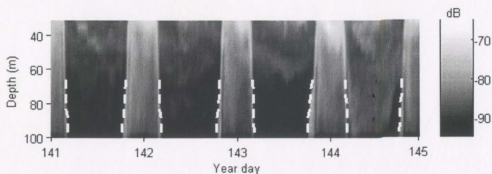


Figure 5.2.2 Trinity Bay 2001 mooring A. Results of edge-detection algorithm used to determine migration timing from backscatter data.

<i>Mooring</i>	<i>Evening difference (minutes)</i>	<i>p-value</i>	<i>Morning difference (minutes)</i>	<i>p-value</i>
Trinity Bay 2001				
A	-7.32	0.44	-1.52	0.9
B	-12.57	0.31	22.51	0.04
C	-11.11	0.21	18.96	0.01
Trinity Bay 2002				
A	-17.25	0.02	11.25	0.11
B	-17.93	0.17	27.58	0.17
C	-11.03	0.16	8.57	0.17
D	-23.29	0.01	15.3	0.01
E	1.44	0.82	10.56	0.18
F	-20.71	0.01	6.45	0.51

Table 5.2.1 Difference of migration timing on overcast days from that on clear days, and associated p -values. Timings are obtained using an edge-detection algorithm on the bottom 20 m of backscatter data, then averaging times, eliminating the two outliers. The sample size varied from $n = 70$ to 80 (with $n - 2$ degrees of freedom), with the exception of mooring B in Trinity Bay 2002, where the sample size was 38. Grey boxes are those with p -value of 0.05 or less.

Temperature

Changes in temperature can affect zooplankton in many ways, particularly by altering rates of metabolism and development. Hiršhe (1987) observed increased metabolic rates among Arctic copepods with increased temperature. Torres and Childress (1983) found that temperature has a substantial effect on the oxygen consumption rate, and therefore the metabolic rate, of *Euphausia pacifica* at high swimming speeds. Egg development time and hatching rate have also been seen to be a function of temperature (cf. Geller, 1986; McLaren, 1974; Nielsen *et al.* 2002). Consider for example Bělehrádek's temperature function,

$$D = a(T - \alpha)^{-b} \quad , \quad (5.4)$$

where D is development time to hatching, T is temperature, and the other values are empirically determined constants (cf. McLaren, 1974). Since sea water temperature is highly stratified in the vertical, temperature is expected to be an important factor in the vertical migration of zooplankton.

As with the light intensity analysis, the migrating layer is treated as a whole for the temperature analysis. In reality, different species within the layer may respond to temperature in different ways (Geller, 1986), particularly at night when the layer within ADCP range likely has a more diverse taxonomic composition. Given the data, species differentiation within the scattering layer is not possible. A collective response by the whole layer to changes in temperature dynamics is still apparent, and some statistical analysis seems appropriate.

Changes in temperature profiles in the study region correspond to longer time

scales than changes in light intensity. Responses to light intensity are seen at a high temporal resolution and therefore dominate the migration cycle, driving migrators to cross temperature gradients every day. The response to temperature is therefore secondary and should not be so immediate, but is apparent on longer time scales (Fig 5.2.3). The focus here is thus on behaviour during the time intervals between migrations, as opposed to during migration.

The ADCPs only view the upper portion of the water column, so the composition of the scattering layers within this range differs between day and night. The examination of temperature response is therefore divided into day and night because of the difference in migrating groups between these two periods. The data are day-normalized. The day time series include the 6 hour intervals centred at noon, and night time series include the 6 hour intervals centred at midnight. These 6 hour intervals are each averaged to give one data point per day (Fig 5.2.4). For example, for the biomass median depth, the day time series Z_{day} would be calculated as

$$Z_{day}(t) = \frac{1}{N} \sum_{9:00}^{15:00} B_t, \quad (5.5)$$

where t is year day, B_t is the day-normalized biomass median depth time series on day t , and N is the number of data points between 9:00 and 15:00. The night biomass median depth, Z_{night} is calculated analogously, and the same averaging can be performed for any time series. This method will also be used here to calculate day and night time series of isotherm depths. Scattering layer depth is denoted Z and isotherm depth D , with a temporal resolution of 1 data point per day. The 6 hour intervals centred at 6:00 and at 18:00 are not included because they correspond to migration events, when the scattering

layer behaviour is dominated by a response to light.

The next step is to determine the temporal scale at which temperature dynamics become significant. The correlation coefficient r is found between Z and D , as a function of time scale q . Running averages are taken over the time interval q , in days, and correlation coefficients are determined between resulting time series Z^q and D^q .

Explicitly,

$$r_q = \frac{\sum (Z_i^q - \bar{Z}^q) \sum (D_i^q - \bar{D}^q)}{\sqrt{\sum (Z_i^q - \bar{Z}^q)^2 \sum (D_i^q - \bar{D}^q)^2}}, \quad (5.6)$$

where over-bars indicate means taken over all i , Z^q is defined by

$$Z_i^q = \sum_{k=0}^{q-1} \frac{1}{q} Z_{i+k}, \quad (5.7)$$

and D^q is defined analogously. This calculation is performed for both day and night time series.

Finally, the coherence between Z_{day} and D_{day} , and between Z_{night} and D_{night} , are determined. Power spectra and cross spectrum are calculated by fast Fourier transform, and coherence is determined as a function of frequency. Coherence at a given frequency is a measure of the correlation between the components at that frequency of the two time series (Chatfield, 1996).

These analyses were performed for Trinity Bay 2002 moorings A, C, D, E, and F, for day and for night series (Figs 5.2.5 - 5.2.9). Analysis of day time series used the depth of the 0 °C isotherm, and analysis of night time series used the depth of the 1 °C isotherm. In most cases, the entire time series was used; in a few cases, the isotherm dropped out of ADCP range near the end of the deployment, so the final 20 days were dropped. Trinity

Bay 2002 mooring B and the Funk Island Bank mooring were not used because of their short durations. Moorings from Trinity Bay 2001 were not used because there are no temperature data for the upper half of the ADCP range. Placentia Bay 1999 data were not used because the moorings had no thermistors.

The remaining five moorings reveal some consistent patterns. The same dip in biomass median depth around year day 170 that was seen in § 5.1 (Fig 5.1.6) is apparent in this analysis, and appears to correspond to similar dips in the isotherm depths occurring at the same time (Figs 5.2.5 – 5.2.9). This implies a response by migrators to large, relatively abrupt changes in temperature stratification.

The statistical analyses show low frequency correlations between biomass median depth and isotherm depth. For the day time series, the time-scale dependent correlation coefficient r_q shows high correlations between 20-50 day time scales. For lower q , correlation drops off, and for $q > 50$, the statistic behaves strangely due to the fact that the time series are of length ≤ 100 data points. For the night time series, there is no clear consistent behaviour of r_q .

The primary result of the coherence analysis is a very high coherence (typically greater than 0.9) at frequencies of 0.05 day^{-1} or less, present in all moorings, for both day and night time series. This implies a significant response by migrators to temperature dynamics of period 20 days or longer.

For higher frequency changes in temperature stratification, a consistent direct response is not perceived. Certain organisms within the scattering layer may be responding in a more immediate sense, but cannot be resolved with these data.

Nevertheless, the response of the layer as a whole to low frequency temperature dynamics is a significant result. It also indicates that these methods are effective and could be applied to more taxonomically detailed data.

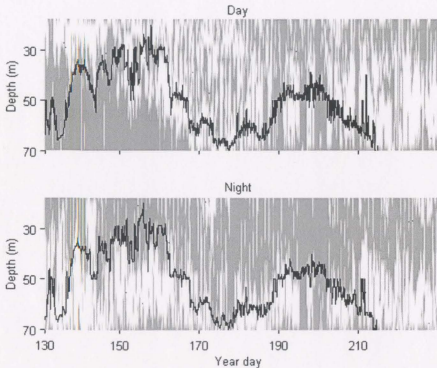


Figure 5.2.3 Trinity Bay 2002 mooring C. Scattering layers (white) defined by identifying a range of backscatter intensity values with high vertical velocities (outside of 2 standard deviations; see § 4.2). Series is day-normalized, and separated into day and night portions. Line shows $-0.5\text{ }^{\circ}\text{C}$ isotherm.

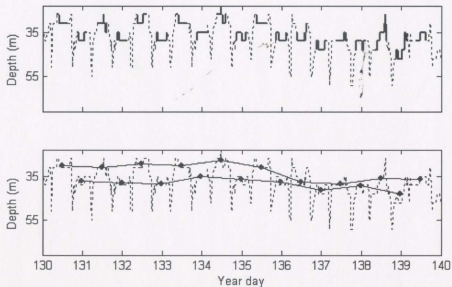


Figure 5.2.4 Data from a 10 day period at Trinity Bay 2002 mooring A. Top: biomass median depth with 6-hour intervals centred at noon and midnight highlighted. Bottom: day and night time series derived by averaging the biomass median depth over the 6-hour intervals shown above.

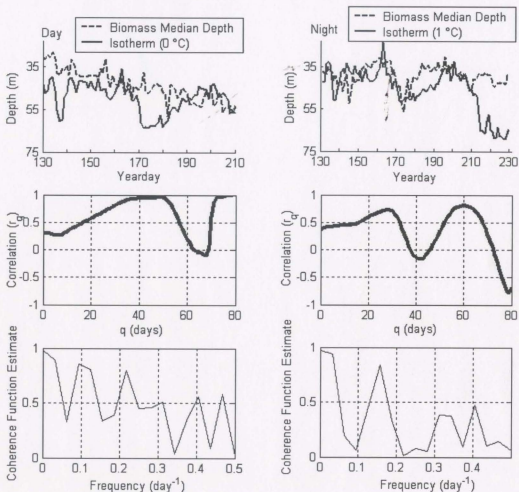


Figure 5.2.5 Trinity Bay 2002 mooring A. Left column shows day time series, and right column shows night time series. Top: biomass median depth and isotherm depth (0 °C for day and 1 °C for night). Middle: correlation between the two time series as a function of time scale q , the time scale at which the running average is taken. Bottom: coherence between the power spectra of biomass median depth and isotherm depth.

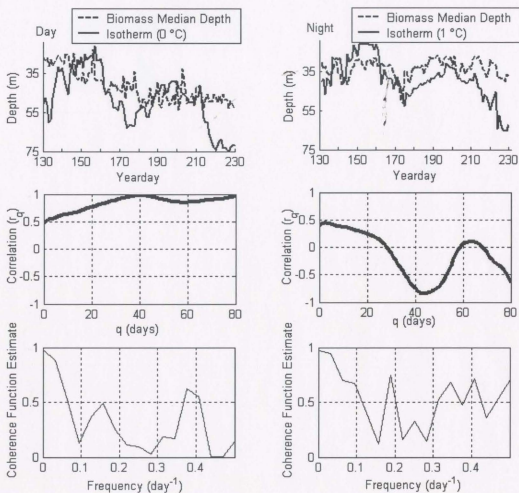


Figure 5.2.6 Trinity Bay 2002 mooring C. Left column shows day time series, and right column shows night time series. Top: biomass median depth and isotherm depth (0°C for day and 1°C for night). Middle: correlation between the two time series as a function of time scale q , the time scale at which the running average is taken. Bottom: coherence between the power spectra of biomass median depth and isotherm depth.

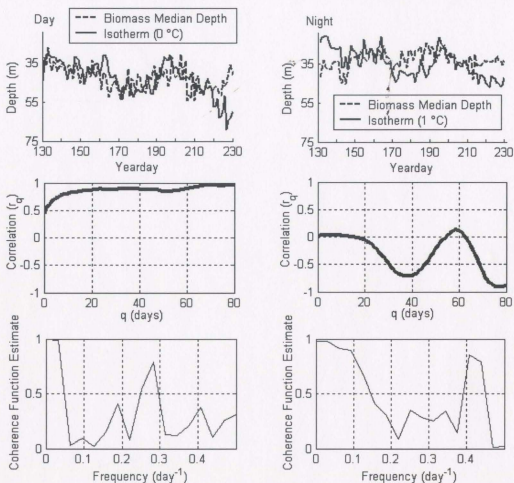


Figure 5.2.7 Trinity Bay 2002 mooring D. Left column shows day time series, and right column shows night time series. Top: biomass median depth and isotherm depth (0 °C for day and 1 °C for night). Middle: correlation between the two time series as a function of time scale q , the time scale at which the running average is taken. Bottom: coherence between the power spectra of biomass median depth and isotherm depth.

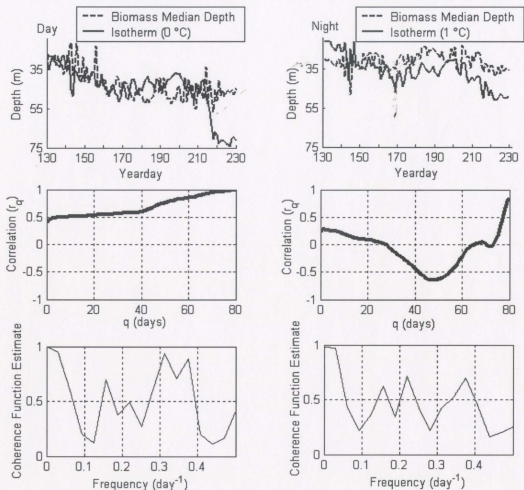


Figure 5.2.8 Trinity Bay 2002 mooring E. Left column shows day time series, and right column shows night time series. Top: biomass median depth and isotherm depth (0 °C for day and 1 °C for night). Middle: correlation between the two time series as a function of time scale q , the time scale at which the running average is taken. Bottom: coherence between the power spectra of biomass median depth and isotherm depth.

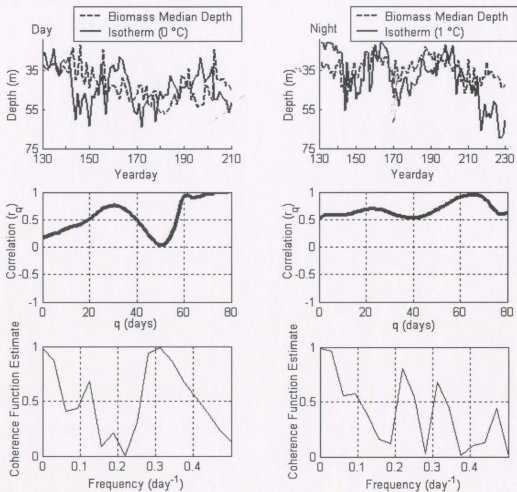


Figure 5.2.9 Trinity Bay 2002 mooring F. Left column shows day time series, and right column shows night time series. Top: biomass median depth and isotherm depth (0 °C for day and 1 °C for night). Middle: correlation between the two time series as a function of time scale q , the time scale at which the running average is taken. Bottom: coherence between the power spectra of biomass median depth and isotherm depth.

5.3 Anomalies

This section identifies and briefly discusses anomalies, presenting no analysis. These can be considered points of possible further inquiry for the 2005 and 2006 field seasons of the capelin ecosystem strategic project and other studies related to zooplankton migration. They are points of interest in particular because similar phenomena have been observed in other studies.

Reverse migration

Some of the ADCP data show what appear to be instances of reverse migration. This migration is the inverse of normal nocturnal migration, with daylight hours spent at the surface and night hours spent at depth. One explanation is a corollary of the predation avoidance hypothesis of diel vertical migration. If carnivorous zooplankton are migrating nocturnally, avoiding predators, then their zooplankton prey will adopt reverse migration to avoid the nocturnally migrating carnivorous zooplankton (Hays, 2003; Lampert, 1989).

On occasion, the column of abnormally large velocity measurements caused by strongly upward migrating zooplankton is immediately followed by a similar column of strong downward velocity values. In the corresponding backscatter data, there sometimes appears to be a faint descending scattering layer (Fig 5.3.1 a, b). Though these features are difficult to perceive at this low temporal resolution, they have an effect on methods used for quantifying scattering layers. For example, the strong downward velocities in the vertical velocity data truncate the migration path of the scattering layer derived from the adjusted Heywood simulation method (Fig 5.3.1 c). The flux-velocimetry method

captures this downward velocity, but it is weaker than in the measured vertical velocity data (Fig 5.3.1 d).

The phenomena that appear to be reverse migration are rarely seen in these data, occurring only 2 to 5 times during a 100 day deployment. If they are occurring on a daily basis, the configuration of the ADCP is such that they are obscured by the dominant nocturnally migrating zooplankton. This may be due to ADCP signal frequency, low spacial or temporal resolution, or the restriction of the ADCP range to the upper portion of the water column. In general, they are more apparent in the Trinity Bay deployments than in the other deployments.

Midnight sinking

Some nocturnal migrators have been observed to ascend to the surface at night, then descend somewhat during the middle hours of the night, and ascend again just before the morning descent to depth. This is known as twilight migration, or midnight sinking, and has been observed for certain stages of *Calanus finmarchicus* (Cushing, 1951). This behaviour is apparent on occasion in the Trinity Bay data (Fig 5.3.2). No clear relationship between midnight sinking and the lunar cycle was found using any of the quantification techniques. Such anomalies serve to illustrate the complexity of the problem of migration, the diversity of migration patterns, and the limitations of single-frequency acoustic observation and analysis.

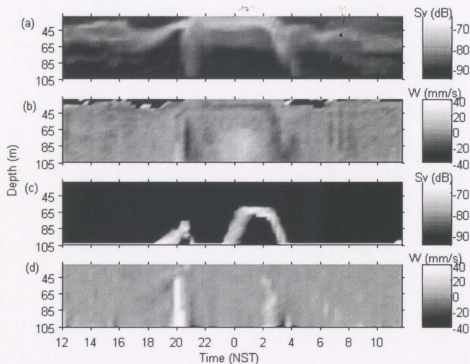


Figure 5.3.1 Data anomaly that appears to be reverse migration, Trinity Bay 2001 mooring A, year day 198-199. Backscatter coefficient (a) and vertical velocity data (b) from ADCP, showing downward migration immediately following upward migration at 20:00. Simulations of backscatter intensity using the adjusted Heywood method (c) and of vertical velocity using the flux-velocimetry method with the bootstrap correction (d).

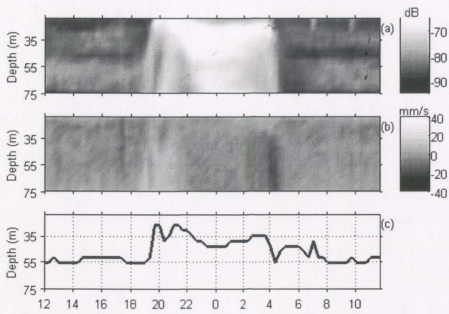


Figure 5.3.2 Data anomaly that appears to be midnight sinking, Trinity Bay 2002 mooring D, year day 234-235. Backscatter coefficient (a) and vertical velocity data (b) from ADCP, showing moderate sinking of the strong scattering layer just after 20:00 NST. Calculation of the biomass median depth (c) shows a similar path.

CHAPTER 6: EMPIRICAL MODEL AND CONCLUSIONS

Models of migrating zooplankton typically attempt to model layer depth, and sometimes thickness, as a function of the cues believed to influence migration (Fisken & Giske, 1995; Han & Straškraba, 1998, 2001). Such a model is inappropriate in this case because it would rely on too many assumptions about the portion of the water column below the ADCP, where no data were collected. Instead, the model focuses on only the upper portion of the water column.

Backscatter coefficient in time and depth is modelled as a function of the known physical variables: light, and temperature. An attempt is made to reconstruct a backscatter array based on the data on these variables and an empirically determined functional response. The modelled backscatter is then compared to the backscatter measured by the ADCP. The comparison gives an interpretation of how much variability can be explained by these physical cues, and how much remains unexplained. Following the model is a discussion of the results and conclusions of this project.

6.1 Model

The objective of the model is to generate a predicted backscatter coefficient, S_v' , based on the measured physical properties of the surrounding water. An empirical approach is taken, based on the observed responses by scatterers to changes in light intensity and temperature. The level of accuracy with which the model reproduces the measured backscatter data gives an indication of how much migration variation is due to

changing physical conditions. The variation not represented in the model is likely due to other factors not represented in the available data, such as food availability and the presence of predators.

Temperature-depth signature

In the following model formulation, functions will be denoted using boldface font, and independent variables using normal font. Measured backscatter, $S_v(t,z)$ is a function of time t and depth z (positive downward). Thermistor data also provide an associated temperature, $T(t,z)$, at each time and depth.

Depth is considered to play a role in migrator response to temperature and light because of the vertical stratification of the ocean in terms of temperature, pressure, illumination, food availability, and other factors important to zooplankton life. For example, a migrator that tends to depths near or below the thermocline would be accustomed to temperatures between -1 and 1 °C, whereas a migrator that spends a substantial amount time nearer the surface would be exposed to a much wider range of temperatures. Because of the dependence on depth, each 4-metre depth bin is considered separately.

A “temperature-depth signature” is an empirical function that gives a mean backscatter value as a function of temperature and depth. It is constructed by averaging, for each (T, z) pair, all S_v values in the data associated with that temperature and depth:

$$S_{TZ}(T, z) = \frac{\sum_{t=1}^n S_v(t, z) \theta_T(t)}{\sum_{t=1}^n \theta_T(t)}, \quad (6.1)$$

where $\theta_T(t) = 1$ if $T(t, z) = T$, and 0 otherwise; n is the number of data points in the time series. Because scattering layer composition differs greatly between day and night, data are divided into day and night portions as in § 5.2, using the 6 hours centred at day-normalized noon and midnight respectively. The day and night temperature-depth signatures are each calculated separately, so that

$$S_{TZ \text{ day}}(T, z) = \frac{\sum_{t=1}^n S_v(t, z) \theta_T(t) \delta_{\text{day}}(t)}{\sum_{t=1}^n \theta_T(t) \delta_{\text{day}}(t)}, \quad (6.2)$$

where $\delta_{\text{day}}(t) = 1$ if t is in the 6 hours centred at day-normalized noon, and 0 otherwise.

$S_{TZ \text{ night}}$ is defined analogously.

In the numerical formulation, depth is divided by 4 m bins to match the ADCP resolution. Temperature values are divided by 0.1 °C bins centred at multiples of 0.1 °C. The resulting signatures show qualitatively the temperature preference of scatterers at any given depth, by day and by night (Fig 6.1.1 – 6.1.3). Temperature frequency distributions at each depth are included to give a relative indication of the number of S_v values averaged for each (T, z) pair.

The Trinity Bay 2002 moorings have the most complete data for this analysis, having temperature data through the entire range of the ADCP. There are some consistent patterns seen in the temperature-depth signatures, showing apparent trends in

the response by migrators to temperature. There is also some variability for which interpretation is difficult. Three moorings are included here as examples.

The temperature-depth signatures for the day time, S_{Tzday} , (Figs 6.1.1 – 6.1.3 tops) all indicate that migrators avoid warm temperatures near the surface. In the depth range of 20 – 40 m, temperatures can range from about -1 to 15 °C. However, for temperatures above 5 °C, backscatter is very low (less than -90 dB). This implies that during the day, migrators tend to inhabit this depth range only when temperatures are relatively low and avoid it otherwise.

At depths below 50 m, the day time behaviour is different, and not consistent throughout all moorings. Moorings C and E (Figs 6.1.1 and 6.1.3 resp.) show a drop in backscatter intensity for temperatures less than -1 °C, suggesting that migrators are avoiding very cold temperatures. However, mooring D (Fig 6.1.2) shows a slight increase at these low temperatures.

The temperature-depth signatures for the night time, $S_{Tznights}$, (Figs 6.1.1 – 6.1.3 bottoms) show different behaviour. Mooring E (Fig 6.1.3 bottom) shows the same aversion to high temperatures near the surface, though to a lesser degree. In the deeper water, high backscatter intensity is associated with both the maximum and minimum temperatures for all moorings, and lower backscatter values are associated with the intermediate temperature range. Though fairly consistent, the causes underlying this pattern are uncertain. It may represent two distinct groups of migrators with different temperature preferences.

Construction of backscatter array

The modelled backscatter array is constructed based on the response to temperature and light. Response to temperature is determined by the temperature-depth signatures described above, separately for day and night. Response to light determines the timing of the transition between day and night.

The timing of the day-night transition is determined at each depth using the method applied in § 5.2—by locating the time of the maximum S_v gradient. The dependence of timing on cloud cover established in § 5.2 is approximated using linear regression between timing on clear days compared with overcast days (approximately a 20 minute difference). This gives the timing of ascent, $t_A(C_A, z)$, and the timing of descent, $t_D(C_D, z)$, as functions of cloud cover during ascent C_A , cloud cover during descent C_D , and depth. These two values of timing determine at each depth, and for each day, which points are associated with day time, and which points are associated with night time.

A simulated backscatter array, S_v' , is then modelled based on these empirical functions. At any time t and depth z , there is an associated temperature, $T(t, z)$. The simulated backscatter value assigned is based on the temperature-depth signature value, either $S_{TZ\text{day}}(T(t, z), z)$ or $S_{TZ\text{night}}(T(t, z), z)$. Timings of ascent and descent, t_A and t_D , determine whether the day or night temperature-depth signature is used. That is, each day is modelled by:

$$S_v'(t, z) = \left\{ \begin{array}{ll} S_{TZ\text{day}}(T(t, z), z) & \text{if } t_D(C_D, z) < t < t_A(C_A, z) \\ S_{TZ\text{night}}(T(t, z), z) & \text{otherwise} \end{array} \right\}. \quad (6.3)$$

For any (T, z) pairs not represented in the temperature-depth signatures, the missing values are linearly interpolated.

The final product is a backscatter array constructed based on temperature, depth, and cloud cover (Fig 6.1.4). The temperature-depth signatures used here are constructed from the entire deployment duration, but this is not necessary. It is possible to construct long periods of modelled backscatter based on just a few days of ADCP data provided that the temperature and cloud data are available.

Cross sections of S_v' along a constant depth show that although the average S_v value is modelled well, the high frequency variation is not (Figs 6.1.5, 6.1.6). Furthermore, strong S_v values that occur during twilight transitions are not modelled. This can be seen in the difference between the daily averages (Fig 6.1.7), and is due to the fact that the transition between day and night at any given depth is modelled as being instantaneous. Otherwise, the daily averages are very close.

The intent of the model is to simulate the distribution of scatterers in the water column. A quantitative assessment can be made by calculating the biomass median depth and comparing it to that of the measured backscatter. The result is that the high frequency variation is lost in the simulation, but the average value across a day or night is accurately simulated (Fig 6.1.8). Therefore the correlation between the two series is low ($r \approx 0.5$), but the correlations between day series and between night series, constructed as in § 5.2, are consistently higher ($r \approx 0.7$), confirming the low-frequency influence of temperature found in § 5.2. The averages of the simulated and measured time series are also always within 1 m of each other, at an order of magnitude smaller than the grid size,

indicating that the average distribution of scatterers is simulated well (Table 6.1.1).

The fact that higher frequency variations in scatterer distribution are modelled poorly is expected. The two physical cues examined in this study—light and temperature—typically have little variation during the day or during the night. Higher frequency changes in scattering layer depth are most likely due to other cues, such as the sudden presence or absence of predators.

The strategy here of reproducing the entire backscatter array, rather than simply modelling layer depth as a function of time, was followed because of the vertical limitation of the ADCP data. The strategy is still applicable to data that span the entire water column, and its results can be reduced to a single time series that represents layer depth as a function of time. It is, however, more calculation-intensive than a simpler functional approach. Further refining of this model based on more empirical data could produce a good tool for estimating low frequency trends in scatterer distribution based on temperature and light data. The model can also be easily modified to incorporate additional variables representing other factors that may influence scatterer distribution.

Mooring	Mean difference (m)	St. dev. difference (m)	Correlation coefficients (r)		
			Whole series	Day series	Night series
A	-0.41	6.54	0.52	0.72	0.74
B	0.6	6.88	0.51	0.73	0.75
C	-0.53	6.86	0.57	0.82	0.6
D	0.07	7.12	0.55	0.39	0.4
E	-0.03	7.12	0.64	0.81	0.6
F	-0.13	8.58	0.47	0.37	0.68

Table 6.1.1 Trinity Bay 2002, all moorings. Comparisons between the biomass median depth of measured backscatter data and that of simulated backscatter data. The difference used for the mean and standard deviation is *simulated - observed*. The day series and night series are constructed as in § 5.2.

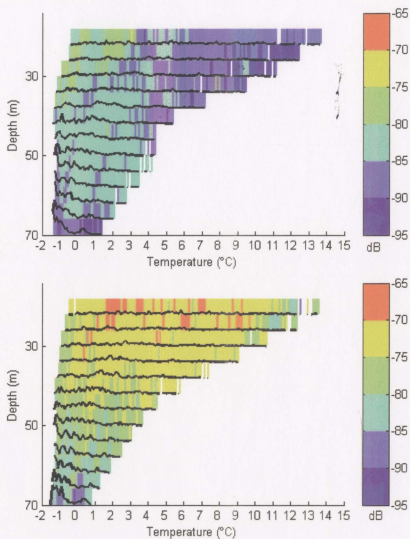


Figure 6.1.1 Trinity Bay 2002 mooring C. Temperature-depth signature of S_v values. Colour plot shows the average S_v value for each temperature-depth pair. Solid lines show the distribution of temperature values at each depth. Averages are taken over the entire deployment period. Top: day. Bottom: night.

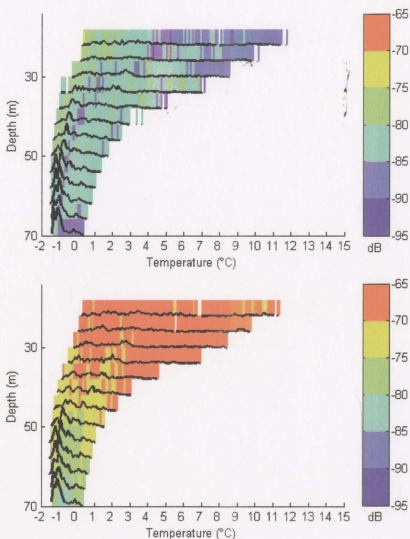


Figure 6.1.2 Trinity Bay 2002 mooring D. Temperature-depth signature of S_v values.

Colour plot shows the average S_v value for each temperature-depth pair. Solid lines show the distribution of temperature values at each depth. Averages are taken over the entire deployment period. Top: day. Bottom: night.

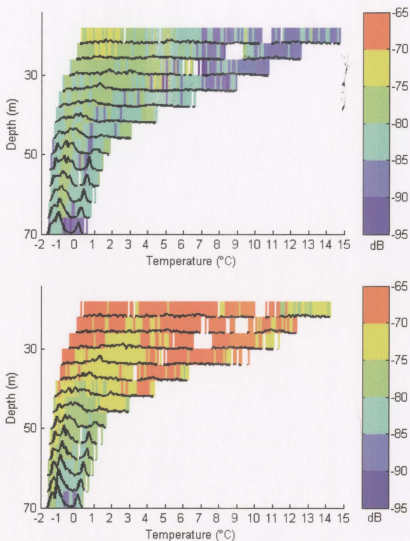


Figure 6.1.3 Trinity Bay 2002 mooring E. Temperature-depth signature of S_v values.

Colour plot shows the average S_v value for each temperature-depth pair. Solid lines show the distribution of temperature values at each depth. Averages are taken over the entire deployment period. Top: day. Bottom: night.

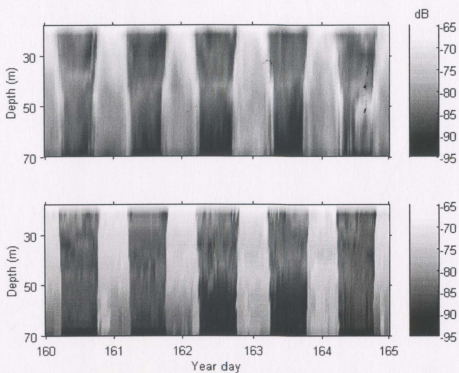


Figure 6.1.4 Trinity Bay 2002 mooring A. Top: measured backscatter. Bottom: simulated backscatter using empirical model.

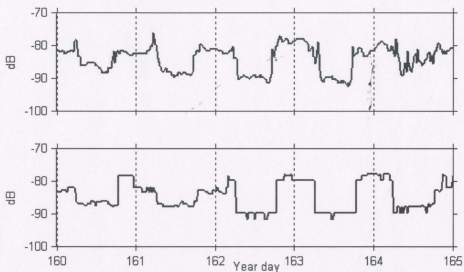


Figure 6.1.5 Trinity Bay 2002 mooring A. Measured (top) and modelled (bottom) backscatter at a depth of 55 m.

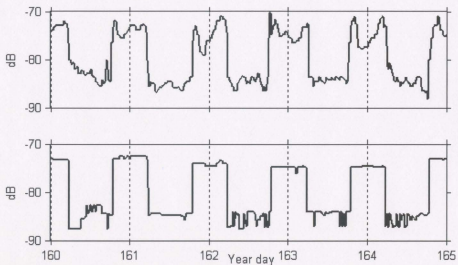


Figure 6.1.6 Trinity Bay 2002 mooring A. Measured (top) and modelled (bottom) backscatter at a depth of 30 m.

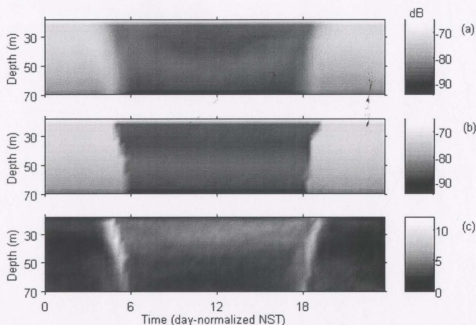


Figure 6.1.7 Trinity Bay 2002 mooring A. Daily average of measured backscatter (a), modelled backscatter (b), and absolute value of difference (c).

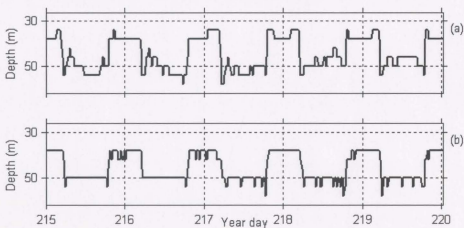


Figure 6.1.8 Trinity Bay 2002 mooring A. Biomass median depth of measured backscatter (a) and simulated backscatter (b).

6.2 Conclusions

In the absence of ADCP calibration and taxonomic differentiation, it is often the case that bioacoustic data are restricted to qualitative applications. However, quantitative analysis of bioacoustic data in the absence of taxonomic data can be a valuable tool in examining the behaviour of the scattering layer as a whole for a number of reasons:

1. The bioacoustic data collection is not as time intensive as sampling and does not disrupt the water column;
2. Bioacoustic data are also often collected automatically with physical data, as is the case with ADCPs, and are often part of standard data collection during surveys, sometimes without complementary tow data;
3. Results from modelling and species-specific laboratory studies are often difficult to integrate with *in situ* DVM patterns because of the complexity of the migrating zooplankton community;
4. Large scale ecosystem projects, such as the capelin ecosystem strategic project, often require simplifications to be made. It is not practical, for example, to model every trophic interaction within a complex zooplankton community.

In order to interpret the bioacoustic data, reliable methods of quantification are developed. These methods have been catalogued in Chapter 4. This includes methods found in the literature as well as methods developed for this thesis. Brief comparison and assessment of these methods show that each may be better suited to a different purpose, and so appropriate consideration should be made before interpreting bioacoustic data. A detailed review using data that span the entire water column would be a useful reference

for future studies of this kind.

Applying methods of quantification to bioacoustic data allows for statistical comparisons to environmental data. Significant relationships between migration behaviour and the available temperature and cloud data were found, as well as horizontal spacial correlations between moorings. Application of techniques for quantification yielded the following results.

1. **Migration velocities** – Measured descent velocities were consistently higher than measured ascent velocities, particularly in Trinity Bay. This is likely related to the negative buoyancy of the animals. With detailed information on the size, morphology, and swimming behaviour of the zooplankton, this velocity difference can be interpreted in the context of the theoretical argument presented in § 2.1.

2. **Relative biomass index** - A strong relationship was found between backscatter intensity (S_v) and observed dry weight of zooplankton collected with a bongo net ($r^2 = 0.77$). This relationship essentially represents a difference between depth-integrated night and day data. The tow data were not directed toward the purpose of correlating backscatter to dry weight, so the method of determining the relationship relied on assumptions about the spatial and temporal persistence of the diel pattern. The resulting conversion from backscatter to biomass is an index that is considered to be accurate in a relative sense, but not in an absolute sense.

3. **Horizontal homogeneity** - Correlations between quantifications at moorings were found to decrease with increasing distance between moorings. The same relationship held when comparing beams within the same mooring. This type of analysis can be used in determining how much horizontal area should be represented by a single mooring. These results indicate a high correlation even at a separation distance of 10s of km for the average daily pattern ($r \approx 0.9$), but a lower correlation for seasonal variations on the same horizontal scale ($r \approx 0.7$).

4. **Response to cloud cover** - The uncertainty inherent in using cloud cover data to represent light (see § 2.2, 4.2) limited analysis to a comparison between clear and overcast days. On overcast days, migrators ascended approximately 20 minutes earlier and descended approximately 20 minutes later than on clear days. This implies that zooplankton are maximizing time spent at the surface under darkness. It also suggests that a threshold light level, rather than a change in light level or endogenous rhythms, cues migration. This is consistent with the predation avoidance hypothesis of DVM, suggesting that zooplankton leave the surface waters in response to the threat of visually hunting predators.

Of the various tools for quantifying migration timing, the most effective for this analysis was an edge detection algorithm, identifying timing by the time of the maximum and minimum gradients dS/dt along a range of depths. The methods of converting backscatter to a single layer, such as biomass median depth, were highly influenced by the truncation of data below the ADCP, particularly during migration events, so these

methods were not useful in quantifying migration timing. They should not be disregarded for this purpose, however, until they are tested on data that include the entire migration cycle.

The high statistical significance of the relationship between timing and cloud cover warrants further investigation. If more refined and location-specific light data were collected at the sea surface, rather than relying on cloud data from a distant weather station, it may be possible to find a functional response by migrators to light level. It is also important to determine whether the ADCP is observing predominantly one type of zooplankton, or if a diverse community is being tracked. It is possible that many types of zooplankton coordinate migration timing with each other to a fairly high temporal resolution since carnivorous zooplankton rely on smaller zooplankton for food.

5. **Response to temperature** - A strong relationship was found between scattering layer depth and isotherms depth on time scales of 20 days or more. This suggests that temperature plays a role in determining the preferred depth toward which migrators tend during times between migration events. In the Trinity Bay 2002 data, there was also a clear response by migrators to an abrupt change in temperature stratification around year day 170.

The response to temperature was expected to occur on a longer time scale than the response to light because of the driving influence of light on the migration cycle. Different types of zooplankton have been seen to have different thermal preferences (Geller, 1986), and taxonomic differentiation was not possible for most of the data.

These methods of analysis could also be applied to more taxonomically detailed data to determine more specific responses to temperature by certain types of zooplankton.

The Model

The strategy of modelling the entire backscatter array, rather than simply the layer depth or thickness, was adopted because of the limited range of ADCP data. Although it is more calculation intensive, this method produces a good simulation that illustrates the extent to which scatterer distribution is a function of light and temperature. High frequency fluctuations are not simulated well, and it is believed that these fluctuations are caused by other factors, such as predation. The model is applicable to more complete data sets, and it can be easily adapted to incorporate other cues believed to influence migration.

Future considerations

Because of constraints in resources, this thesis relied largely on data originally collected for other purposes. The methods of quantification and analysis were developed to be robust enough to deal with imperfect data sets. However, for future studies, the following pieces of data should be considered. These considerations will be accounted for in the 2005 field season for the capelin ecosystem project.

1. **Acoustic data spanning the full water column** - The truncation of data below the ADCP depth restricted analysis. Techniques for quantification and analysis are

expected to be more effective when the entire migration cycle is recorded. However, this limitation of the data was valuable in developing robust quantification techniques. The convenience and availability of bioacoustic data is countered by the fact that collection of these data is not always honed to a specific purpose. It is therefore important for these quantification and analysis techniques to be applicable to imperfect and incomplete data sets.

2. **More complete temperature and light data** - The entire spacial range viewed by the ADCP was not always covered by thermistors. This made the temperature response difficult to determine, particularly for the Trinity Bay 2001 deployment. Ideally, the entire water column should be represented.

Relying on cloud cover as an indicator of light intensity led to some degree of uncertainty. Light data should be measured directly, rather than relying on cloud data, and should be taken closer to the moorings.

3. **Directed tows near the ADCP mooring** - It is important to determine what organisms make up the observed scattering layers during various times of the day. A fairly high correlation between backscatter and copepod biomass was found. However, the sampling technique used bongo nets, designed specifically to sample copepods. Other zooplankton may be present, and taxonomic differentiation may explain different migratory behaviours of the scattering layers. Furthermore, the tow data used were taken as part of a survey over a very large region, and without specific attention paid to time of

day. A sampling regime should be designed for the mooring location with specific attention paid to nautical twilight times.

REFERENCES

- Alcaraz, M. and J. R. Strickler, 1988. Locomotion in copepods: pattern of movements and energetics of *Cyclops*. *Hydrobiologia*, **167/168**, 409-414.
- Ashjian, C. J., S. L. Smith, C. N. Flagg, A. J. Mariano, W. J. Behrens, P. V. Z. Lane, 1994. The influence of a Gulf Stream meander on the distribution of zooplankton biomass in the Slope Water, the Gulf Stream, and the Sargasso Sea, described using a shipboard acoustic Doppler current profiler. *Deep-Sea Research I*, **41(1)**, 23-50.
- Ashjian, C. J., S. L. Smith, C. N. Flagg, and C. Wilson, 1998. Patterns and occurrence of diel vertical migration of zooplankton biomass in the Mid-Atlantic Bight described by an acoustic Doppler current profiler. *Continental Shelf Research*, **18**, 831-858.
- Ashjian, C. J., S. L. Smith, C. N. Flagg, and N. Idrisi, 2002. Distribution, annual cycle, and vertical migration of acoustically derived biomass in the Arabian Sea during 1994-1995. *Deep-Sea Research II*, **49**, 2377-2402.
- Bosch, H.F., and W.R. Taylor, 1973. Diurnal Vertical Migration of an Estuarine Cladoceran, *Podon polyphemoides*, in the Chesapeake Bay. *Marine Biology*, **19**, 172-181.
- Brierley, A. S., M. A. Brandon, and J. L. Watkins, 1998. An assessment of the utility of an acoustic Doppler current profiler for biomass estimation. *Deep-Sea Research I*, **45**, 1555-1573.
- Budyko, M.I., 1974. *Climate and Life*. Academic Press, Inc., pp. 45-48.
- Bundy, M. H., T. F. Gross, D. J. Coughlin, and J. R. Strickler, 1993. Quantifying copepod searching efficiency using swimming pattern and perceptive ability. *Bulletin of Marine Science*, **53(1)**, 15-28.
- Burks, R. L., D. M. Lodge, E. Jeppesen, and T. L. Lauridsen, 2002. Diel horizontal migration of zooplankton: costs and benefits of inhabiting the littoral. *Freshwater Biology*, **47**, 343-365.
- Buskey, E. J., C. Coulter, and S. Strom, 1993. Locomotory patterns of microzooplankton: potential effects on food selectivity of larval fish. *Bulletin of Marine Science*, **53(1)**, 29-43.
- Carscadden, J. E., B. S. Nakashima, and K. T. Frank, 1997. Effects of fish length and temperature on the timing of peak spawning capelin (*Mallotus villosus*). *Can. J.*

Fish. Aquat. Sci., **54**, 781-787.

- Carscadden, J. E., K. T. Frank, and W. C. Leggett, 2001. Ecosystem changes and the effects on capelin (*Mallotus villosus*), a major forage species. *Can. J. Fish. Aquat. Sci.*, **58**, 73-85.
- Chatfield, C., 1996. *The Analysis of Time Series, An Introduction*, Fifth edition. CHAPMAN & HALL/CRC, p. 142.
- Clark, C. W., and D. A. Levy, 1988. Diel vertical migrations by juvenile sockeye salmon and the antipredation window. *The American Naturalist*, **131(2)**, 271-290.
- Clarke, G.L., 1930. Change of phototropic and geotropic signs in *Daphnia* induced by changes of light intensity. *J. Exp. Biol.*, **7(2)**, 109-131.
- Clarke, G. L., 1932. Quantitative aspects of the change of phototropic sign in *Daphnia*. *J. Exp. Biol.* **9**, 180-211.
- Cushing, D. H., 1951. The vertical migration of planktonic Crustacea. *Biological Reviews*, **26**, 158-192.
- Dalley, E. L., J. T. Anderson, and D. J. Davis, 2001. Decadal Time-Series of Invertebrate Zooplankton on the Newfoundland Shelf and Grand Banks 1991-1999. Canadian Science Advisory Secretariat, Res. Doc. 2001/110, 1-29.
- Deines, K. L., 1999. Backscatter estimation using broadband acoustic Doppler current profilers. *Proceeding of the IEEE 6th working conference on current measurement, San Diego, CA*, 249-253.
- Dodson, S., 1988. The ecological role of chemical stimuli for the zooplankton: Predator-avoidance behavior in *Daphnia*. *Limnol. Oceanogr.*, **33(6, part 2)**, 1431-1439.
- Enright, J. T., 1977a. Problems in estimating copepod velocity. *Limnol. Oceanogr.* **22**, 160-162.
- Enright, J. T., 1977b. Diurnal vertical migration: Adaptive significance and timing. Part 1. Selective advantage: A metabolic model. *Limnol. and Oceanogr.*, **22(5)**, 856-872.
- Enright, J. T., and H.-W. Honegger, 1977. Diurnal Diurnal vertical migration: Adaptive significance and timing. Part 2. Test of the model: Details of timing. *Limnol. and Oceanogr.*, **22(5)**, 873-886.
- Environment Canada, 2004. REFERENCE GUIDE TO THE AUTOMATED

WEATHER OBSERVATION SYSTEM (AWOS) SECOND EDITION January 2004. Originating Authority: Atmospheric Monitoring and Water Survey Directorate, Issued Under the Authority of the Assistant Deputy Minister. http://www.msc-smc.ec.gc.ca/msb/manuals/awos/chap1_e.html#1210_e

- Fielding, S., G. Griffiths, and H. S. J. Roe, 2004. The biological validation of ADCP acoustic backscatter through direct comparison with net samples and model predictions based on acoustic-scattering models. *ICES Journal of Marine Science*, **61**, 184-200.
- Fisken, Ø., and J. Giske, 1995. Vertical distribution and population dynamics of copepods by dynamic optimization. *ICES J. mar. Sci.*, **52**, 483-503.
- Flagg, C. N., and S. L. Smith, 1989. On the use of the acoustic Doppler current profiler to measure zooplankton abundance. *Deep-Sea Research*, **36(3)**, 455-474.
- Flagg, C. N., C. D. Wirick, and S. L. Smith, 1994. The interaction of phytoplankton, zooplankton and currents from 15 months of continuous data in the Mid-Atlantic Bight. *Deep-Sea Research II*, **41(2/3)**, 411-435.
- Forward, R. B. Jr., 1988. Diel vertical migration: zooplankton photobiology and behaviour. *Oceanogr. Mar. Biol. Annu. Rev.*, **26**, 361-393.
- Gabriel, W. and B. Thomas, 1988. Vertical Migration of Zooplankton as an Evolutionarily Stable Strategy. *The American Naturalist*, **132** No. 2, 199-216.
- Gal, G., E. R. Loew, L. G. Rudstam, and A. M. Mohammadian, 1999. Light and diel vertical migration: spectral sensitivity and light avoidance by *Mysis relicta*. *Can. J. Fish. Aquat. Sci.*, **56**, 311-322.
- Garthe, S., S. Benvenuti, and W. A. Montevecchi, 2003. Temporal patterns of foraging activities of northern gannets, *Morus bassanus*, in the northwest Atlantic Ocean. *Can. J. Zool.*, **81**, 453-461.
- Geller, W., 1986. Diurnal vertical migration of zooplankton in a temperate great lake (L. Constance): A starvation avoidance mechanism? *Arch. Hydrobiol.*, **Suppl. 74**, 1-60.
- Gill, C. W., 1987. Recording the beat patterns of the second antennae of calanoid copepods, with a micro-impedance technique. *Hydrobiologia*, **148**, 73-78.
- Gliwicz, M. Z., 1986. Predation and the evolution of vertical migration in zooplankton. *Nature*, **320**, 746-748.

- Greene, C. H., 1988. Foraging tactics and prey-selection patterns of omnivorous and carnivorous calanoid copepods. *Hydrobiologia*, **167/168**, 295-302.
- Hairston, N. G. Jr., 1976. Photoprotection by carotenoid pigments in the copepod *Diatomus nevadensis*. *Proc. Nat. Acad. Sci. USA*, **73(3)**, 971-974.
- Han, B-P., and M. Straškraba, 1998. Modeling patterns of zooplankton diel vertical migration. *Journal of Plankton Research*, **20**, 1463-1487.
- Han, B-P., and M. Straškraba, 2001. Control Mechanisms of Diel Vertical Migration: Theoretical Assumptions. *J. theor. Biol.*, **210**, 305-318.
- Hays, G. C., 2003. A review of the adaptive significance and ecosystem consequences of zooplankton diel vertical migrations. *Hydrobiologia*, **503**, 163-170.
- Hein, R. G., D. M. Krueger, and S. Richman, 1993. Feeding and energy relations in *Daphnia galeata mendotae*. *Bulletin of Marine Science*, **53(1)**, 115-127.
- Heywood, K. J., 1996. Diel vertical migration of zooplankton in the Northeast Atlantic. *Journal of Plankton Research*. **18(2)**, 163-184.
- Heywood, K. J., S. Scrope-Howe, and E. D. Barton, 1991. Estimation of zooplankton abundance from shipborne ADCP backscatter. *Deep-Sea Research*, **38(6)**, 677-691.
- Hirche, H. J., 1987. Temperature and plankton. II. Effect on respiration and swimming activity in copepods from the Greenland Sea. *Marine Biology*, **94**, 347-356.
- Holliday, D. V., and R. E. Pieper, 1995. Bioacoustical oceanography at high frequencies. *ICES J. mar. Sci.*, **52**, 279-296.
- Hugie, D. M., and L. M. Dill, 1994. Fish and game: a game theoretic approach to habitat selection by predators and prey. *Journal of Fish Biology*, **45** (Supplement A), 151-169.
- Hutchison, G. E., 1967. A treatise on limnology, Volume I, Geography, Physics, and Chemistry. John Wiley & Sons, Inc., pp. 725-779.
- IPCC**, 2001: *Climate Change 2001: Synthesis Report. A Contribution of Working Groups I, II, and III to the Third Assessment Report of the Intergovernmental Panel on Climate Change* [Watson, R.T. and the Core Writing Team (eds.)]. Cambridge University Press, Cambridge, United Kingdom, and New York, NY, USA, 398 pp.

- Iwasa, Y., 1982. Vertical migration of zooplankton: a game between predator and prey. *The American Naturalist*, **120**(2), 171-180.
- Jiang, H., T. R. Osborn, and C. Meneveau, 2002. The flow field around a freely swimming copepod in steady motion. Part I: Theoretical analysis. *Journal of Plankton Research*, **24**(3), 167-189.
- Kerfoot, W. B., 1970. Bioenergetics of vertical migration. *The American Naturalist*, **104**(940), 529-546.
- Kirk, J. T., 1994. Light and Photosynthesis in Aquatic Ecosystems. 2nd edition, Cambridge University Press, pp. 31-33
- Klyashtorin, L. B., and A. A. Yarzhombek, 1973. Energy consumption in movement of planktonic organisms. *Oceanology*, **13**, 575-580.
- Kundu, P. K., and I. M. Cohen, 2002. Fluid Mechanics, Second Edition. Elsevier Science. pp. 260, 264-266, 297-302.
- Lalli, C. M., and T. R. Parsons, 1993. Biological Oceanography: an Introduction. Pergamon Press. p. 81, 100-101, 107
- Lampert, W., 1989. The adaptive significance of diel vertical migration of zooplankton. *Functional Ecology*, **3**, 21-27.
- Lampert, W., R.-D. Schmitt, and P. Muck, 1988. Vertical migration of freshwater zooplankton: test of some hypotheses predicting a metabolic advantage. *Bulletin of Marine Science*, **43**(3), 620-640.
- Large, W. G., and S. Pond, 1981. Open Ocean Momentum Flux Measurements in Moderate to Strong Winds. *Journal of Physical Oceanography*, **11**, 324-336.
- LaRow, E. J., 1970. The effect of oxygen tension on the vertical migration of *Chaoborus* larvae. *Limnology and Oceanography*, **15**, 357-362.
- Lehman, J. T., 1977. On calculating drag characteristics for decelerating zooplankton. *Limnol. Oceanogr.* **22**, 170-172.
- Leishman, J. G., 2000. Principles of helicopter aerodynamics. Press Syndicate of the University of Cambridge, pp. 33-42.
- Liu, S-H., S. Sun, and B-P. Han, 2003. Diel vertical migration of zooplankton following optimal food intake under predation. *Journal of Plankton Research*, **25**, 1069-1077.

- Lorke, A., D. R. McGinnis, P. Spaak, and A. Wüest, 2004. Acoustic observations of zooplankton in lakes using a Doppler current profiler. *Freshwater Biology*, **49** (10), 1280-1292.
- Lougee, L. A., S. M. Bollens, and S. R. Avent, 2002. The effects of haloclines on the vertical distribution and migration of zooplankton. *Marine Biology*, **278**, 111-134.
- Luo, J., P. B. Ortner, D. Forcucci, S. R. Cummings, 2000. Diel vertical migration of zooplankton and mesopelagic fish in the Arabian Sea. *Deep-Sea Research II*, **47**, 1451-1473.
- MacLennan, D. N., and D. V. Holliday, 1996. Fisheries and plankton acoustics: past, present, and future. *ICES Journal of Marine Science*, **53**, 513-516.
- Madin, L. P., E. F. Horgan, and D. K. Steinberg, 2001. Zooplankton at the Bermuda Atlantic Time-series Study (BATS) station: diel, seasonal and interannual variation in biomass, 1994-1998. *Deep Sea Research II*, **48(6-9)**, 2063-2082.
- Marcus, N. H., 1988. Photoperiodic conditions, food patchiness and fecundity. *Bulletin of Marine Science*, **43(3)**, 641-649.
- Martin, L. V., T. K. Stanton, P. H. Wiebe, and J. F. Lynch, 1996. Acoustic classification of zooplankton. *ICES Journal of Marine Science*, **53**, 217-224.
- Mauchline, J., 1998. The biology of calanoid copepods. *Advances in Marine Biology*, **33**, 1-710.
- McAllister, C. D., 1969. Aspects of Estimating Zooplankton Production from Phytoplankton Production. *Journal of the Fisheries Research Board of Canada*, **26**, 199-220.
- McLaren, I. A., 1963. Effects of Temperature on Growth of Zooplankton, and the Adaptive Value of Vertical Migration. *Journal of the Fisheries Research Board of Canada*, **20(3)**, 685-727.
- McLaren, I. A., 1974. Demographic strategy of vertical migration by a marine copepod. *The American Naturalist*, **108(959)**, 91-102.
- Montevecchi, W. A., and R. A. Myers, 1996. Dietary changes of seabirds indicate shifts in pelagic food webs. *Sarsia*, **80**, 313-322.
- Morris, M. J., G. Gust, and J. J. Torres, 1985. Propulsion efficiency and cost of transport

- for copepods: a hydromechanical model of crustacean swimming. *Marine Biology*, **86**, 283-295.
- Neill, E. W., 1990. Induced vertical migration in copepods as a defence against invertebrate predation. *Nature*, **345**, 524-526.
- Nelson, D. R., J. N. McKibben, W. R. Strong Jr., C. G. Lowe, J. A. Sisneros, D. M. Schroeder, and R. J. Lavenberg, 1997. An acoustic tracking of a megamouth shark, *Megachasma pelagios*: a crepuscular vertical migrator. *Environmental Biology of Fishes*, **49**, 389-399.
- Newman, S., 1994. The foundations of helicopter flight. Simon Newman, pp. 27-30.
- Nielsen, T. G., E. F. Møller, S. Satapoomin, M. Ringuette, and R. R. Hopcroft, 2002. Egg hatching rate of the cyclopoid copepod *Oithona similis* in arctic and temperate waters. *Marine Ecology Progress Series*, **236**, 301-306.
- Ohman, M. D., 1990. The Demographic Benefits of Diel Vertical Migration by Zooplankton. *Ecological Monographs*, **60(3)**, 257-281.
- Ott, M. W., 2005. The accuracy of acoustic vertical velocity measurements: instrument biases and the effect of Zooplankton migration. *Continental Shelf Research*, **25**, 243-257.
- Pickard, G. L. and W. J. Emery, 1990. Descriptive Physical Oceanography, An Introduction. 5th enlarged edition, Butterworth-Heinemann, p. 40.
- Planque, B., 1996. Spatial and temporal fluctuations in *Calanus* populations sampled by the Continuous Plankton Recorder. Benjamin Planque, Université Pierre et Marie Curie (Paris IV), pp. 13-17.
- Plueddemann, A. J., and R. Pinkel, 1989. Characterization of the patterns of diel migration using a Doppler sonar. *Deep-Sea Research*, **36(4)**, 509-530.
- Raymont, J. E. G., 1983. Plankton and productivity in the oceans. Volume 2—Zooplankton. 2nd edition, Pergamon Press. p. 166.
- Renard, B., 2003. Inversion of Acoustic Zooplankton Measurement for Adaptive Physical-Biological Ocean Forecast. Bertrand Renard, Dept. of Ocean Engineering and Material Science and Engineering, MIT, pp. 16-17.
- Rippeth, T. P. and J. H. Simpson, 1998. Diurnal signals in vertical motions on the Hebridean Shelf. *Limnol. Oceanogr.* **43(7)**, 1690-1696.

- Robertis, A. D., 2002. Size-dependent visual predation risk and the timing of vertical migration: An optimization model. *Limnology and Oceanography*, **47(4)**, 925-933.
- Schillinger, D.J., P. Simmons, and B. de Young, 2000. Analysis of the Mean Circulation in Placentia Bay: Spring and Summer 1999. Physics and Physical Oceanography Data Report 2000-1. *Dept. of Phys. And Phys. Oceanogr. Memorial Univ. of Newfoundland*.
- Sekino, T, and N. Yamamura, 1999. Diel vertical migration of zooplankton: optimum migrating schedule based on energy accumulation. *Evolutionary Ecology*, **13**, 267-282.
- Sindlinger, L. R., D. C. Biggs, and S. R. DiMarco, 2005. Temporal and spatial variability of ADCP backscatter on a continental slope. *Continental Shelf Research*, **25**, 259-275.
- Small, L. F., and J. F. Hebard, 1967. Respiration of a vertically migrating marine crustacean *Euphausia pacifica* Hansen. *Limnol. Oceanogr.*, **2**, 272-280.
- Smith, P. C., and J. I. MacPherson, 1987. Cross-Shore Variations of Near-Surface Wind Velocity and Atmospheric Turbulence at the Land-Sea Boundary During CASP. *Atmosphere-Ocean*, **25(3)**, 279-303.
- Stanton, T. K., P. H. Wiebe, D. Chu, M. C. Benfield, L. Scanlon, L. Martin, and R. L. Eastwood, 1994. On acoustic estimates of zooplankton biomass. *ICES Journal of Marine Science*, **51**, 505-512.
- Stanton, T. K., D. Chu, and P. H. Wiebe, 1996. Acoustic scattering characteristics of several zooplankton groups. *ICES Journal of Marine Science*, **53**, 289-295.
- Stanton, T. K. and D. Chu, 2000. Review and recommendations for the modelling of acoustic scattering by fluid-like elongated zooplankton: euphausiids and copepods. *ICES Journal of Marine Science*, **57**, 793-807.
- Stich, H.-B., and W. Lampert, 1981. Predator evasion as an explanation of diurnal vertical migration by zooplankton. *Nature*, **293**, 396-398.
- Strickler, J. R., 1975. Swimming of planktonic *Cyclops* species (Copepoda, Crustacea): pattern, movements, and their control. In: *Swimming and flying in nature*, Vol. 2. pp 599-613. Ed. by T. Y. T. Wu, C. J. Brokaw and C. Brennan. New York: Plenum Press 1975.
- Strickler, J. R., 1977. Observation of swimming performances of planktonic copepods.

Limnol. Oceanogr. **22**, 165-169.

- Strickler, J. R., 1982. Calanoid Copepods, Feeding Currents, and the Role of Gravity. *Science*, **218**, 158-160.
- Svetlichnyi, L. S., Yu. A. Zagorodnyaya, and V. N. Stepanov, 1977. Bioenergetics of copepods *Pseudocalanus elongatus* during migration. *Soviet Journal of Marine Biology*, **3**, 430-436.
- Tarling, G. A., J. B. L. Matthews, R. Saborowski, and R. Bochholz, 1998. Vertical migratory behaviour of the euphausiid, *Meganyctiphanes norvegica*, and its dispersion in the Kattegat Channel. *Hydrobiologia*, **375/376**, 331-341.
- Taylor, J. R., 1982. An Introduction to Error Analysis, The Study of Uncertainties in Physical Measurements. University Science books, p. 144.
- Thomson, R. E., and S. E. Allen, 2000. Time series acoustic observations of macrozooplankton diel migration and associated pelagic fish abundance. *Can. J. Fish. Aquat. Sci.*, **57**, 1919-1931.
- Tiselius, P., and P. R. Jonsson, 1990. Foraging behaviour of six calanoid copepods: observations and hydrodynamic analysis. *Marine Ecology Progress Series*, **66**, 23-33.
- Tittensor, D.P., B. de Young, and J. Foley, 2002a. Analysis of Physical Oceanographic Data from Trinity Bay, May – August 2001. Physics and Physical Oceanography Data Report 2002-1. *Dept. of Phys. And Phys. Oceanogr. Memorial Univ. of Newfoundland*.
- Tittensor, D.P., B. de Young, and J. Foley, 2002b. Analysis of Physical Oceanographic Data from Trinity Bay, May – August 2002. Physics and Physical Oceanography Data Report 2002-2. *Dept. of Phys. And Phys. Oceanogr. Memorial Univ. of Newfoundland*.
- Tjossem, S. F., 1990. Effects of fish chemical cues on vertical migration behavior of *Chaoborus*. *Limnol. Oceanogr.*, **35(7)**, 1456-1468.
- Torres, J. J., and J. J. Childress, 1983. Relationship of oxygen consumption to swimming speed in *Euphausia pacifica*. I. Effects of temperature and pressure. *Marine Biology*, **74**, 79-86.
- Torres, J. J., 1984. Relationship of oxygen consumption to swimming speed in *Euphausia pacifica*. II. Drag, efficiency and a comparison with other swimming organisms. *Marine Biology*, **74**, 79-86.

- Vlymen, W. J., 1970. Energy expenditure of swimming copepods. *Limnol. Oceanogr.*, **15**, 348-356.
- Vlymen, W. J., 1977. Reply to comment by J. T. Enright. *Limnol. Oceanogr.* **22**, 162-165.
- Westerweel, J., 1997. Fundamentals of digital particle image velocimetry. *Meas. Sci. Technol.*, **8**, 1379-1392.
- Wiebe, P. H., D. G. Mountain, T. K. Stanton, C. H. Greene, G. Lough, S. Kaartvedt, J. Dawson, and N. Copley, 1996. Acoustical study of the spatial distribution of plankton on Georges Bank and the relationship between volume backscattering strength and the taxonomic composition of the plankton. *Deep-Sea Research II*, **43**(No. 7-8), 1971-2001.
- Zaret, T. M. and J. S. Suffern, 1976. Vertical migration in zooplankton as a predator avoidance mechanism. *Limnol. Oceanogr.*, **21**(6), 804-813.

Appendix A

The energetics discussion in § 2.1 omitted some details of the derivations so as not to disrupt the continuity of the discussion. These details are presented here.

A.1 Energetic requirement for hovering at constant depth

This derivation assumes that the animal hovers by creating a continuous uniform flow, so that the problem becomes similar to calculating the energetic cost of a hovering helicopter. For details on derivations for a hovering helicopter and assumptions made see Newman (1994), Leishman (2000). Remaining stationary by creating such a flow is also a feeding tactic for some zooplankton, such as *Neocalanus cristatus*, as the flow is generated by the mouthparts, and entrains food particles (Greene, 1988).

The animal's shape is approximated as a sphere of radius a , and the downward flow generated is considered to have a cross-sectional area of πa^2 (Fig A.1.1). A current is generated by the mouthparts with velocity w_1 , and pressure p just above, so that Bernoulli's law gives

$$p_0 = p + \frac{1}{2} \rho w_1^2, \quad (\text{A.1})$$

where p_0 is the pressure of undisturbed water far above, and ρ is the fluid density. The flow is modelled by a constant pressure difference across the plane of the mouthparts, so just below the mouthparts, the pressure is increased to $p + \Delta p$, and further below the animal the pressure is again equal to the undisturbed pressure p_0 , with some wake velocity w_2 . Bernoulli's law gives

$$p + \Delta p + \frac{1}{2} \rho w_1^2 = p_0 + \frac{1}{2} \rho w_2^2 \quad (\text{A.2})$$

$$\Rightarrow \Delta p = \frac{1}{2} \rho w_2^2 \quad (\text{A.3})$$

The generated flow moves a mass of water equal to $\rho(\pi a^2)(w_1 t_T)$, where t_T is the total time spent hovering. The kinetic energy required to move this mass is

$$E_k = \frac{1}{2} [\rho(\pi a^2)(w_1 t_T)] w_2^2 \quad (\text{A.4})$$

The thrust that the animal must generate to move this water can be expressed in three ways—in terms of the mass flux of water (M), in terms of the generated pressure, and in terms of the force balancing gravity; respectively:

$$T = M w_2 = \pi a^2 \rho w_1 w_2 \quad (\text{A.5})$$

$$T = \pi a^2 \Delta p = \pi a^2 \frac{1}{2} \rho w_2^2 \quad (\text{A.6})$$

$$T = F_g' \quad (\text{A.7})$$

Equating these gives expressions for velocities:

$$w_1 = 2 w_2 \quad (\text{A.8})$$

$$w_2 = \sqrt{\frac{2 F_g'}{\rho \pi a^2}} \quad (\text{A.9})$$

and substitution into (A.4) gives

$$W = E_k = \left[\frac{(2 F_g')^{3/2}}{(2 \rho \pi a^2)^{1/2}} \right] t_T \quad (\text{A.10})$$

The actual work required by the zooplankter to generate this energy depends on the mechanical efficiency of the animal and mode of propulsion, discussed in § 2.1.

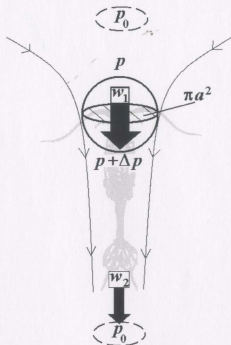


Figure A.1.1 Schematic of a copepod hovering by producing a continuous downward flow.

A.2 Time and distance required to coast to a stop

Consider a spherical zooplankter moving upward with an initial velocity w_1 . The forces acting to decelerate are the adjusted force of gravity, F_g' , and the drag force F_D , which is a function of velocity. Using the definitions for these forces given by equations (2.2) and (2.3), the acceleration is given by

$$\frac{dw}{dt} = \frac{-6\pi\mu a w - \Delta\rho \frac{4}{3}\pi a^3 g}{\Delta\rho \frac{4}{3}\pi a^3} \quad (\text{A.11})$$

Let

$$A = \frac{-9\mu}{2\Delta\rho a^2} \quad \text{and} \quad B = -g \quad (\text{A.12})$$

Then

$$\frac{dw}{dt} = Aw + B \quad (\text{A.13})$$

The amount of time required to come to rest is then

$$\int_{\Delta t} dt = \int_{w_1}^0 \frac{dw}{Aw + B} \quad (\text{A.14})$$

$$\Delta t = \frac{1}{A} \ln |Aw + B| \Big|_{w_1}^0 \quad (\text{A.15})$$

$$\Delta t = \frac{1}{A} \ln \frac{B}{Aw_1 + B} \quad (\text{A.16})$$

Similarly, the distance required to come to rest is

$$\int_{\Delta z} dz = \int_{w_1}^0 \frac{w dw}{Aw + B} \quad (\text{A.17})$$

$$\Delta z = \frac{Aw+B}{A^2} - \frac{B}{A^2} \ln |Aw+B| \Big|_{w_1}^0 \quad (\text{A.18})$$

$$\Delta z = -\frac{w_1}{A} - \frac{B}{A^2} \ln \frac{B}{Aw_1+B} \quad (\text{A.19})$$

A zooplankter of size $a = 0.001$ m travelling at $w = 0.05$ m s⁻¹ (approximately the maximum velocity found in the measured data) will come to rest in $\Delta t = 0.004$ s and in $\Delta z = 8 \times 10^{-5}$ m. It should be noted that more elaborate formulations of copepod swimming yield coasting distances that are not as small (*cf.* Morris *et al.*, 1985).

A.3 Work requirement for hop-and-sink swimming at a nonzero mean velocity

A zooplankter is assumed to hop upward at a constant velocity w_j and to sink at a constant terminal velocity w_s , as given by equation (2.6). Acceleration and deceleration times are neglected (see Appendix A.2). The mean rate of ascent, \bar{w} , is also known. This rate is a combination of hopping upward and sinking downward:

$$\bar{w} = \frac{z_j - |z_s|}{t_j + t_s} = \frac{z_j - |w_j|t_s}{t_j + t_s}, \quad (\text{A.20})$$

where z_j and t_j are respectively the distance and time passed in one hop, and z_s and t_s are respectively the distance and time passed sinking between the end of one hop and the start of the next. This time spent sinking is unknown, and depends upon the mean velocity.

Rearranging (A.20) gives:

$$t_s = \frac{z_j - \bar{w}t_j}{\bar{w} + |w_j|} \quad (\text{A.21})$$

The work done by the zooplankter for a single hop is $F_{up}z_j$, where F_{up} is

determined as in equation (2.1). The number of hops N over total time t_T is

$$N = \frac{t_T}{t_j + t_s}, \quad (\text{A.22})$$

so the total work done is

$$W_T = F_{up} N z_j = F_{up} \left[\frac{z_j}{t_j + t_s} \right] t_T. \quad (\text{A.23})$$

Substitution for t_s and some simple algebra gives

$$W_T = F_{up} \left[\frac{w_j (\bar{w} + |w_i|)}{w_j + |w_i|} \right] t_T. \quad (\text{A.24})$$

